

**Alma Mater Studiorum – Università di Bologna**

**DOTTORATO DI RICERCA IN  
INGEGNERIA CIVILE, AMBIENTALE E DEI MATERIALI**

**Ciclo XXX°**

**Settore Concorsuale: 08/B3**

**Settore Scientifico Disciplinare: ICAR/09**

**SEISMIC VULNERABILITY ASSESSMENT AND FRAGILITY  
ANALYSIS OF INDUSTRIAL RC PRECAST STRUCTURES**

**Presentata da: Elena Ongaretto**

**Coordinatore Dottorato**

**Prof. Luca Vittuari**

**Supervisore**

**Prof. Ing. Marco Savoia;**

**Co-Supervisore**

**Dott. Ing. Nicola Buratti**

**Esame finale anno 2018**

Copyright by Elena Ongaretto 2018  
All Rights Reserved

## TABLE OF CONTENTS

<b>1. INTRODUCTION</b>	<b>1</b>
1.1 Motivation and objectives	1
1.2 from Past Earthquakes	2
1.3 Feature of the 2012 Emilia earthquakes	4
1.4 Evolution of the seismic classification in the Emilia region	8
1.5 Evolution of building codes for RC precast structures	10
<b>2. DAMAGE DATABASE FOR INDUSTRIAL BUILDINGS AFTER THE EMILIA EARTHQUAKES</b>	<b>12</b>
2.1 Definition of the building stock interested by the Emilia earthquakes	12
2.2 Damage data collection and inventory	14
2.3 The electronic database	18
2.4 Database consistency and spatial distribution.	23
<b>3. TYPOLOGIES OF PRECAST BUILDINGS IN THE EMILIA REGION:</b>	<b>30</b>
3.1 Introduction	30
3.2 Types of precast buildings: a personal classification.	31
3.3 Damage data analysis considering different typologies of precast building	36
3.4 Typological features of the precast industrial buildings in the area of interest	41
<b>4. RECURRENT DAMAGES AND COLLAPSES IN PRECAST INDUSTRIAL BUILDINGS DURING EMILIA EARTHQUAKE</b>	<b>43</b>
4.1 Introduction	43
4.2 Classification of damage and collapse mechanisms in reinforced concrete precast industrial buildings	44
4.3 Statistical analysis of damages observed in Emilia region after 2012 earthquakes	48
4.4 Summary of post-earthquake reconnaissance activity	52
<b>5. OBSERVATIONAL FAILURE ANALYSIS OF PRECAST BUILDINGS AFTER THE 2012 EMILIA EARTHQUAKES AND RELATED RETROFIT INTERVENTIONS.</b>	<b>54</b>
5.1 Introduction	54

5.2	Parameters of seismic intensity adopted in the study _____	54
5.3	First correlations between damage and seismic intensities _____	56
5.4	Conclusions _____	62
<b>6.</b>	<b><i>EMPIRICAL SEISMIC FRAGILITY FOR THE PRECAST RC INDUSTRIAL BUILDINGS DAMAGED BY THE 2012 EMILIA (ITALY) EARTHQUAKES</i></b> _____	<b>64</b>
6.1	Introduction _____	64
6.2	Damage distribution vs. ground-motion intensity _____	65
6.2.1	Definition of ground-motion intensity _____	65
6.2.2	Damage distribution versus PGA _____	67
6.3	Damage analysis and fragility _____	68
6.3.1	Damage data _____	68
6.3.2	Point estimates of fragility _____	69
6.4	Parametric fragility curves _____	71
6.4.1	General approach _____	71
6.4.2	Fragility curves based on individual damage levels _____	72
6.4.3	Fragility curves using ordinal models _____	74
6.4.4	Ground-motion uncertainty _____	76
6.5	Fragility curve distinguished for the different types of precast buildings _____	79
<b>7.</b>	<b><i>Conclusions</i></b> _____	<b>82</b>
7.1	General conclusions _____	82
7.2	Further developments _____	83
	<b>REFERENCES</b> _____	<b>85</b>

## LIST OF FIGURES

<i>Figure 1. Damages from l’Aquila eathquakes (2009): a)Plastic hinge formation in the column,b) un-seating of the beam .....</i>	<i>4</i>
<i>Figure 2. Damages from l’Aquila eathquakes (2009): collapse of the roof elementh, failureof curtain waall .....</i>	<i>4</i>
<i>Figure 3. Ground-motion recording stations. Temporary stations were installed after May 20<sup>th</sup> mainshock close to the epicenters. The MRN (permanent) and MRO2 (temporary) stations are overlapped on the map, their relative distance is about 2.7 km [24]. .....</i>	<i>6</i>
<i>Figure 4. Investigated area. Epicenters (stars): May 20th mainshocks (ML=5.9). May 29th mainshock (ML=5.8). June 3rd mainshock (ML=5.1). For the sites cited, the cumulative macroseismic intentensities are reported in brackets [8]. .....</i>	<i>6</i>
<i>Figure 5. Epicenters of the 2012 Emilia earthquake sequence. The color scale indicates the earthquakes dates [24]. ..</i>	<i>7</i>
<i>Figure 6. Geological structures in the region struck by the Emilia earthquakes [24]. .....</i>	<i>8</i>
<i>Figure 7. Seismic classification before 1998, according to De Marco and Marsan (1986), (a); and actual classification according to the official hazard data (Stucchi et al, 2011) employed in DM 14/01/2008, (b). .....</i>	<i>9</i>
<i>Figure 8. Soil classification on geological basis of the area struck by the earthquake. ....</i>	<i>10</i>
<i>Figure 9. Map of the territory hit by 2012 Emilia earthquake reporting the distribution of the industrial building stock (green circle data points) and the epicentres of the two mainshocks (red stars). .....</i>	<i>13</i>
<i>Figure 10. Industrial building in San Giacomo Roncole (Mirandola, MO): (a) the building after May 20<sup>th</sup> earthquake, and (b) after May 29<sup>th</sup> earthquake.....</i>	<i>15</i>
<i>Figure 11. Form1_Building identification .....</i>	<i>19</i>
<i>Figure 12. Form 2_Building identification .....</i>	<i>20</i>
<i>Figure 13. Form 3_Building structural description. ....</i>	<i>21</i>
<i>Figure 14. Example of two built-up area located in San Felice sul Panaro (Mo).....</i>	<i>22</i>
<i>Figure 15. Form 4_Columns caracterists .....</i>	<i>22</i>
<i>Figure 16. Form 5_Damages and interventions to structural and non structural elements. ....</i>	<i>23</i>
<i>Figure 17. Percentage of each damage level for the whole database, a) Five damage levels, b) Three damage levels. ....</i>	<i>24</i>
<i>Figure 18. Normalized cumulative number of industrial buildings versus distance from the nearest epicentre. ....</i>	<i>24</i>
<i>Figure 19. GIS representation of the spatial distribution of the buildings collected in the damage database. ....</i>	<i>26</i>
<i>Figure 20. GIS overview representation of the buildings analyzed in the database located in the most damaged industrial clusters. ....</i>	<i>26</i>
<i>Figure 21. GIS overview representation of the buildings analyzed in the database located in San Felice industrial area. ....</i>	<i>27</i>
<i>Figure 22. GIS overview representation of the buildings analyzed in the database located in Finale Emilia industrial area. ....</i>	<i>27</i>
<i>Figure 23. Percentage of each damage level for the main damaged industrial clusters. . ....</i>	<i>28</i>
<i>Figure 24. Type 1 Building with double slope precast beams simply-supported at the top of the columns and masonry cladding panels.....</i>	<i>31</i>
<i>Figure 25. a) Buildings type 0 with double slope precast beams simply-supported at the top of the columns and orizontal precast cladding panels placed between the columns, b) a typical roof of building types 0 characterized by TT elements. ....</i>	<i>32</i>
<i>Figure 26. Type 2: buildings with double slope precast beams simply-supported at the top of the columns with external precast heavy cladding panels fixed esternally to the columns a) horizontal panels or b) vertical panels....</i>	<i>32</i>

Figure 27. Type 3 - Buildings with long span planar roof: a) example of external and internal view; b) types of cladding panels: horizontal and vertical. ....	33
Figure 28. Shed roof: a) beams “knee” b) oblique beams c) picture of a building catalog as type 4. ....	34
Figure 29. Buildings with plan irregularity. ....	35
Figure 30. Type 5 due to the presence of a cast in place portion of the building. Due to this irregularity a portion on the building totally collapsed. ....	35
Figure 31. a) Percentage of each of the 7 types of precast buildings considering a damage database of 1767 units; b) Percentage of each of type of buildings considering type 0 and type 1 belonging to the same type. ....	36
Figure 32. Percentage of each damage level for each of type of precast buildings. ....	37
Figure 33. Percentage of each building type for the main industrial clusters present in the area struck by the 2012 Emilia earthquakes. ....	38
Figure 34. Number of buildings belonging to each interval of PGA, for each type of building and for each damage level. ....	39
Figure 35. Damage levels distribution for each type of building considering three range of PGA. ....	40
Figure 36. Type 0/1: probability distributions of the length of the main beam, of frame spacing and column height. ....	41
Figure 37. Type 2: probability distributions of the length of the main beam, of frame spacing and column height. ....	42
Figure 38. Type 3: probability distributions of the length of the main beam, of frame spacing and column height. ....	42
Figure 39. Google Earth images of a building located in Medolla (MO): a) before the seismic events 2011 b) after the seismic event 2014. ....	44
Figure 40. Roof collapses in precast buildings: two examples of partial collapse due to interaction with masonry curtain walls. ....	45
Figure 41. Collapse of (a) a masonry curtain wall not restrained by the RC structure. ....	45
Figure 42. Roof collapses in precast buildings: (b) extended collapse in a modern prefabricated building. ....	46
Figure 43. Collapse RC cladding panels due to failure of the steel channel profiles supporting them. ....	46
Figure 44. Damages in precast RC columns: (a) rotation of external columns; and (b) large base rotation due to formation of a plastic hinge with yielding and buckling of longitudinal steel bars. ....	47
Figure 45. Local damages in precast RC columns: (a) failure mechanism due to interaction with masonry infills; and (b) damage of the upper fork of a column due to flexural-torsional displacements of the precast beam. ....	47
Figure 46. Damages in precast RC columns: (a) extended building collapse caused by large column rotation due to foundation settlement; and (b) column rotation due to settlement at the foundation level, counteracted by the presence of an industrial concrete pavement. ....	48
Figure 47: Damage of the main components of the precast structures among the different damage levels. ....	49
Figure 48. distribution of different types of column damage among the 5 damage levels. ....	51
Figure 49. distribution of different types of roof damages among the 5 damage levels. ....	51
Figure 50. distribution of different types damages on masonry curtain wall among the 5 damage levels. ....	52
Figure 51. distribution of different types damages on RC cladding panels among the 5 damage levels. ....	52
Figure 52. Horizontal PSA versus period for (a) the seismic station at Mirandola (first and second mainshocks), and (b) those at San Felice sul Panaro and Moglia (second mainshock) ....	55
Figure 53. Map reporting the locations of severely damaged to collapsed buildings (damage levels D3, D4 and D5, black data points) and of epicentres of the two mainshocks (red stars). ....	57
Figure 54. Cumulative frequencies of buildings belonging to damage levels D3 (dashed lines), D4 (line with symbols) and D5 (solid line) versus (a) distance from the nearest epicentre, and (b) corresponding PSA at 1 s. ....	57
Figure 55. Map reporting the locations slightly to moderately damaged buildings (damage levels D1 and D2, black data points) and of epicentres of the two mainshocks (red stars) ....	58

Figure 56. Cumulative frequencies of buildings belonging to damage levels D1 and D2 versus (a) distance from the nearest epicentre, and (b) corresponding PSA at 1 s .....	58
Figure 57. Map reporting the locations of undamaged buildings (damage level D0, black data points) and of epicentres of the two mainshocks (red stars) .....	58
Figure 58. Cumulative frequencies of the three classes of damage levels plotted versus the distance from the nearest epicentre .....	59
Figure 59. Bar charts with (a) cumulative number of buildings investigated, and (b) cumulative frequencies of buildings versus epicentral distance for the three classes of damage levels .....	60
Figure 60. Cumulative frequencies of the three classes of damage levels versus (a) PSA at 1 s corresponding to the nearest epicentre, and (b) maximum experienced PGA .....	60
Figure 61. Single-storey single-bay precast frame (a) without masonry infill and (b) with an infill wall provided with a strip window between precast beam and wall .....	62
Figure 62. Shakemaps for (a-b) the median value of the horizontal PGA, and (c-d) for its logarithmic standard deviation (SD), for (a, c) the 20 May and (b, d) 29 May earthquakes. Grey dots and black squares indicate the locations of the buildings in database associated to the PGA of 20 May and 29 May, respectively. ....	66
Figure 63. Cumulative number of industrial buildings, in the survey area, which experienced a peak ground acceleration less or equal to the PGA values reported in abscissa: building stock from cadastral data (right axis), all buildings in the database ( $D \geq D_0$ ), buildings with damage level $D \geq D_1$ , and $D \geq D_3$ . ....	68
Figure 64. (a-e) comparison among failure probabilities for damage levels $D_1$ to $D_5$ , point-estimates from damage matrices (black circles), lognormal (LN) and log-logit (LL) parametric fragility curves obtained by maximum likelihood estimation; (f) LL parametric fragility curves for the various damage levels. ....	70
Figure 65. (a) PDF and (b) CDF for $y_i^*   IM_i, \beta$ and $y_j^*   IM_j, \beta$ , with $IM_j > IM_i$ and $\beta > 0$ . The boundaries of the intervals used to map the continuum latent variables $y_i^*$ and $y_j^*$ to the ordinal damage variables $y_i$ and $y_j$ are indicated by dashed lines. The areas corresponding to the probability of observing damage $D_i = D_1$ (i.e. $y_i = 1$ ) and $D_j = D_1$ (i.e. $y_j = 1$ ) are hatched in (a). ....	75
Figure 66. Dataset used for the ordinal regression. Figures a) to f) correspond to damage levels $D_0$ to $D_5$ , respectively. Each point represents the median PGA value assigned to a building, colours indicate the earthquake that produced the ground-motion (20 May and 29 May). Vertical bars represent $\pm$ standard deviation intervals on the logarithm of PGA, centred on the median PGA value. ....	78
Figure 67. Comparison of fragility curves obtained from the log-logit models (LL), the ordinal log-logistic model (OLL) and the ordinal log-logistic model taking ground-motion uncertainty into account (OLL-R). ....	79

## LIST OF TABLES

<i>Table 1. total estimated loss for the 3 main seismic recent events in Italy.</i>	12
<i>Table 2 Damage levels adopted in the present investigation and correspondences with definitions reported by Emilia-Romagna Regional Decree No. 57/2012</i>	17
<i>Table 3 Correspondence of the damage levels used in the present analysis with those introduced by EMS-98 (1998)</i>	17
<i>Table 4. Number of buildings analyzed for each damage level.</i>	24
<i>Table 5. Number of surveyed buildings for the thirty cities with the highest number of industrial buildings collected inside the damage database</i>	29
<i>Table 6. Number of buildings analyzed for each damage level after grouping the structures by type.</i>	36
<i>Table 7. Geometrical dimensions characteristic of the building stock belonging to Emilia damage database.</i>	41
<i>Table 8. Distribution among the three damage classes of the buildings affected by a <math>PGA \geq 0.28g</math></i>	61
<i>Table 9. Damage matrix for all buildings collected in the database: number of buildings for each damage level vs. intervals of PGA.</i>	69
<i>Table 10. Cumulative damage matrix for all buildings in the database.</i>	69
<i>Table 11. Estimated failure probability for each damage level.</i>	71
<i>Table 12. Mean value (E) and standard deviation (SD) of the posterior distribution of the parameters of the log-logistic models (LL) for the different damage states.</i>	73
<i>Table 13. Mean value (E) and standard deviation (SD) of the posterior distribution of the parameters of the ordinal log-logistic models with (OLL-R) and without (OLL) ground-motion uncertainty.</i>	<b>Errore. Il segnalibro non è definito.</b>

# 1. INTRODUCTION

## 1.1 Motivation and objectives

The 2012 earthquake sequence in Northern Italy (Emilia earthquake) is considered the most severe seismic event in terms of damages and collapses suffered by precast RC industrial buildings.

Issues and collapses related to precast buildings were reported by many authors after past earthquakes in the world [1][2][3][4][5][6][7] and in Italy [8] but the extent and the severity of the collapses observed after the Emilia earthquake are unprecedented in Italy.

The region struck by the earthquake mainshocks is one of the most productive areas in Italy, and is characterized by medium-to-small clusters of industrial buildings located in the various municipalities. The two mainshocks caused extended damages and collapses in prefabricated RC buildings and in some industrial areas close to the epicenters (e.g., Mirandola Nord, S. Giacomo Roncole, Cavezzo, Medolla), up to 70% of buildings were significantly damaged or collapsed. The main causes of the collapses were vulnerabilities related to the structural characteristics of Italian precast buildings not designed with seismic criteria, since the region was not covered by seismic code requirements until October 2005. To underline the gravity of the seismic event it's worth to know that the total estimated loss for Emilia earthquakes is € 13 bn, equal to the 0.8% of 2012 Italy GDP, even more higher than Aquila and Amatrice earthquakes were the number of death and injured was much higher.

After an earthquake, the collection of damage data and their inventory represents an essential tool for predicting the response of the buildings to future earthquakes. So, through a critical elaboration of the huge amount of case studies, provided by the 2012 earthquake, the aim of my Ph.D research was to evaluate the fragility of Italian RC precast buildings.

Seismic fragility is a measure of how prone a building is to suffer damage for a given severity of the ground shaking, and it can be mathematically formulated by fragility curves, which describe the conditional probability of exceeding a certain damage limit state given the intensity of the ground motion.

In order to achieve this goal, it was developed an electronic database to catalog observational damage data related to a wide range of precast RC buildings struck by the Emilia earthquake. The building damages are classified using a six level damage scale derived from EMS-98. The completeness of the database and the spatial distribution of the buildings investigated are analyzed using cadastral data as a reference.

In the very first part of the research, the damages of 1890 buildings were related with the epicentral distance and to the peak ground acceleration.

Subsequently the damages were examined first, by deriving damage matrices and then estimating empirical fragility curves. The intensity of the ground motion is quantified by the

maximum horizontal peak ground acceleration (PGA), which is estimated for each site from available shakemaps. The fragility curves obtained in the present work, when compared to literature fragilities for cast in place RC frame buildings, indicate that precast industrial buildings are significantly more vulnerable. Therefore, specific fragility models should be used for assessing the seismic risk related to prefabricated buildings.

Subsequently, the precast buildings of the whole damage database have been classified as belonging to a particular type of precast structures. The precast buildings were grouped into seven different typologies and fragility curves were developed for each of them underling the difference in the seismic response.

Communicating seismic risk and structural performance is a complex but essential task assigned to the technical community, in order to enable owners of earthquake prone buildings and other stakeholders to consider the implementation of seismic vulnerability reduction interventions and to make informed retrofit decisions. That said, the last phase of the research activity was related to the application of Performance-Based-Earthquake-Engineering (PBEE) methodology according to FEMA P-58 guidelines. In particular, to exercise and evaluate P-58 guidelines, while making a comparison with the Italian damage data collected, was used the software SP3, developed by Haselton and Baker risk group. Significant cases study were then chosen to perform a loss assessment analysis and evaluate the cost-effectiveness of alternative retrofit options to support decision making to better suit the client priorities and needs. This part of the research is still going on and will be part of further development.

## **1.2 from Past Earthquakes**

Since Spitak (Armenia) earthquake in 1988, precast industrial buildings lacking of a suitable seismic design have showed a unique behaviour, generally characterized by extended collapses of girders and roof elements [9]. During that earthquake, multi-storey precast frame-panel buildings showed poor performances, especially due to the low ductility of the connections [10]. Heavy damages strictly related to deficiencies of connections between precast members and inadequate flexural reinforcement in precast RC columns were also documented after the 1999 Kocaeli (Turkey) earthquake [11]. The results obtained from several non-linear time history analyses of typical Turkish single-storey precast industrial buildings indicated that flexural damages at the base of the columns should mainly be ascribed to near-fault earthquakes [12]. Sezen and Whittaker [13] categorized observational damage data from Kocaeli earthquake according to a performance scale composed by five and four levels of structural and non-structural damages, respectively. The effects of infill walls on the seismic response of precast industrial buildings in Turkey was highlighted by Korkmaz and Karahan (2011) [14], who performed a series of non-linear analyses. In the presence of masonry curtain walls, the stability and integrity of the precast structures resulted often to be enhanced, even if the stiffening effects of the walls may lead to an increase of the

earthquake actions. With regard to another, more recent destructive earthquake occurred in Turkey, i.e. the 2011 Van earthquake, the effects of improper design and detailing of connections in precast concrete structures under construction were reported by Ozden et al. (2014) [5]. The strong vulnerability of totally or partially precast structures not designed for the earthquake resistance was also highlighted after the 2008 Sichuan (China) earthquake. In particular, many schools built using a hybrid structural system with unreinforced masonry walls, cast-in-place concrete beams, and precast concrete floor elements suffered from a disproportionate number of collapses (Miyamoto et al. 2008, China Earthquake Field Investigation Report 2008) [15]. During the 2010 Haiti earthquake and 2011 sequence of events around Christchurch (New Zealand), considerable damages occurred in numerous low-rise industrial buildings [16]. In particular, many modern industrial structures, based on the use of load-bearing concrete panels, or steel frames with concrete or unreinforced masonry cladding, suffered significant structural and non-structural damages.

In Italy, the high vulnerability of precast concrete cladding panels in industrial buildings was evidenced, probably for the first time, after the 2009 L'Aquila earthquake, that revealed the inadequacy of typical steel connections between panels and main structural elements [6]. Recently, numerical models were developed to study the role of the wall panel connections for different degrees of interaction with the precast structure [17].

Unlike the Aquila earthquake, the Emilia Romagna earthquake affected an area that only recently was included in the Italian seismic design provisions. Some deficiencies in the performance of precast buildings could be observed in both regions, others could be noticed only in Emilia Romagna, where in the majority of the cases the structures have been designed for static forces only.

Faggiano et al. [2009] [18] illustrate how structural elements of industrial precast buildings responded to the L'Aquila earthquake in compliance with the provisions of the code they were designed with: none of the columns failed, in some cases plastic hinges developed due to the intensity of the seismic action (Figure 1 a). Many buildings presented damage to the beam column joint, but just in one case the beam fell down for loss of support (Figure 1 b). In this case the resistance of the connection did not rely only on friction, as we could often observe in Emilia, but failure instead occurred due to spoiling of the concrete covering the steel reinforcement in the joint (Cassotto C., Ph.D Thesis [2015]). The same mechanism affected the roof-beam connection (Figure 2 a). The most severe and common damage was related to the curtain wall system, especially masonry walls, but also the anchoring systems of the precast panels proved to be inefficient (Figure 2b).



Figure 1. Damages from l'Aquila earthquakes (2009): a) Plastic hinge formation in the column, b) un-seating of the beam



Figure 2. Damages from l'Aquila earthquakes (2009): collapse of the roof element, failure of curtain wall

### 1.3 Feature of the 2012 Emilia earthquakes

The earthquakes that struck the Northern Italy in May 2012 can be collected in two main sequences, with mainshocks of comparable energy. They occurred on May 20<sup>th</sup> and 29<sup>th</sup>, with epicentral coordinates and local magnitude N44.889, E11.228,  $M_L = 5.9$  and N44.851, E11.086,  $M_L = 5.8$ , respectively [19]. The epicentre of the first shock was between Finale Emilia, Bondeno and Sermide and the depth of ipocenter was about 6.3 kilometres (4 mi). Two main aftershocks occurred, one approximately an hour after the main event and another approximately eleven hours after the main event. Seven people were killed. Main damage involved historical buildings, masonry buildings, industrial structures, and in some cases also reinforced concrete structures, as shown by in-filed reports after the earthquake (e.g., EPICentre Field Observation Report No. EPI-FO-200512, 2012; EPICentre Field Observation Report No. EPI-FO-290512, 2012). The second

main shock occurred more than 20 km to the west of the first one, close to Medolla, at a depth of about 10 kilometres (6 mi), causing more damage in the affected area and the deaths of 20 people out of a total of 27 fatalities. The first main shock occurred 2012 at 04:03 local time (02:03 UTC), if the Emilia event had occurred during the day the number of casualties would have been much higher, since the employees of the industrial buildings would have been at work. The second main shock occurred at 09:00 CEST, 07:00 UTC, when a lot of buildings were still closed due to the first event.

The first mainshock (May 20<sup>th</sup>) was recorded also from the station of San Nicandro Garganico, located in Southern Italy, at a distance from the epicentre of about 500 km. The horizontal (subscript “h”) and vertical (subscript “v”) Peak Ground Accelerations (PGA) recorded on May 20<sup>th</sup> at Mirandola (epicentral distance  $R_{\text{epi}} = 12.3$  km), the only fixed station initially located in the epicentral area, were  $\text{PGA}_h = 2.60$  m/s<sup>2</sup> and  $\text{PGA}_v = 3.00$  m/s<sup>2</sup>. Peak Ground Velocities (PGV) were  $\text{PGV}_h = 0.47$  m/s and  $\text{PGV}_v = 0.06$  m/s (INGV 2012). After the first mainshock, 10 additional real-time stations were positioned within few tens of kilometres from the epicentre by the Italian National Institute of Geophysics and Vulcanology (INGV), and 11 additional temporary stations were installed in the epicentral area by the Italian Department of Civil Protection (DPC), see the paper by Cultrera et al. (2014) and Figure 3. Therefore, the second mainshock (May 29<sup>th</sup>) was much better monitored than the first event. In this case, the strong motion data obtained from the station of Mirandola, once again the closest to the epicentre (epicentral distance  $R_{\text{epi}} = 4.1$  km), were  $\text{PGA}_h = 2.90$  m/s<sup>2</sup> and  $\text{PGV}_h = 0.57$  m/s for the strongest horizontal component, and  $\text{PGA}_v = 9.00$  m/s<sup>2</sup> and  $\text{PGV}_v = 0.28$  m/s for the vertical component (INGV 2012). Note the very high value of  $\text{PGA}_v$ , typical of near-fault earthquakes. The ground-motion records used in the present work were obtained from the ITACA database [20] [21] containing processed accelerograms mostly recorded in Italy [22].

The macroseismic survey, which was updated after the second strong event, involved about 190 localities. The maximum intensity derived from the cumulative effects of the two main events was equal to VII-VIII MCS (Figure 4). The second shock of May 29, along with the main aftershocks that followed the earthquake of May 20, significantly increased damage in the western part of the stricken area. In addition, significant co-seismic effects were observed, such as soil liquefaction phenomena [23], especially in the villages of Mirabello, San Carlo, and Sant’Agostino.



epicentres during the sequence, displayed in Fig. 10, it can be noted that they are located almost at the same latitude but with a remarkably different longitude. During the seismic sequence, the epicentres migrated to the west, with epicentral distance between May 20 and June 3 events equal to about 23 km. The migration of epicentres during the seismic sequence increases uncertainty on the selection of the reference earthquake to be considered in the post-event surveys for usability evaluation [25].

It's worth noticing that, on 90% of the territory, the maximum seismic intensity was recorded during the May 20th or 29th, 2012, earthquakes. All other subsequent shocks were significant for the remaining 10% of the struck area .

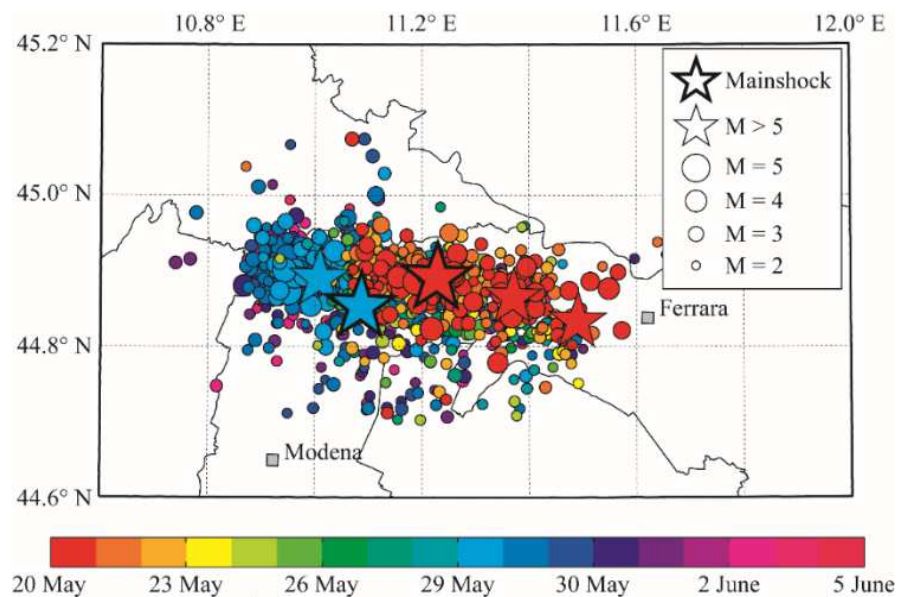


Figure 5. Epicenters of the 2012 Emilia earthquake sequence. The color scale indicates the earthquakes dates [24].

In the past, the same area was struck in 1996 by a  $M_w = 5.4$  earthquake and by other smaller earthquakes, in 1986 and 1967. The most destructive historical events were the November 15th, 1570, Ferrara earthquake, with an estimated  $M_w = 5.48$ , and the March 17th, 1574 event ( $M_w = 4.7$ ), that produced damage in Finale Emilia [26], [27]

The seismic-tectonic structure of the area is characterized by the northern Apennines frontal thrust systems, composed of a pile of NE-verging tectonic units as a consequence of the collision between the European plate and the Adria plate [28]. The geometries of the thrusts below the Po Valley have been studied by various authors [29][30]. Three major curved thrust fronts are identified, as depicted in Figure 6: the Monferrato, the Emilia, and the Ferrara-Romagna Arcs. Active NE-SW shortening has been documented by various authors [31][32].

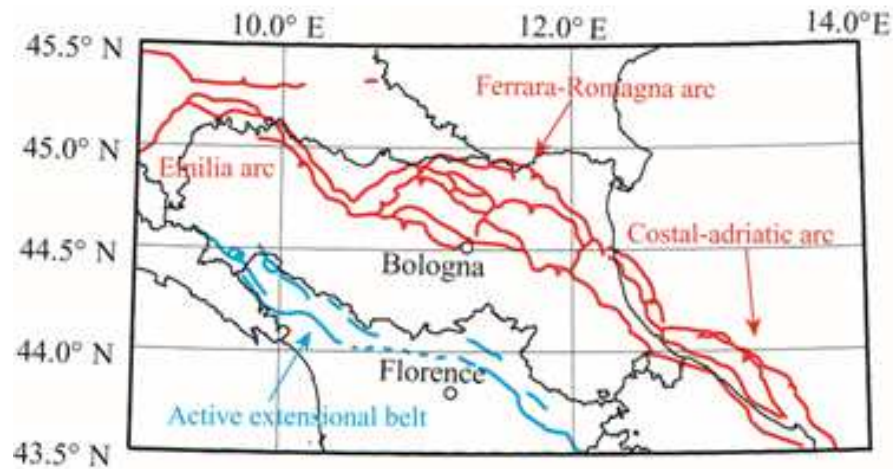


Figure 6. Geological structures in the region struck by the Emilia earthquakes [24].

#### 1.4 Evolution of the seismic classification in the Emilia region

The region struck by the earthquake was not covered by seismic design regulations until October 2005. Therefore, most of the buildings were lacking of proper design and detailing for earthquake resistance. This circumstance undoubtedly represented the main cause of collapses in precast RC industrial buildings [7]. In addition, acceleration and displacement response spectra of the two mainshocks exhibited significant amplifications in the medium-to-long period range, typical of precast RC structures (1 s–3 s), due to the peculiar soil characteristics of the Po River Plain, with the presence of very deep alluvial deposits [19].

Seismic classification in Italy and in general in all seismically prone areas is quite often a result of disastrous earthquakes. In Italy, the first seismic hazard map for Italy was prepared after the destructive Messina earthquake in 1908 and thus the first classification was released in 1909. Obviously such a classification was updated at the knowledge of the time. After this first classification every five or ten years, typically after the occurrence of strong earthquakes, a new update of seismic classification and code provisions were provided [33].

The most important improvement was achieved in 1996 [34] when four seismic zones, corresponding to different seismic hazard levels, were identified in Italy: the first zone was characterized by the largest value of horizontal seismic-actions, while for the fourth zone no seismic actions were prescribed for design. The zone boundaries followed administrative boundaries (i.e. municipalities). The Emilia region was mostly classified a non-seismic zone, with the exception of some upland areas (far from the areas struck by the 2012 earthquakes). The seismic hazard map was then significantly updated in 2003 [35], after the San Giuliano earthquake, and 2008 [36]. The 2003 design provisions (OPCM 3274, 2003), introduced also modern design rule such as the so called capacity design. On the other hand, it should be noted that such rules worked

as recommendation, since they have never become compulsory, and it was still possible to design new structures according to the previous building code (DM 16/01/1996). Even if the 2003 classification and the design provisions were not compulsory, they represented the “Copernican revolution” of Italian earthquake engineering, since it was the first step towards the European unified design approach provided by Eurocodes and the first introduction of modern seismic design rules [37]. In particular, the OPCM 3274 (2003) was very similar to the provisions provided in Eurocode 8 or EC8 (CEN, 2004).

The last step in terms of seismic classification was made in 2008, when the DM 14/01/2008 [38] was released. The new map was based on a site-specific probabilistic seismic hazard assessment, significantly increasing the number of municipalities belonging to seismic areas (Figure 7). Almost the entire Emilia region is presently classified as a low to medium-hazard zone. With reference to a 475 years return period, the current hazard map predicts  $PGA_h$  values ranging from 0.14g to 0.17g on rock soils, and 0.22g - 0.26g on soft soils, such as those in the area hits by 2012 earthquakes.

In Figure 8 the geological classification of the soil according to EC8. It is worth noting that the area of interest is mostly characterized by soft soil classes D .

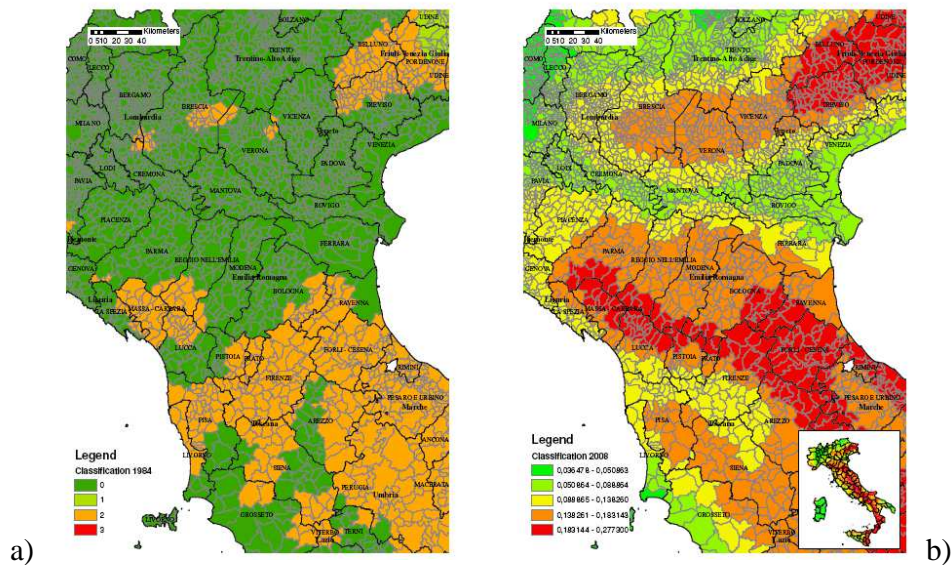


Figure 7. Seismic classification before 1998, according to De Marco and Marsan (1986), (a); and actual classification according to the official hazard data (Stucchi et al, 2011) employed in DM 14/01/2008, (b).

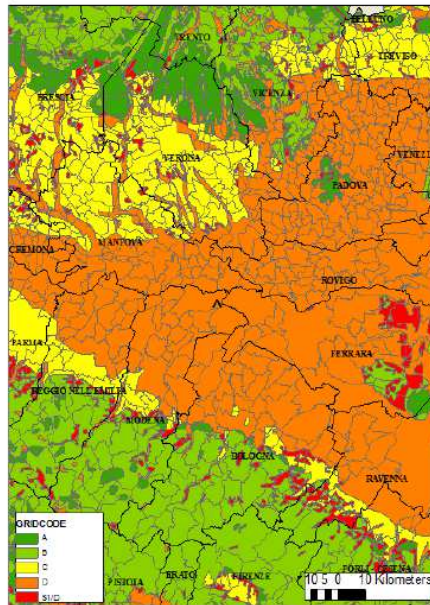


Figure 8. Soil classification on geological basis of the area struck by the earthquake.

It should be finally noted that the 2008 code became the official Italian code and the only one to be employed only in July 2009, after the 2009 Aquila earthquake.

According to the previous observations, and considering that most of the building stock was realized between sixties and eighties it is easy to recognize that most of the area struck by the 2012 Emilia earthquake was designed for gravity loads. Another support reason for the choice of gravity load designed structures as representative of the whole RC building stock of the area is that in the case of mid rise RC buildings and medium-low seismicity design the gravity loads still rule the design, as long as capacity design is not employed (e.g., [39]).

### 1.5 Evolution of building codes for RC precast structures

Being Emilia (including the area hit by the earthquake) mostly classified as non-seismic region until 2006, precast concrete structures were often inadequate to support the horizontal seismic actions.

The first complete law regulating design rules for reinforced concrete structures in non-seismic regions dates back to 1971 (N. 1086, November 5<sup>th</sup>, 1971), followed in 1974 by the first law (N. 64, February 2<sup>nd</sup>, 1974) regulating the design of structures in seismic regions. These laws did not indicate specific provisions for precast structures.

The 1976 Friuli earthquake produced extensive damage and failures of industrial buildings, which exhibited all the critical issues typical of structures built without proper seismic design

criteria. After this earthquake, a sequence of decrees and guidelines were published. Among them, the most important documents as far as the design of precast RC structures is concerned were the CNR 10025/84 [40] guidelines and the DM 3 December 1987 [34] decree. CNR 10025/84 guidelines defined the basis of design for precast concrete structures as well as requirements on materials, manufacturing processes and end products (manufacturing tolerances and dimensions, surface quality, etc.). For some elements, typical of precast structures (pocket foundations, corbels, etc.), detailed design procedures were defined. For all other structural elements, such as for beams and columns, only general rules were given referring to further national codes for details on design, minimum dimensions or reinforcement ratios.

The CNR 10025/84 guidelines defined specific rules for design of connections between monolithic elements (rubber bearings, steel connections and dowels, etc). The use of dowels to connect precast beams with columns was clearly recommended in seismic areas. Their ultimate shear strength was defined as:

$$V_{Rd} = c\phi^2 \sqrt{f_{yd}f_{cd}} \quad (1)$$

where  $\phi$  is the dowel diameter,  $f_{yd}$ ,  $f_{cd}$  the design strengths of steel and concrete,  $c$  a coefficient depending on concrete confinement ( $c = 1.2$  for unconfined concrete or  $c = 1.6$  for well confined concrete). It is worth nothing that Eqn. (1) is formally analogous to modern design criteria (see for instance Eurocode 2 [41]) and also conservative if compared with the most recent experimental evidences [42], [43].

Three years later, the 3 December 1987 Decree defined the basis of design for precast concrete structures in seismic areas; the use of simply-supported bearings or friction-based support without mechanical connectors was forbidden. Of course, those prescriptions were mandatory only in municipalities belonging to areas classified as seismic, whereas in the municipalities interested by the May 2012 earthquakes beam-column connections based on friction were still allowed.

In the following years, several decrees were issued to update the design criteria for concrete structures and for seismic actions. The 14 February 1992 [44] and the 9 January 1996 [45] decrees defined requirements for the design of RC and prestressed structures, design rules and verification criteria. Minimum dimensions for columns (250 mm x 250 mm) were specified, a minimum reinforcement ratio was set to 0.3% and a maximum longitudinal spacing between stirrups was imposed (250 mm). For seismic areas, 16 January 1 1996 [46] decree defined new design criteria for earthquake resistant structures. The minimum reinforcement ratio was increase to 1%, and prescription of stirrups to be fully anchored at the ends through 135° hooks was added. Minimum dimensions for columns were increased to 300 mm x 300 mm, but no capacity-design rules were given. Of course, these rules were not prescribed in municipalities interested by the May 2012 earthquakes.

## 2. DAMAGE DATABASE FOR INDUSTRIAL BUILDINGS AFTER THE EMILIA EARTHQUAKES

### 2.1 Definition of the building stock interested by the Emilia earthquakes

Emilia–Romagna is one of the richest, most developed regions in Europe, and it has the third highest “gross domestic product” per capita in Italy. This region is characterized by medium-to-small industrial zones, located in various municipalities. The number of industrial buildings located in the whole Emilia-Romagna region is almost 80000, corresponding to approximately 12% of the industrial buildings in Italy [Errore. L'origine riferimento non è stata trovata., Errore. L'origine riferimento non è stata trovata.].

The May 20th mainshock caused the collapse of several precast RC buildings in the industrial areas of S. Agostino, Bondeno, Finale Emilia and S. Felice sul Panaro, whereas the May 29th earthquake was particularly severe for industrial buildings in Mirandola, Cavezzo and Medolla. The first post-earthquake surveys indicated that, in some industrial areas, almost 70% of precast RC buildings, collapsed or were severely damaged [7].

It's worth notice that, since the Emilia earthquakes struck a very industrialized area, the total estimated loss after the event is even bigger than the ones from Aquila or Amatrice where number of death and injured was much higher (Table 1). The total estimated loss for Emilia earthquakes is € 13 bn, equal to the 0.8% of 2012 Italy GDP.

	AQUILA	EMILIA		AMATRICE
Year	2009	2012		2016
Day	6 of April	20 of May	29 of May	24 of August
Hour	3.30 a.m	2.03 a.m	9.00 a.m	3.36 a.m
Magnitude	6.3	5.9	5.8	6.2
Death	309	7	20	292
Injured	1,600	50	350	400
homeless	65,000	15,000		2,925
<b>Total estimated loss</b>	<b>€10bn</b>	<b>€13bn</b>		<b>€5bn</b>

Table 1. total estimated loss for the 3 main seismic recent events in Italy.

In the present work, the total number of industrial buildings located within the area of interest was estimated using cadastral data. In Italy, the cadastre has the role of public registry of real estates and land properties and is established mainly for fiscal purposes.

The elementary urban real estate unit is defined as the smallest real estate asset with functional autonomy and ability to produce income. The Italian cadastre is divided into categories related to the activities undergoing in real estate units. In the present study, the building stock was defined

with reference to two specific cadastral categories, labelled D/1 and D/7, and corresponding to “factories” and “buildings hosting a specific industrial activity”, respectively. Since in some cases one building can be constituted by more than one real estate unit, the actual number of industrial buildings forming the reference population does not correspond to the number of cadastral units included into categories D/1 and D/7. A detailed analysis was then performed and the number of actual (independent) buildings, evaluated using aerial photography and some field-surveys, was compared with the number of cadastral units for 18 representative municipalities selected among the total of 35 in the area of interest. This analysis showed that the ratio of actual buildings over cadastral units is, on average, about 0.52. The total size of the building stock (number of independent industrial buildings) for the 17 municipalities not analysed in detail was then estimated by multiplying the total number of real estate units obtained from the cadastral register [**Errore. L'origine riferimento non è stata trovata.**] by 0.52. It is worth noticing that the procedure adopted possibly overestimated the actual number of prefabricated industrial RC buildings because the cadastre might classify in categories D/1 and D/7 also cast-in-place concrete and masonry structures which might not have been identified from aerial photography and field surveys.

The distribution of the building stock within the region of interest, estimated as described above, is reported in the map of Figure 9, where green circles are located on the administrative centres of the municipal territories. The maximum concentration of industrial buildings is observed in the Carpi district.

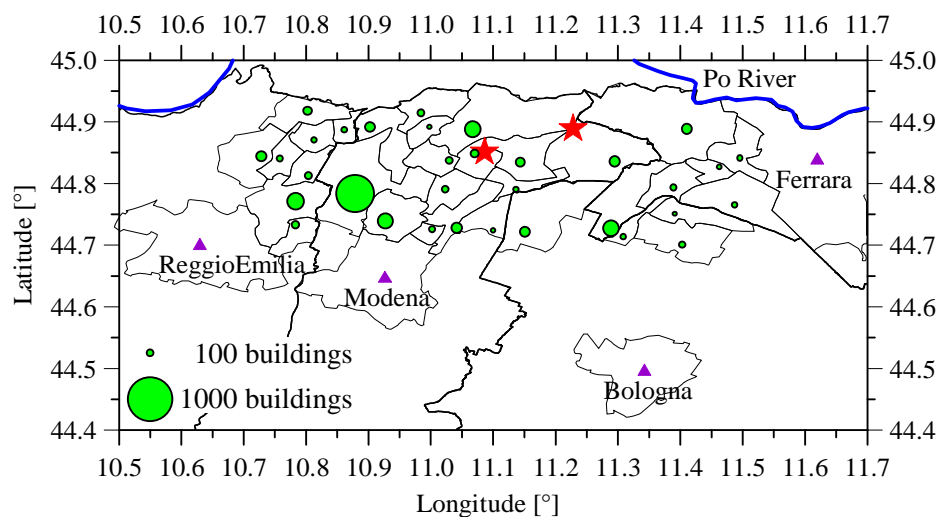


Figure 9. Map of the territory hit by 2012 Emilia earthquake reporting the distribution of the industrial building stock (green circle data points) and the epicentres of the two mainshocks (red stars).

## 2.2 Damage data collection and inventory

After an earthquake, the collection of damage data and their inventory represent an essential tool for predicting the response of the buildings to future earthquakes.

The post-earthquake survey procedures usually adopted worldwide are rapid assessment protocols for assisting the surveyors in making a decision about the usability of the buildings based on the observed damages. In Italy, the official protocol was developed from the experience acquired since the 1997 Umbria-Marche earthquake, and combines observational damage data with information on possible sources of seismic risk. This procedure is based on AeDES inspection form (Baggio et al. 2007) and is restricted to ordinary buildings.

As far as the precast industrial buildings struck by the 2012 Emilia earthquakes, designed in most cases without any seismic design criteria, are concerned, this standard survey-forms was not applicable at all. In fact, the absence of mechanical connections between the precast elements caused many very brittle failures, often without any preceding damage indicating the possible vulnerability of the structure. This aspect became particularly evident after May 29<sup>th</sup> mainshock, that caused heavy damages and collapses even to buildings which did not suffer any damage during May 20<sup>th</sup> mainshock, even if the first earthquake was characterized by comparable and even larger values of some macroseismic parameters (see Section 1.2).

As an example, two pictures of a single-storey two-bay industrial building with variable height roof beams simply-supported in correspondence of the columns and perimeter masonry curtain walls, taken after the first and the second mainshock, are reported in Figure 10. Industrial building in San Giacomo Roncole (Mirandola, MO): (a) the building after May 20<sup>th</sup> earthquake, and (b) after May 29<sup>th</sup> earthquake (a) and (b), respectively. The maximum accelerations in that area were comparable, but the effects of the second mainshock on many buildings were significantly heavier [47]. In that building, May 20<sup>th</sup> earthquake caused only the detachment of a masonry curtain wall on the front without any displacement between beams and columns at the roof level. On the contrary, May 29<sup>th</sup> earthquake caused the falling of the two front beams with a mechanism.

One of the most critical issues in a post-earthquake emergency is assessing the usability of buildings since it definitely plays a major role in the recovery of the essential social and economic activities of the affected communities. Yet, the usability of a structure represents a delicate calculation, involving the safety of individuals because of the possibility of significant aftershocks [48]. The example just illustrated, shows that some buildings have to be judged not usable despite having no or very little damage.

Assessing usability determines if there is a significant risk to human life in using the affected and possibly damaged buildings, thus minimizing the risk which people could be subjected to when returning to their houses/work activities once the initial panic has ended. Considering this objective, being conservative in such an evaluation appears mandatory. On the other hand, timely usability inspections are essential in order to minimize the number of homeless hosted in provisional or temporary structures and in order to reduce the economic loss related to the

downtime of the work activities. Too conservative evaluations can be detrimental, causing unnecessary discomfort, and therefore they should be avoided.



Figure 10. Industrial building in San Giacomo Roncole (Mirandola, MO): (a) the building after May 20<sup>th</sup> earthquake, and (b) after May 29<sup>th</sup> earthquake

In DPC (2000) and [48] usability is defined as follows: “The evaluation of usability in the post-earthquake emergency is a temporary and rough evaluation - i.e., based on an expert judgment and carried out in a short time, on the basis of a simple visual inspection and of data which can be easily collected - aiming at determining whether, in case of a seismic event, buildings affected by the earthquake can still be used with a reasonable level of life safety”.

Usability surveys are first and foremost focused on the short-term use of the buildings under examination [49]. However, together with the usability survey, a global damage assessment can be done to provide data and directions useful in establishing long-term strategies on the affected building stock.

The field, surveys conducted after the Emilia earthquakes, highlighted the following main sources of seismic vulnerability for the precast industrial buildings, additional with respect to the cast-in-situ RC structures:

- ✓ the lack of connecting devices between precast monolithic elements, and in particular between roof slab elements and main girders and between main girders and columns;
- ✓ the inadequacy of steel connections of precast RC cladding panels to the structural elements (i.e., columns and beams);
- ✓ the presence of very heavy shelves without any bracing systems suitable for resisting horizontal forces.

The aforementioned shortcomings being the cause of a huge number of partial or full collapses, their removal, even for undamaged buildings, became mandatory after the second mainshock in 52 municipalities close to the epicentre, in order to allow for restarting the working activities (Legislative Decree No. 74/2012). The resulting area is approximately 100 km long (E-W) and 40 km wide (N-S) and 35 of the 52 municipalities considered are in the Emilia-Romagna region.

In particular, a two-phase intervention strategy was planned. In the first short term phase, interventions aimed at removing the three mentioned vulnerabilities had to be scheduled in order to re-obtaining the temporary usability of the buildings. The second long term phase required seismic risk assessment and, if necessary, the design of structural retrofitting interventions. According to Legislative Decree No. 74/2012 (2012), the retrofitting interventions shall ensure a safety level not lower than 60% of that required for a new construction.

In the present study, given the absence of information from a specific fast survey procedure, dedicated to precast industrial buildings, damage data were collected from reports prepared by structural engineers, obtaining more detailed and accurate damage estimates than from fast surveys.

These reports were prepared by professional engineers, representing building owners and charged of estimating the damages as partial requirement for obtaining regional funds for either reconstruction or retrofit, in accordance with Regional Decree 57/2012 [81]. These reports were also validated by a public in-house company charged of assessing the coherence of the public economical contribution for the interventions.

In the present study, damage data were classified according to the six level damage scale reported in Table 2, from the absence of both structural and non-structural damages (level D0) up to building collapse (level D5). These levels substantially coincide with those introduced by EMS-98 (1998)\*\*, reported in Table 3 for comparison. Furthermore, levels D1 (slight damage), D2 (moderate damage), D3 (severe damage), D4 (heavy damage) and D5 (collapse) considered in the present analysis correspond to damage classes “c”, “b”, “d”, “e” and “a”, respectively, established by Decree No. 57/2012 (2012) of Emilia-Romagna region. In particular, the latter diversifies the damage classes according to the percentage of damaged elements (i.e., slabs, roof, including the supporting beams, and cladding panels) and damaged columns (Table 2). Earthquake-induced foundation settlements are also considered by the recent updates of Regional Decree No. 57/2012, but they do not appear explicitly in Table 2. As a matter of fact, rotations of the pocket foundation at the column base, observed in some cases, may be taken into account in the form of a permanent column drift.

Regional Decree No. 57/2012 granted specific non-repayable funds to the manufacturing companies for the interventions on damaged buildings. In particular, the funds dedicated to buildings belonging to damage levels D1 and D2 covered the costs for local repair interventions and structural strengthening, and could be increased to cover the seismic retrofitting. Funds for severely and heavily damaged buildings (levels D3 and D4) covered all the refurbishment costs, including seismic retrofitting. Funds for partially or fully collapsed buildings (level D5) covered reconstruction costs. Finally, for undamaged buildings (level D0), financial support to realize short term interventions (e.g., connecting devices at the roof or slab level to avoid sliding of monolithic elements), but also for seismic retrofitting, was periodically made available (Emilia-Romagna Regional Decree No. 91/2013).

Nonetheless some building owners decided to not apply for funding as per Regional Decree 57/2012 for three main reasons:

- i) buildings were not occupied;
- ii) they preferred to apply for national funds for building refurbishment, which were convenient in some cases;
- iii) they had private insurances covering seismic damage.

Table 2 Damage levels adopted in the present investigation and correspondences with definitions reported by Emilia-Romagna Regional Decree No. 57/2012

Damage level	D0	D1	D2	D3	D4	D5
	No damage	Slight damage	Moderate damage	Severe damage	Heavy damage	Collapse
Damage class according to Regional Decree 57/2012		c	b	d	e	a
Local or distributed structural damages to horizontal and/or vertical partitions without collapses <sup>1</sup>	-	< 20%	≥ 20%	-	-	-
Severe structural damages to horizontal and/or vertical external surfaces with collapses <sup>2</sup>	-	-	-	≤ 15%	≤ 30%	> 30%
Residual column drift $\theta > 2\%$ <sup>3</sup>	-	-	-	at least 1 column	≤ 20%	> 20%
Plastic hinges at the column base sections <sup>3</sup>	-	-	-	-	≤ 20%	> 20%

<sup>1</sup> Percentages referred to all horizontal and vertical partitions in the building

<sup>2</sup> Percentages referred to all horizontal and vertical outer surfaces in the building, such as roof and curtain walls

<sup>3</sup> Percentages referred to the whole number of columns in the building

Table 3 Correspondence of the damage levels used in the present analysis with those introduced by EMS-98 (1998)

Damage scale		Damage level					
Present		D0	D1	D2	D3	D4	D5
EMS-98			1	2	3	4	5
	Non-structural damage	-	Slight	Moderate	Heavy	Very heavy	Total or partial collapse
	Structural damage	-	-	Slight	Moderate	Heavy	collapse

The purpose of the classification reported by Regional Decree No. 57/2012 was to provide for objective elements for the evaluation of damages, being the damage level strictly connected with the funding plateau. However, establishing the damage level of buildings according to Table 2 may result in unconservative damage evaluations. For instance, damage levels D3, D4 and D5 depend on the number of columns whose permanent drift is greater than 2%, but it can be verified that, for precast buildings, this value is too large to be related to a damage condition measured at the end of the seismic event. In fact, for RC columns, a drift of 2% is a typical value usually provided (see Table C1-3 of FEMA 356 2000) to illustrate the overall structural response associated with a Life

Safety Structural Performance Level, and is therefore related to the maximum drift attained during the seismic event. Thus, a value of the residual drift lower than 2% should be used for identifying the damage level at the end of the seismic event. For example, taking second order effects into account according with the nominal curvature method (CEN 2004), it is possible to show that precast RC columns of industrial buildings typical for the struck area, and not designed for the earthquake resistance, can collapse under permanent loads in the presence of a residual drift of approximately 1%. Such a drift value should then be considered as a very heavy damage. Hence, as far as damages related to residual column drifts larger than 2% are concerned, damage levels D3, D4 and D5 defined in Table 2 can be considered as substantially equivalent.

### **2.3 The electronic database**

The first phase of the research consisted in the creation of a electronic database to catalog observational damage data, related to a wide range of precast reinforced concrete buildings struck by the 2012 Emilia earthquake. Field surveys, post-disaster satellite imagery and technical reports prepared by structural engineers for obtaining public funds for reconstruction (§ 2.4) were used.

Since post-earthquake field survey procedure based on AeDES inspection form is restricted to ordinary buildings, to catalog damage information, during the inspections done in the Emilia industrial clusters, a survey form specifically developed by the author was used.

Once the inspections were performed and the reports prepared by structural engineers for obtaining public funds for reconstruction were collected, all the information were digitized, with the further help of satellite imagery to develop a precise georeferentiation of the building stock.

This operation allowed the building of a broad database that provides a clear picture of the surveyed building stock, from the structural typology, damage, and usability judgement points of view. Analysing this database can provide valuable hints for damage estimation that can occur in Italy due to future earthquakes.

Microsoft Access 2016 is the software used to create the damage database, which is composed in the following sections arranged on 5 forms:

Form1) Building identification (Figure 11):

- business name;
- professionals responsible for retrofit interventions;
- address;
- geographic coordinates;
- google earth fast connection to see the building with satellite imagery;
- pictures of the building and usefull attachments.

Figure 11. Form1\_Building identification

Form2) Damage quantification according to the Emilia-Romagna Regional Decree No. 57/2012 (Figure 12):

- damage class established by Decree No. 57/2012 (2012), tab.A;
- cadastral category, ATECO classification of the industrial activity, number of employees before the seismic event;
- non-repayable funds made available, according to the damage class and building characteristics;
- costs of outline specifications;
- total amount granted as specific non-repayable funds (the minor value between the two previous amounts);
- presence/absence of insurance and eventual insurance value;
- presence/absence of activity temporary or permanent delocalization.

Figure 12. Form 2\_Building identification

Form 3) Building structural description (Figure 13): .

- building main dimensions;
- number and height of the floors;
- age of construction;
- designated use;
- type of vertical structures;
- type of roof;
- presence/absence of beam in both directions;
- permanent loads;
- type of curtain walls;
- type of foundations;
- presence/absence of elements that might influence the seismic behaviour of the building: strip windows, skylights, crane support, internal stairwall, etc..
- number and length of the bays in X and Y direction;
- type and distribution of the partitions
- typology of soil;
- orientation of the X axes (main beam direction) according to Nord;
- most significant seismic event (information not often collected);

- detail level of the informations collected.

The industrial clusters, in the Emilia region, are sometimes characterized by building with irregular plan shape, example L shape or, very often, by buildings grew in phases during the years, as the sum of different buildings strictly connected without any seismic joint (Figure 14). Often this build up area is made of buildings with different structural typologies. In these complex situations, the database allows the subdivision of the built-up area in different “zone” to take into account all the building details. In these cases, it would have been wrong to consider the build-up area simply as the sum of different buildings, since, in that way, it would not have been taken into account the structural interaction between them; interaction that can completely change the seismic answer.

Figure 13. Form 3\_Building structural description.



Figure 14. Example of two built-up area located in San Felice sul Panaro (Mo)

Form 4) Columns characteristics (Figure 15):

- Columns size (b\*h);
- Influence domain for each column;
- Percentage of reinforcement;
- vertical load for each type of column (automatically estimated using data from the Form 3).

Pilastrini

**Columns:**

Building name: ABF Imm. 1/1

Zone name: ABF Imm. 1\_blocco 1/1

EXTERNAL COLUMNS- X dir		EXTERNAL COLUMNS- Y dir		INTERNAL COLUMNS		CORNER COLUMNS	
Number	4	Number	26	Number	26	Number	4
b [cm]	50						
h [cm]	40						
Influence domain [m <sup>2</sup> ]	100	Influence domain [m <sup>2</sup> ]	100	Influence domain [m <sup>2</sup> ]	200	Influence domain [m <sup>2</sup> ]	50
% of reinforcement		% of reinforcement		% of reinforcement		% of reinforcement	
N [kN]	315,00	N [kN]	315,00	N [kN]	630,00	N [kN]	157,50

Record: 1 di 1 | Filtrato | Cerca

Figure 15. Form 4\_Columns characteristics

Form 5) Damages and interventions to structural and non structural elements (Figure 16):

- List of damages experienced by structural and not structural components: columns, roof, external precast cladding panel or masonry cladding panel, partitions, foundations, etc.
- List of interventions performed on structural and not structural components. The eventual option of demolition and reconstruction is also considered.

The screenshot shows a software interface for recording damage and interventions. The main title is "Damage and interventions". On the left, there are input fields for "Building name" (ABF Imm. 1/1), "Zone name" (ABF Imm. 1\_blocco 1/1), and "Behaviour factor q". On the right, there is a "List of damages" section with a table. The table has two columns: "Elements" and "Interventions". The "Elements" column lists: Columns, Roof, External precast cladding pannel, Masonry cladding panels and partitions, Overturning of racks, and Suspended ceilings falling or breacking. The "Interventions" column lists: Cerniera plastica alla base; Rottura seggi, Trave\_perdita d'appoggio; Impalcato\_per, Spostamenti reciproci; Rottura connessio, Window break, and Foundations failure. Below this is an "Interventions" section with a dropdown menu set to "ABF Imm. 1\_blocco 1/1". This section is divided into two columns: "Elements" and "Interventions". The "Elements" column lists: Columns, Roof, and Masonry infills and precast panles. The "Interventions" column lists: Foundations, Connections, and New structures. At the bottom, there is a "% of retrofit" field and a "Demolition and reconstruction" checkbox which is checked.

Figure 16. Form 5\_Damages and interventions to structural and non structural elements.

## 2.4 Database consistency and spatial distribution.

The total number of precast buildings included into the damage database gathered for the present study is 1890. All industrial buildings considered in the database are located in municipalities of Emilia-Romagna region lying in the area where assessment of seismic vulnerability was mandatory, with a distance from the closest epicenter lower than 37 km.

The number of buildings belonging to each damage level is reported in Table 4. Figure 17 represent the percentage of each damage level for the whole database considering a) 5 or b) 3 damage levels were  $D_0$ ,  $D_1+D_2$ ,  $D_3+D_4$ ,  $D_5$ .

The normalized cumulative number of buildings investigated, defined as the cumulative number of buildings divided by the total number of buildings (i.e. 1890), is plotted, in

Figure 18 (curve labelled  $D \geq D_0$ ), against the epicentral distance, defined as the distance of each building from the nearest epicentre, between those of the two mainshocks. For more than 70% of the buildings, this distance is associated to the second mainshock (29 May).

Damage level	$D_0$	$D_1$	$D_2$	$D_3$	$D_4$	$D_5$	$D_1+\dots+D_5$
No. of buildings in the database	967	371	174	105	76	197	1890

Table 4. Number of buildings analyzed for each damage level.

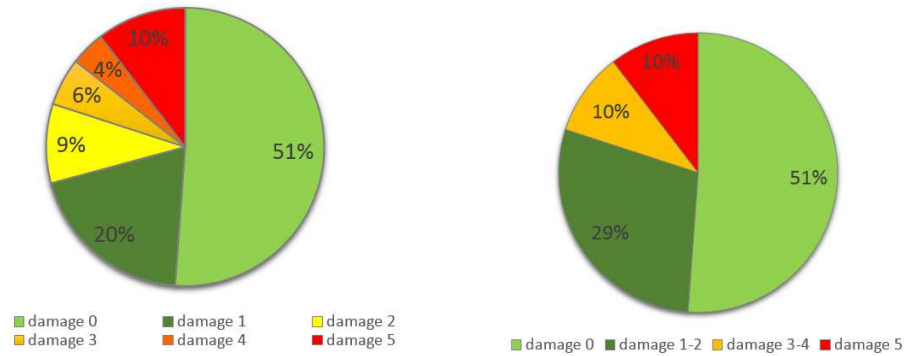


Figure 17. Percentage of each damage level for the whole database, a) Five damage levels, b) Three damage levels.

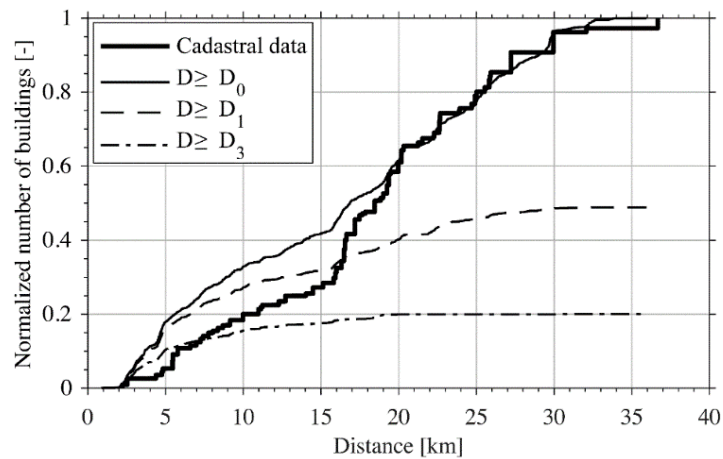


Figure 18. Normalized cumulative number of industrial buildings versus distance from the nearest epicentre.

In order to check the level of completeness of the data collected, the normalized cumulated number of buildings, estimated from cadastral data as described in 2.1, is also reported in the same figure (curve labelled “cadastral data”). This curve is normalized to the total number of buildings estimated from cadastral data. The positions of these buildings were defined based on the main industrial areas identified by aerial photography, in particular all the buildings in each industrial area were assumed at its centre. The shapes of the curves corresponding to the database and to the cadastral estimate are in good agreement. The sudden increase in the building density between distances of 16 km to 20 km corresponds to a series of large industrial zones in Carpi, in the Modena district. That area is peculiar in the region. In fact, it contains mainly large textile manufactories, a production sector which, in the Emilia region, was severely affected by an economic crisis started in 2009. For this reason, many buildings in the Carpi area were not-in use at the time of the earthquakes and their owners did not submit reports to the authority to obtain funds; therefore their damage was not classified.

About 96% of buildings considered in the database are located at no more than 30 km from the nearest epicentre and, in such range of epicentral distances, they represent approximately 30% of the whole number of precast industrial buildings struck by the seismic sequence estimated from cadastral units. For epicentral distances larger than 30 km, the data reported in the database are not significant because only few buildings were subjected to survey so far from the epicentres.

It is worth noticing that the building distribution in the area is not uniform, otherwise the curve representing the cumulated distribution of buildings would be quadratic in terms of epicentral distance. Finally,

Figure 18 also shows the normalized cumulative number of buildings against the distance to the nearest epicentre for  $D \geq D_1$  (i.e., the total number of damaged buildings in the database), and  $D \geq D_3$  (the number of buildings with severe damages up to partial or total collapse). Note that most of the buildings with  $D \geq D_3$  are located within 15-20 km from the nearest epicentre. For epicentral distances shorter than 10 km, a clear predominance of damaged buildings is observed.

Figure 19 shows a GIS representation (ArcMap 10.5.1), of the spatial distribution of the buildings collected in the damage database, each of them distinguished with a different color according to the damage level. The two black stars indicate the position the epicenters of the two main shocks. Figure 20, Figure 21 and Figure 22 represent an overview of main industrial clusters struck by the seismic events, as Mirandola, San Giacomo Roncole, San Felice sul Panaro, Medolla, Cavezzo, Concordia sulla Secchia and Finale Emilia.

Figure 23 shows through pie plots, the percentage of each damage level for the main damaged industrial clusters. Finally, to better understand the consistency of the damage database, Table 5 shows the number of surveyed industrial buildings for the thirty cities with the highest number of buildings analyzed in this study.

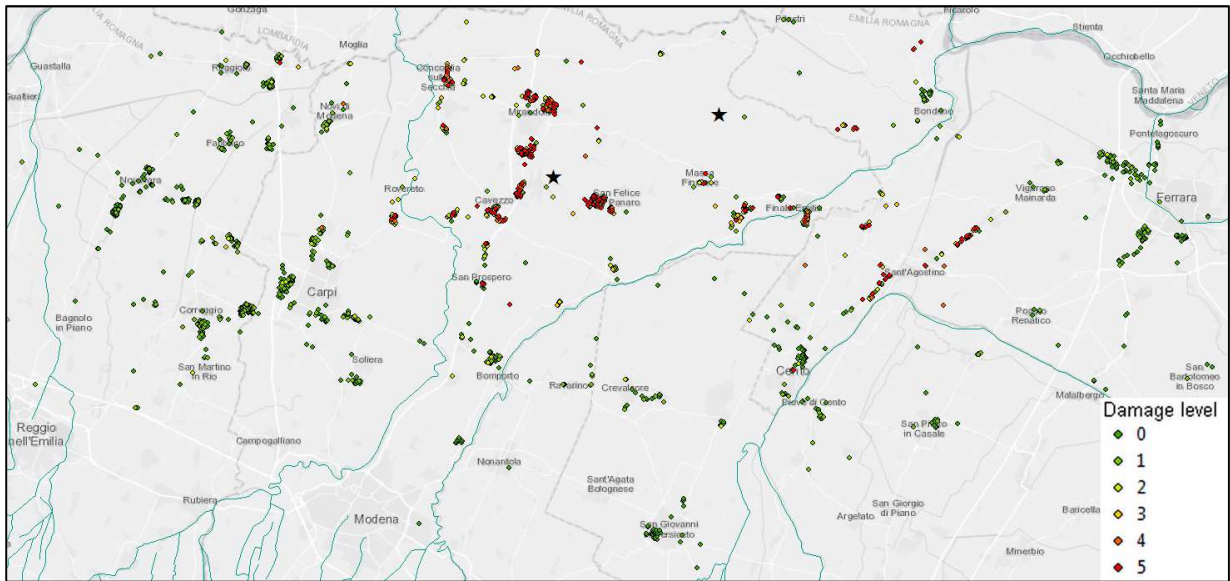


Figure 19. GIS representation of the spatial distribution of the buildings collected in the damage database.

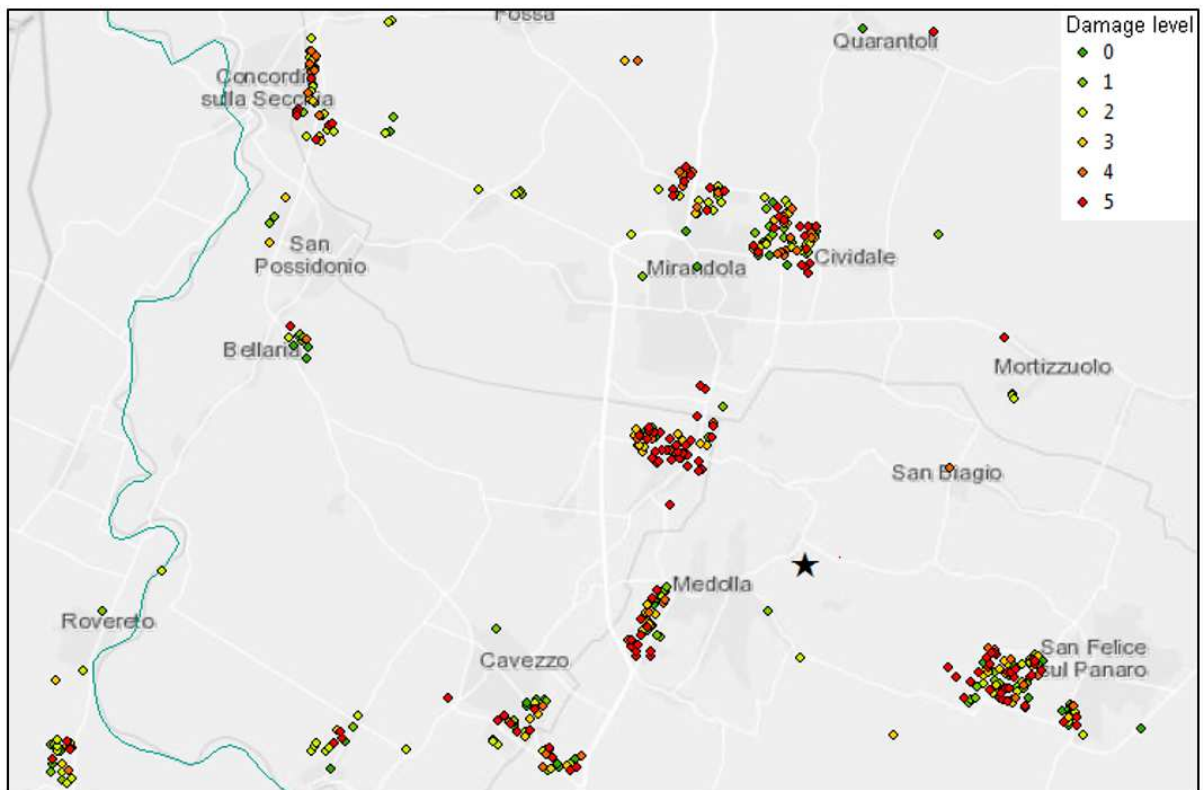


Figure 20. GIS overview representation of the buildings analyzed in the database located in the most damaged industrial clusters.

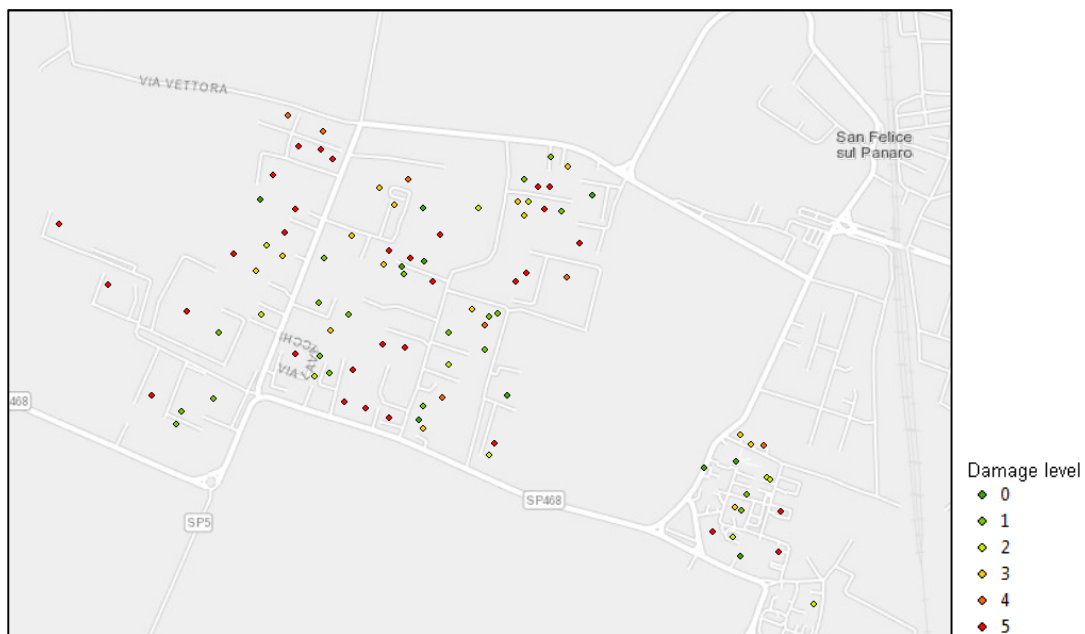


Figure 21. GIS overview representation of the buildings analyzed in the database located in San Felice industrial area.

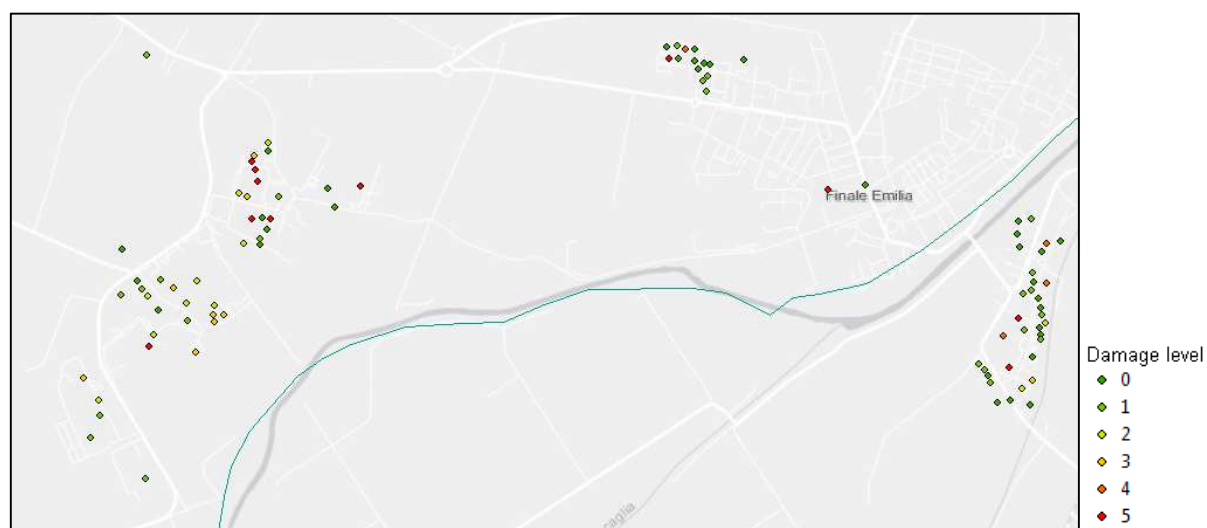


Figure 22. GIS overview representation of the buildings analyzed in the database located in Finale Emilia industrial area.

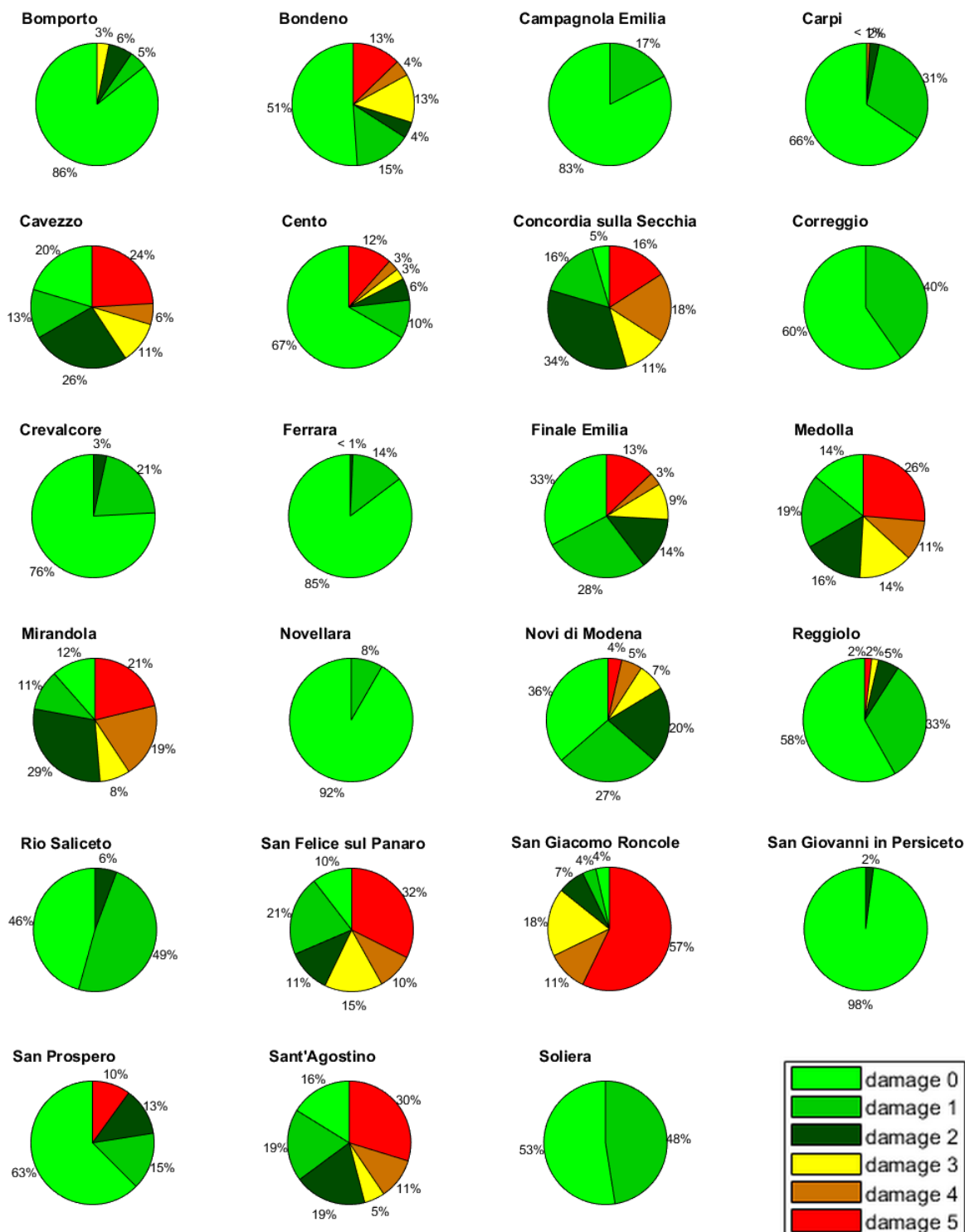


Figure 23. Percentage of each damage level for the main damaged industrial clusters. .

Ni	City	Survey buildings
1	Pieve di Cento	16
2	San Pietro in Casale	19
3	San Possidonio	22
4	Fabbrico	24
6	Mirabello	24
8	Crevalcore	29
9	Rio Saliceto	35
10	Sant'Agostino	37
11	San Prospero	40
12	Soliera	40
13	Concordia sulla Secchia	44
14	Campagnola Emilia	46
15	Bondeno	47
16	San Giovanni in Persiceto	49
17	Cavezzo	54
18	Novi di Modena	55
19	Reggiolo	55
20	San Giacomo Roncole	58
21	Medolla	57
22	Bomporto	63
23	Cento	69
24	Novellara	72
25	San Felice sul Panaro	105
26	Mirandola	117
27	Finale Emilia	116
28	Carpi	122
29	Correggio	134
30	Ferrara	143
<b>TOT</b>		<b>1692</b>

Table 5. Number of surveyed buildings for the thirty cities with the highest number of industrial buildings collected inside the damage database

### **3. TYPOLOGIES OF PRECAST BUILDINGS IN THE EMILIA REGION:**

#### **3.1 Introduction**

The typical layout of a single-storey industrial building is composed of a series of basic portal frames, realized as the assembly of monolithic precast elements. Each frame has precast cantilever columns clamped in a pocket foundation, and precast concrete roof girders supported over the columns. Precast slab elements are also simply-supported over the roof beams. In the case of structures not designed with seismic provisions, the beam-column and slab-beam connections were typically friction-based supports, without any connection device and often neoprene pads in order to allow beam end rotations under gravitational loadings. The stability of the structures and their capacity with respect to horizontal actions depend on the cantilever behaviour of the columns [24].

For the industrial buildings struck by the 2012 Emilia earthquakes, [7] identified two main categories of precast RC structures:

- i) buildings constructed from 1970 to 1990 (Type 1), with beam span length from 12 to 20 m, roof slab span length from 6 to 10 m, and masonry infills;
- ii) more recent buildings (Type 2), approximately built after 1990, featuring significantly longer spans of beams and roofing elements, and either horizontal or vertical prefabricated RC cladding panels. These two building types approximately correspond to those identified by Casotto et al. [50].

The construction date may represent an important factor for the analysis the seismic behaviour of the precast buildings struck by the Emilia earthquakes, because of the changes in construction practice and technology occurred over time. However, most of the territory struck by the earthquakes was not considered a seismic area by design codes until October 2005. As a consequence, most of the partial and full collapses were caused by the usage, both in Type 1 and Type 2 buildings, of friction-based slab-beam and beam-column connections.

In the present work, seven types of precast buildings are identified, as described in the following chapter. In section 6.5 fragility curves for each of those types of precast buildings are illustrated. In the Emilia region, most of precast RC buildings have a single-storey structure, typically composed of a series of basic portal frames. Some buildings may have two floors, and others an intermediate floor in a portion of the building, typically along one of the two short edges, where offices are located. The personal classification of building type not considers structures with 2 or more floors since, according to [18], approximately 70% of the industrial buildings in the Emilia-Romagna region are single-storey precast RC structures.

### 3.2 Types of precast buildings:

One of the main objective of this research was to develop empirical fragility curves for industrial precast structures since, nowadays, fragility curves are the most widely used prediction tool for seismic risk assessment. As described in chapter 8, initially these curves were developed considering the whole database of damage data. The next step consisted in developing fragility curves taking into account the difference in building typology. The data were grouped by structural type; seven main typologies of precast RC buildings were considered.

Type 1 - Buildings with double slope precast beams simply-supported at the top of the columns with masonry infills, along both short and long walls (Figure 24). A typical technology adopted in the 70's and in the 80's, and also recently for small and cheap constructions, for instance for agricultural warehouses.

The roof can be made of precast elements with hollow-clay-blocks or, in recent construction, TT or hollow-core concrete elements. Columns are usually quite slender, with square cross-sections with 30-40 cm side. No beam-column connection devices are present. The beam height can be up to 2 m in the centre, and typically have either no or little restraints against out-of-plane movements, with the exception of the presence of an upper pocket support on the top of the columns. These buildings have normally a single storey, eventually with an intermediate floor in a limited portion of the building on one side, where offices are located. Often, the presence of that intermediate floor on one side of the building caused an irregularity in the structural behaviour of the building, with negative effects during ground-motions. It's worth noticing that often there are no beam to link the main frame in transverse direction.



Figure 24. Type 1 Building with double slope precast beams simply-supported at the top of the columns and masonry cladding panels.

Type 0 - Buildings with double slope precast beams simply-supported at the top of the columns with horizontal precast cladding panels placed between the columns (Figure 25). A typical technology adopted in the 70's and in the 80's. From the structural point of view, this typology is very similar to the previous except for the presence of precast cladding panels.

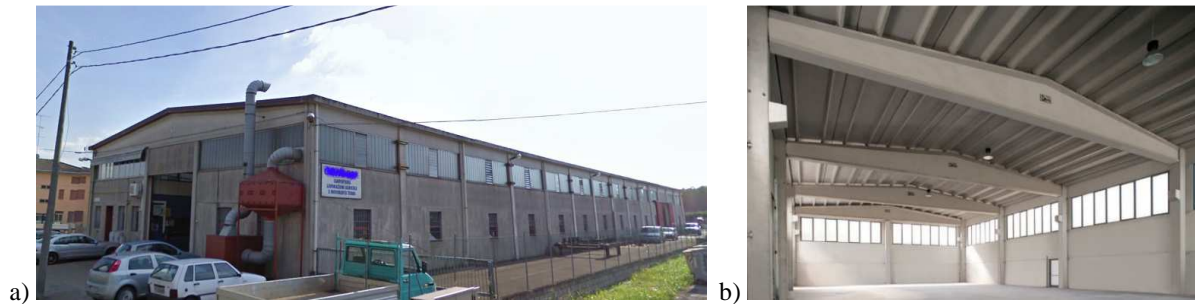


Figure 25. a) Buildings type 0 with double slope precast beams simply-supported at the top of the columns and horizontal precast cladding panels placed between the columns, b) a typical roof of building types 0 characterized by TT elements.

This last type of building has been called 0 since the fragility curves demonstrated (§.6.5) that the seismic behavior of this type of building is very similar to the one showed by The type 1 so much so that they can almost be considered belonging to the same typology.

- Type 2 - Buildings with double slope precast beams simply-supported at the top of the columns with external precast heavy cladding panels fixed externally to the columns. The external cladding panels can be horizontal or vertical (Figure 26). A typical technology adopted after '80. As the previous typologies, "Type 2" can be characterized by different kinds of precast roof or slab elements, according to the span length, as well as the insulation properties and lightning required inside the building.

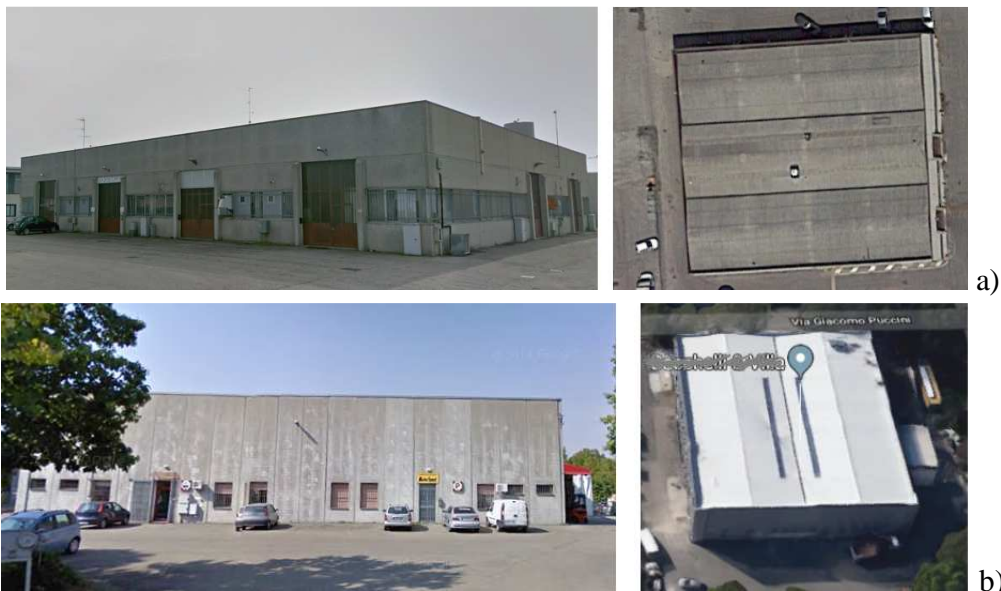


Figure 26. Type 2: buildings with double slope precast beams simply-supported at the top of the columns with external precast heavy cladding panels fixed externally to the columns a) horizontal panels or b) vertical panels.

- Type 3 - Buildings with planar roof, composed of long-span prestressed roof or floor elements simply-supported on (prestressed or not) precast girder beams. This technology was widely used after the 80's, typically for large industrial facilities, in media almost 2 times the plan dimensions of type 0,1 and 2. It allows also the realization of construction with two or more floors and typically it is designed to obtain large empty spaces for working activities with few columns inside. Planar precast RC girders (e.g., I- or omega-shaped beams) are supported on columns. In order to reach significant spans in the slab direction, different kinds of prestressed elements are adopted for roofs or slabs, such as TT or Y-shaped (Figure 27). More recently, the use of precast vaulted thin-web elements (called “wing contours”) allowed to cover roof spans over 30 m long [24]. In this case, curved panels made of glass or transparent polycarbonate are allocated between the structural thin-web elements with the purpose of lighting the interior of the building. When the latter solution is adopted, quite commonly in the last 20 years for large industrial buildings (spans longer than 20 m in both directions), the roof is of course highly deformable in its plane. RC columns have very large cross-sections (with sides up to 60-80 cm) and must bear both vertical and horizontal loads. In fact, cladding walls are reinforced concrete panels, externally fixed to the columns and the upper beams, and do not have any structural function. The cladding panels can be horizontal, vertical or in some case a mixed solution (Figure 27).



Figure 27. Type 3 - Buildings with long span planar roof: a) example of external and internal view; b) types of cladding panels: horizontal and vertical.

- Type 4 - Buildings with a shed roof. A technology adopted since the 70's to 90's but not very common. The shed roof can be realized through beams "knee" shaped, through oblique beams (Figure 28 a) e b) or, less common, through Vierendel or reticular type beams. This type of building is characterized by a very poor seismic behavior, as it will be confirmed by the fragility curves illustrated in the ch.8.

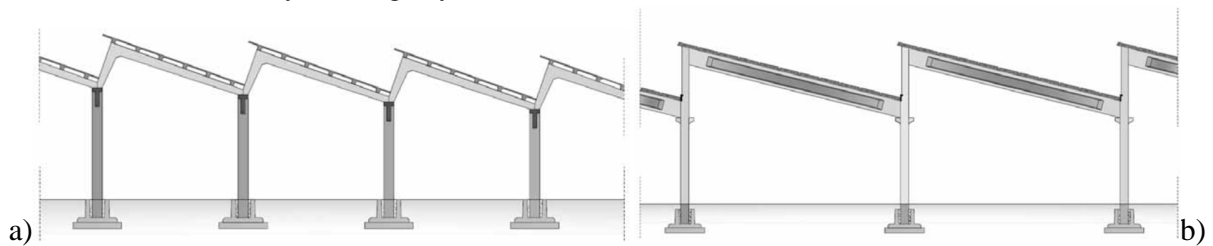


Figure 28. Shed roof: a) beams "knee" b) oblique beams c) picture of a building catalog as type 4.

- Type 5 – In this categories there are all the buildings with a sort of irregularity. The most common situation are the folling:
  - Irregularity in plan:L shape, T shape,ecc... (see Figure 29). ;
  - Irregularity in height;
  - Interaction with adiacient precast buildings builted without seismic joint and caracterized by a different structural typologys;
  - Consistent portion of the building used as offices or residential destination, usually in masonry walls and almost always located in one extremity of the precast structure;
  - Precast structures with a portion cast in place.

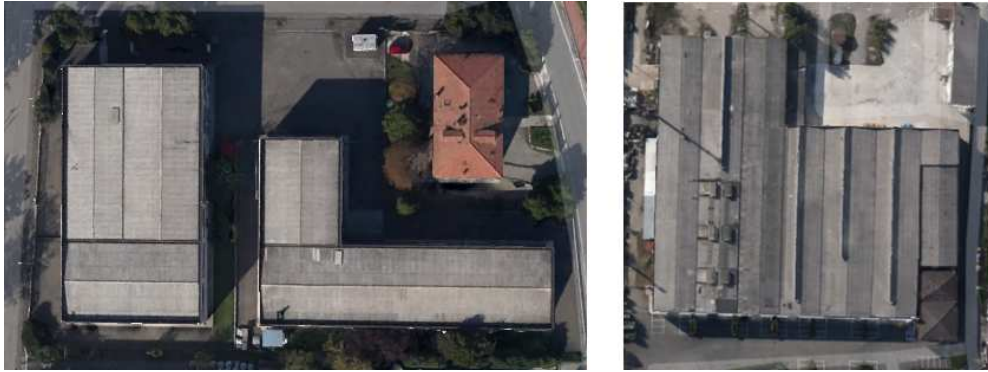


Figure 29. Buildings with plan irregularity.

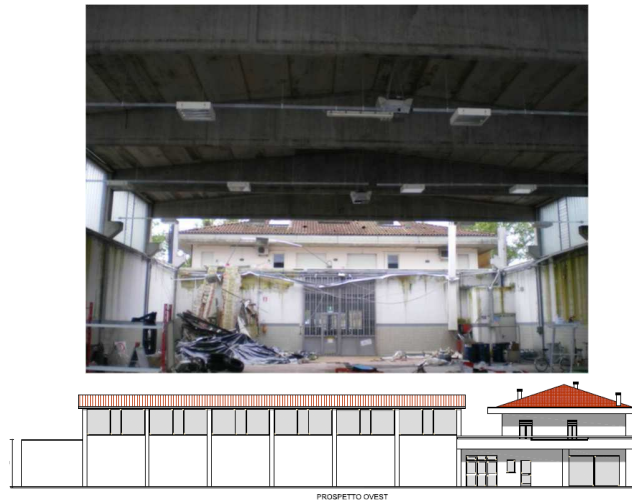


Figure 30. Type 5 due to the presence of a cast in place portion of the building. Due to this irregularity a portion of the building totally collapsed.

- Type 6 – In this category were placed all the precast structures not belonging to one of the previous typologies since characterized by very uncommon characteristics.

### 3.3 Damage data analysis considering different typologies of precast building

Considering that the buildings collected in the database have been grouped by structural type; the total number of building considered for the following static analysis is slightly (see Table 6) since, two floors buildings are not included in any typologies, as well buildings with arch roof or steel roof. It's worth noticing that, compared with Table 4 § 2.4, instead of decreasing, the number of building in the damage levels D1 and D4 increased, since, in this research phase, new damage data became available after field surveys and on-site interviews.

Figure 30 a) shows the percentage of each of the 7 types of precast buildings considering a damage database of 1767 units. Figure 30 b) shows instead the percentage of each of type of buildings considering type 0 and type 1 belonging to the same type. Looking to the pie plots, the type 2 is the most common typology of precast building within the database (percentage of 27 %). followed whit only few percentage points of difference by type 1+type 0 (25%) and then by type 3 (20%). It's worth noticing the high percentage of irregular buildings present in the area (18%). Figure 32 shows on the left the percentage of each damage level for each type of building and on the right, vice versa, the percentage of each type of buildings for each damage level. It's not proper try to understand vulnerability of the different building types looking to these plots since the different typologies are not uniformly distributed in the area and that is clear from Figure 33 who represents the percentage of each building type for the main industrial clusters present in the area struck by the 2012 Emilia earthquakes. All the industrial clusters have at least 50% of the precast buildings cataloged as types 1,2,3 but with different proportions between cluster and cluster. Some industrial cluster show an high predominance of building type 1, as San Felice sul Panaro, Crevalcore e Medolla; others an high predominance of type 2 as Cavezzo and Concordia sulla Secchia; finally some clusters show a predominance of type 3 as Carpi and Ferrara. It's worth noticing the very low percentage of building type 1 in the city of Ferrara.

Damage level	D <sub>0</sub>	D <sub>1</sub>	D <sub>2</sub>	D <sub>3</sub>	D <sub>4</sub>	D <sub>5</sub>	D <sub>1</sub> +...+D <sub>5</sub>
No. of buildings in the database	880	375	159	88	79	186	1767

Table 6. Number of buildings analyzed for each damage level after grouping the structures by type.

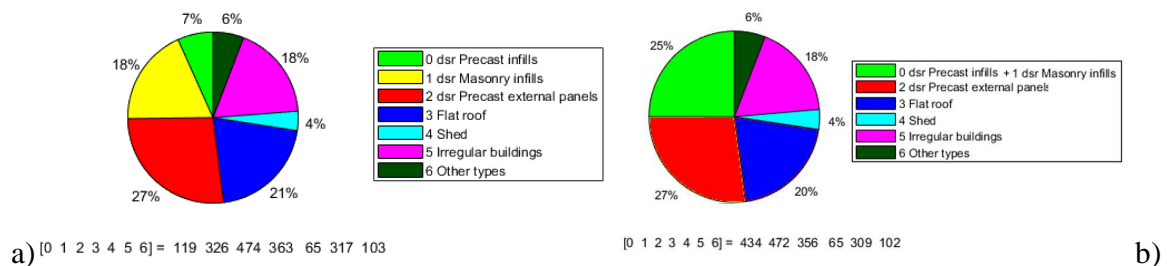


Figure 31. a) Percentage of each of the 7 types of precast buildings considering a damage database of 1767 units; b) Percentage of each of type of buildings considering type 0 and type 1 belonging to the same type.

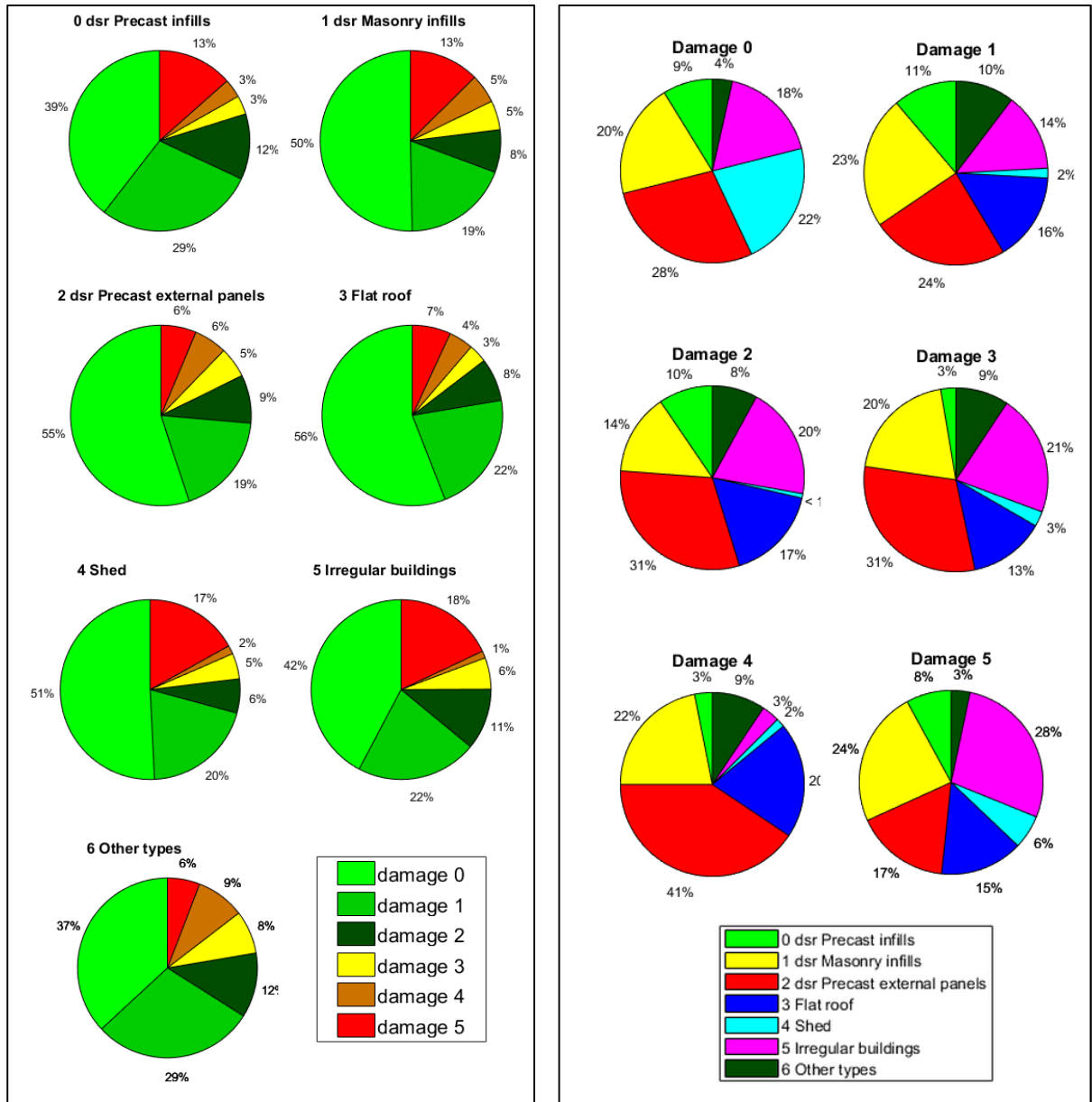


Figure 32. Percentage of each damage level for each of type of precast buildings.

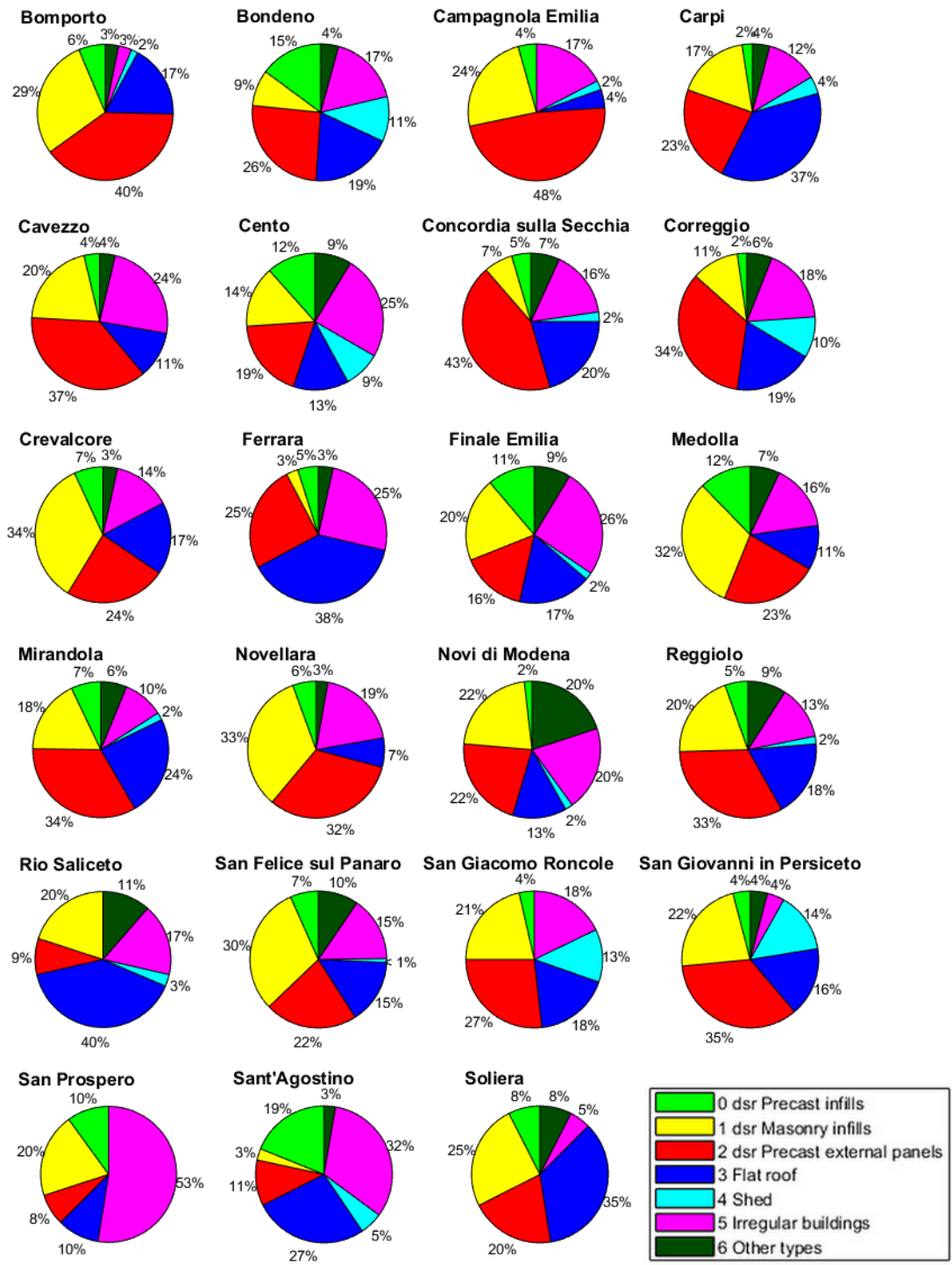


Figure 33. Percentage of each building type for the main industrial clusters present in the area struck by the 2012 Emilia earthquakes.

Fragility curves for different typologies will be illustrated in section 6.5. Anyway, the following Figure 35 and Figure 34 show a first attempt to distinguish the seismic behavior of different typologies, evaluating the damage levels distribution for each type of building considering three range of PGA. The number of buildings belonging to each interval of PGA, for each type of building and for each damage level., is shown in Figure 34. The three range of PGA are selected to group almost the same number of buildings. According with the following two figures, Type 4 (shed) seems to be the most vulnerable typology, followed by Type 5 (Irregular buildings) Type1 (dsr masonry infills), Type 3 (flat roof) and Type 2 (dsr precast external panels). Finally type 0 (dsr precast infills), according to D5, has the same high vulnerability of Type 1 but, considering the sum of D3+D4+D5 (severe damages) Type 0 seems to be the less vulnerable. The fragility curves described in section 6.5 confirmed almost the same results.

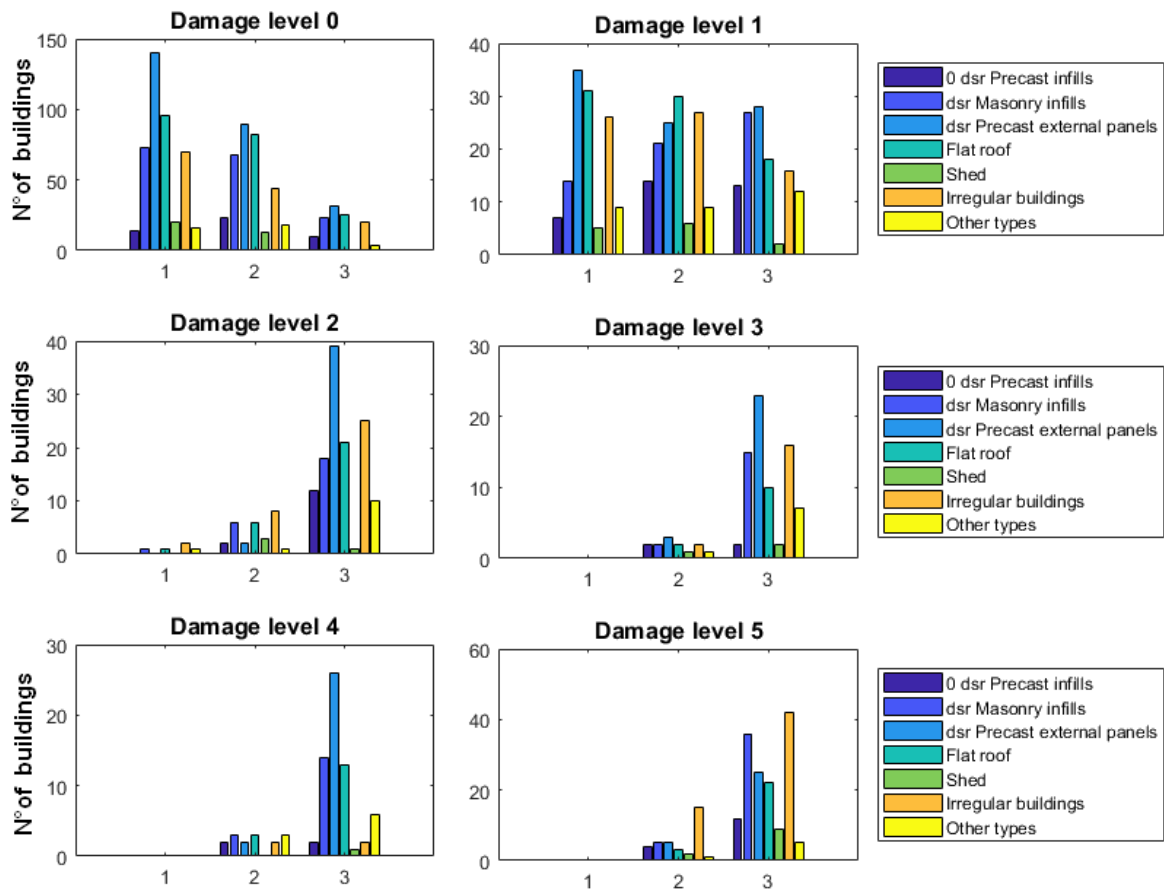


Figure 34. Number of buildings belonging to each interval of PGA, for each type of building and for each damage level.

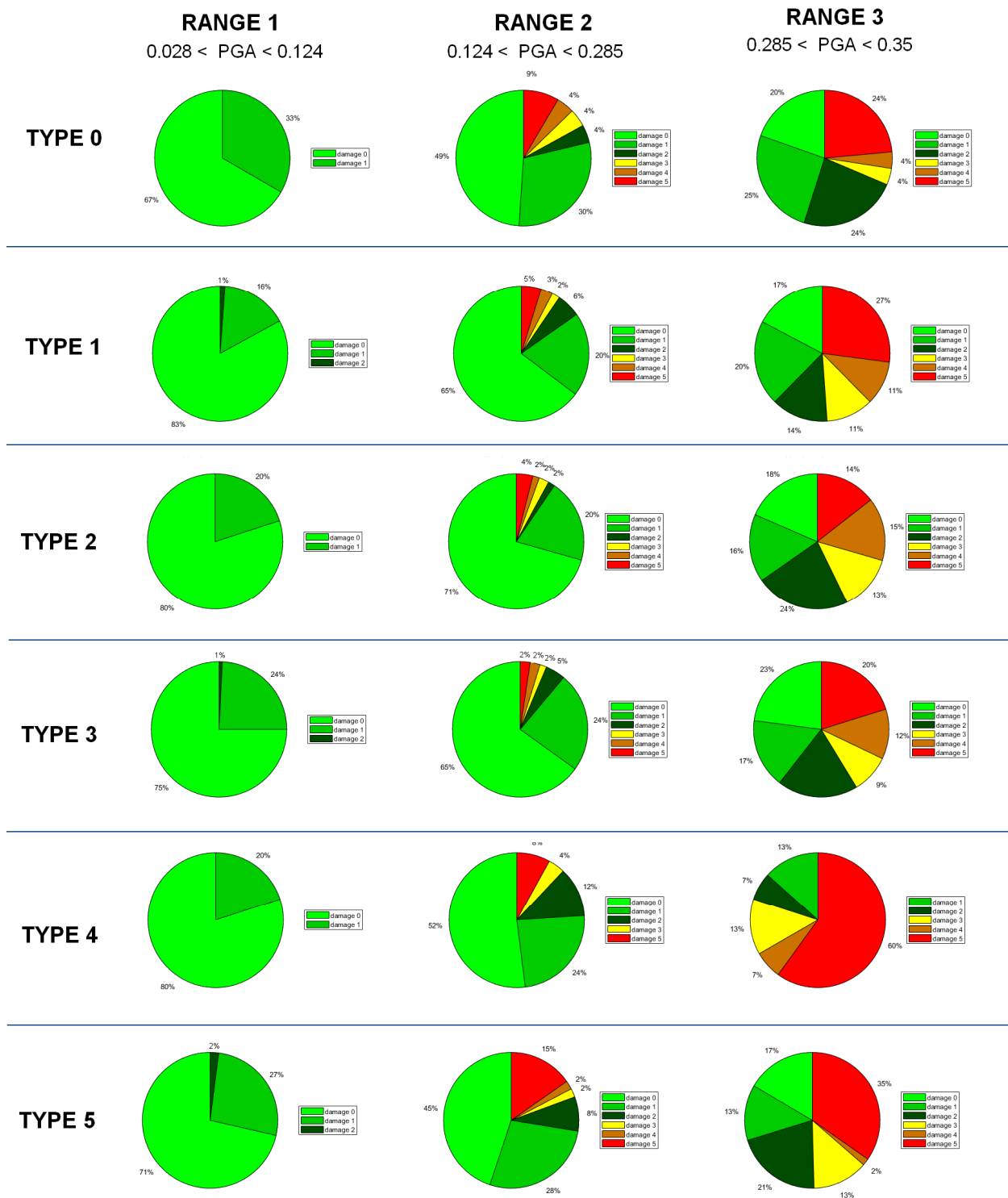


Figure 35. Damage levels distribution for each type of building considering three range of PGA.

### 3.4 Typological features of the precast industrial buildings in the area of interest

The present chapter shows the statistical results obtained after analyzing the distribution of the main geometrical properties of precast structures. Beam span, frame spacing, column height, have been analyzed for the building types 0+1,2 and 3. In this statistical evaluation Type 1 and Type 0 are grouped since are very similar from the geometrical point of view.

The results (Table 7) can be compared with the information present in [50] and related to two building categories, named Type 1 and Type 2, that more or less correspond to Type 1 and Type 2 of the present research. In [50] probability distributions for the main geometrical parameters were obtained starting from a database created from direct surveys of 650 warehouses located in Tuscany, Emilia Romagna and Piedmont regions.

Figure 36, Figure 37 and Figure 38 shows the probability distributions of the main geometrical parameters of type 0/1 type 2 and type 3.

<i>Building configuration</i>	<i>Geometrical parameter</i>	<i>Median value [m]</i>	<i>Logarithmic Std. Dev. [-]</i>	<i>Test <math>\chi^2</math></i>	<i>Min [m]</i>	<i>Max [m]</i>
<i>Type 1</i>	<i>Beam span<sup>(a)</sup></i>	<i>15.64</i>	<i>0.22</i>	<i>YES</i>	<i>8</i>	<i>30</i>
	<i>Frame spacing</i>	<i>6.6</i>	<i>0.23</i>	<i>NO</i>	<i>4</i>	<i>11</i>
	<i>Column height<sup>(a)</sup></i>	<i>5.9</i>	<i>0.18</i>	<i>YES</i>	<i>4</i>	<i>11</i>
<i>Building configuration</i>	<i>Geometrical parameter</i>	<i>Median value [m]</i>	<i>Logarithmic Std. Dev. [-]</i>	<i>Test <math>\chi^2</math></i>	<i>Min [m]</i>	<i>Max [m]</i>
<i>Type 2</i>	<i>Beam span</i>	<i>17.16</i>	<i>0.23</i>	<i>YES</i>	<i>8</i>	<i>10</i>
	<i>Frame spacing</i>	<i>8.9</i>	<i>0.24</i>	<i>YES</i>	<i>4</i>	<i>18</i>
	<i>Column height</i>	<i>6</i>	<i>0.21</i>	<i>YES</i>	<i>4</i>	<i>12</i>
<i>Building configuration</i>	<i>Geometrical parameter</i>	<i>Median value [m]</i>	<i>Std. Dev. [m]</i>	<i>Test <math>\chi^2</math></i>	<i>Min [m]</i>	<i>Max [m]</i>
<i>Type 3</i>	<i>Beam span</i>	<i>13.1</i>	<i>0.43</i>	<i>NO</i>	<i>8</i>	<i>10</i>
	<i>Frame spacing</i>	<i>12.4</i>	<i>0.32</i>	<i>YES</i>	<i>8</i>	<i>23</i>
	<i>Column height</i>	<i>6.15</i>	<i>0.2</i>	<i>NO</i>	<i>4</i>	<i>10</i>

<sup>(a)</sup> Lognormal distribution;

Table 7. Geometrical dimensions characteristic of the building stock belonging to Emilia damage database.

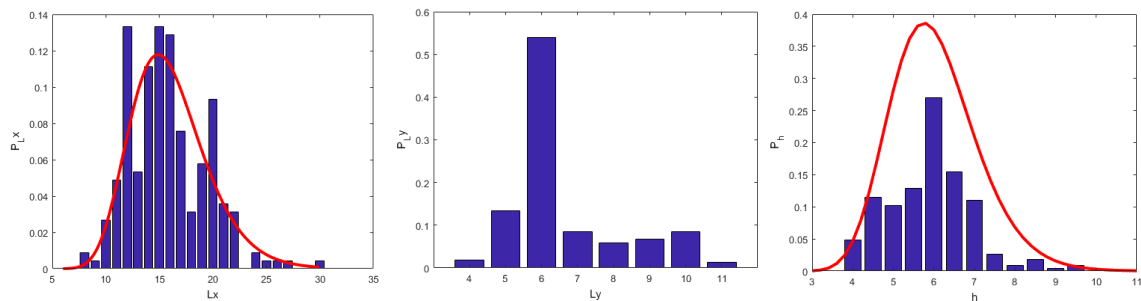


Figure 36. Type 0/1: probability distributions of the length of the main beam, of frame spacing and column height.

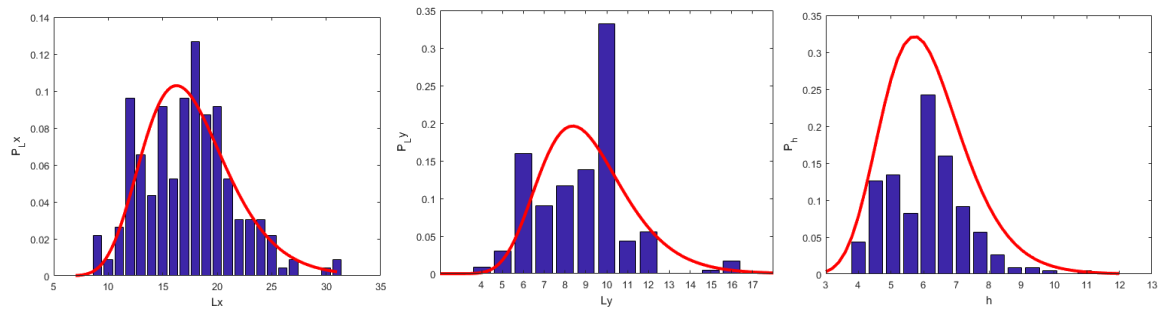


Figure 37. Type 2: probability distributions of the length of the main beam,of frame spacing and column height.

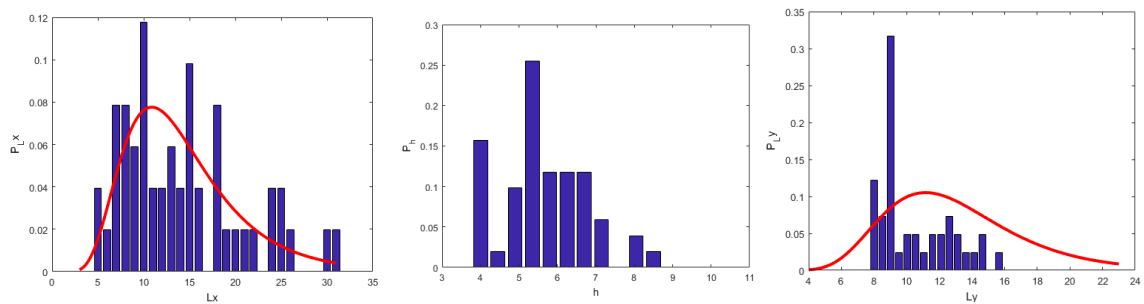


Figure 38. Type 3: probability distributions of the length of the main beam,of frame spacing and column height.

The data analysis on the geometrical parameters is still going on. Future developments consist in processing and correlating the data entered in the database with the purpose of identifying the most significant parameters to achieve a fast method for the analysis of seismic vulnerability. At the end of this first phase, it should become possible to identify the geometric and constructive synthetic parameters, able to uniquely classify the different types of prefabricated buildings.

The evaluation of seismic vulnerability based on synthetic parameters is of interest not only for retrofitting of existing buildings, but also for the benefits that could derive from the application of this provided method, on a larger scale in the recovery of entire industrial areas. In the modern economy, establish the vulnerability of whole industrial areas is very important to plan the civil protection strategies and to predict the costs for restoring or retrofitting the damaged buildings.

## **4. RECURRENT DAMAGES AND COLLAPSES IN PRECAST INDUSTRIAL BUILDINGS DURING EMILIA EARTHQUAKE**

### **4.1 Introduction**

The present chapter presents a comprehensive classification of damage and collapse mechanisms in reinforced concrete precast industrial buildings observed by the author using the following sources:

- technical reports prepared by structural engineers for obtaining public funds for reconstruction as described at section 2.2;
- field surveys;
- satellite imagery (Figure 38 shows an example of damage recognition).

As stressed in the previous chapters, the two mainshocks caused extended damages and collapses in prefabricated RC buildings. In some industrial areas close to the epicenters (e.g., Mirandola Nord, S. Giacomo Roncole, Cavezzo, Medolla), up to 70% of buildings were significantly damaged or collapsed. The main causes of the collapses were vulnerabilities related to the structural characteristics of Italian precast buildings not designed with seismic criteria, since the region was not covered by seismic code requirements until October 2005. In particular, they were typically built as an assembly of monolithic elements (roof elements, main and secondary beams, columns) in simply-supported conditions, without mechanical connectors between the various structural members. In non-seismic regions, mechanical connections were not used. Often, neoprene pads were used to allow end rotations in long span elements, thus reducing even more the friction resistance.

Thus, the most common failure cause identified was the absence of connecting systems between precast monolithic elements (slab-to-beam support, beam-to-column connection) as well, the interaction of structural elements with non-structural walls, the inadequacy of column bending capacity or the foundation rotation, the inadequacy of connections of external precast cladding walls to bearing elements (columns and beams), the overturning of racks in buildings used as warehouses or in automated storage facilities.

Moreover, older buildings with masonry curtain walls between RC columns (with the walls supporting most of the horizontal loading during the earthquake) and more recent buildings with external RC cladding panels (where horizontal forces mainly act on precast columns in clamped-free condition) exhibited very different seismic responses, as presented in [7] [51] and [52]. In the following paragraph a wide illustration of all these types of damages.



Figure 39. Google Earth images of a building located in Medolla (MO): a) before the seismic events 2011 b) after the seismic event 2014.

#### **4.2 Classification of damage and collapse mechanisms in reinforced concrete precast industrial buildings**

The damaged or collapsed buildings illustrated in this paragraph were selected among a total of more than one thousand industrial reinforced concrete precast buildings whose data have been collected in the large database described in chapter 2.4. In most cases, it was possible to identify the reasons of the collapses, in relation with the usual design criteria for non-seismic zones adopted in the region.

The loss of support of roof elements from beams and of beams from column supports, due to the lack of mechanical connections between various precast monolithic elements (columns, beams, slab elements, cladding panels) was the main cause of most collapses, even if the large displacements causing the fall of precast beams from the column supports were, in some cases, amplified by other phenomena.

Some pictures of the most frequent collapses and damages are reported in Figure 40-Figure 46 and described in the following.

Figure 40 (a-b) shows the falling of a precast beam from the column support due to the interaction with the front masonry curtain wall. During the roof oscillation, the infill wall alternatively exerted an additional constraint to only one of the two adjacent columns, leading to a significant increase in the translational stiffness of that column. Therefore, most of the horizontal force was transferred to one beam-column support only, overcoming the friction capacity of the support. This failure was very common in buildings with strip windows between the precast beam and the curtain wall, usually with double slope beams and built until the eighties.

Figure 41 shows the collapse of a) the masonry curtain wall b) the horizontal precast cladding panels placed between the columns. The collapse was caused by the insufficient restraint exerted on the wall by RC columns and upper beam, due to the presence of the strip window. Sometimes, before the collapse of the masonry infill, column damages occurred because of the interaction with the wall: in Figure 41 (a), note also the short column failure of the left column. Short column failure

mechanisms were also documented in Figs. 11-13 reported by [53] , and in Fig. 10 reported by [51].



Figure 40. Roof collapses in precast buildings: two examples of partial collapse due to interaction with masonry curtain walls.



Figure 41. Collapse of (a) a masonry curtain wall not restrained by the RC structure

In modern buildings, with large spans covered with long prestressed beams and prefabricated slab elements, the insufficient flexural capacity of cantilever columns (not designed for horizontal seismic actions but for wind actions at most) or the rotations experienced by the foundations were, in some cases, the onset of progressive and catastrophic collapses. Furthermore, several failures involved reinforced concrete precast cladding panels, because the fastening devices on the bearing elements (columns and beams) were inadequate for the large displacement capacity required at the connection level. Figure 42 a)b) shows an extended roof collapse in a modern precast building due to the absence of slab-beam connections.



Figure 42. Roof collapses in precast buildings: (b) extended collapse in a modern prefabricated building

The picture of Figure 43 illustrates the falling of RC cladding panels due to the damage of the retaining systems, represented by steel channel profiles cast in the column concrete cover. These devices are typically designed against horizontal forces acting perpendicularly to the panels and are not able to support the large building displacements in the direction parallel to the curtain front during the earthquake. This kind of collapse was common in precast buildings with horizontal cladding panels.



Figure 43. Collapse RC cladding panels due to failure of the steel channel profiles supporting them.

Rotations of precast RC columns not designed for the earthquake resistance due to damages at the column base are shown in Figure 44. In the case of Figure 44(a), the rotation was caused by the formation of a plastic hinge at the base. A detail of a plastic hinge, with yielding of longitudinal steel bars in tension and buckling of bars in compression is shown in Figure 44 (b).



Figure 44. Damages in precast RC columns: (a) rotation of external columns; and (b) large base rotation due to formation of a plastic hinge with yielding and buckling of longitudinal steel bars

Local damages occurred frequently in columns due to the interaction with masonry curtain walls (Figure 45(a)), or in the forked supports at the column top (Figure 45 (b)), generally not designed to avoid overturning of the beams during seismic excitations. Typically, these damages were repairable and were restricted to some elements in the building only.



Figure 45. Local damages in precast RC columns: (a) failure mechanism due to interaction with masonry infills; and (b) damage of the upper fork of a column due to flexural-torsional displacements of the precast beam

Sometimes, rigid rotations of columns occurred due to settlements at the foundation level or failure of the precast sleeve footing. In few cases, very large column rotations occurred with very extended collapses (Figure 46 (a)), probably due to the use of fully precast sleeve footings simply-supported on the cast in situ RC foundation. This technology was often used in recent years in order to speed up the construction, but this kind of foundation structure does not exhibit any overstrength capacity when the external bending moment overcomes the stabilizing moment. In other cases, the presence of a RC pavement avoided excessive column rotation and falling of the upper beam (Figure 46 (b)). With regard to the overturning failure of precast RC columns, an analysis was recently presented by [54].



Figure 46. Damages in precast RC columns: (a) extended building collapse caused by large column rotation due to foundation settlement; and (b) column rotation due to settlement at the foundation level, counteracted by the presence of an industrial concrete pavement

### 4.3 Statistical analysis of damages observed in Emilia region after 2012 earthquakes

The present chapter shows through some histograms, a preliminary statistical analysis of the different types of damages among the different damage levels.

Figure 47 shows the damage repartition for the main components of the precast structures (columns, roof, masonry infills and precast panels), among the different damage levels.

It's worth noticing that, in Figure 47 , the percentage of buildings with damages at the columns rise steeply from 36.5% for the damage level 1, to 66.7% for damage level 2. From damage level 2, as the damage level increase, that percentage shows a steady escalation of 5%, up to 85.3% for the damage level

The percentage of buildings who showed roof damages, for each damage level, increases from 65.2% for the damage level 1 to 77.9 % for damage level 5.

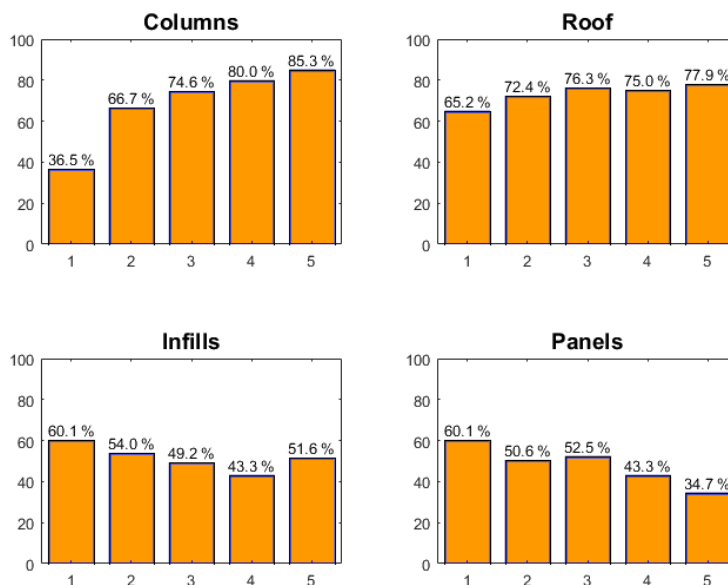
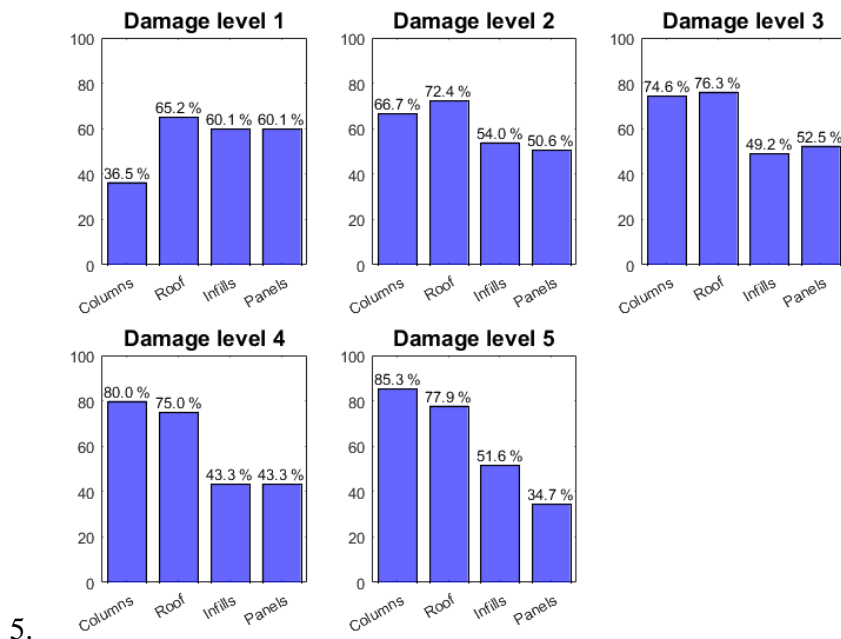


Figure 47: Damage of the main components of the precast structures among the different damage levels.

The histograms of the damage distribution among the different damage levels related to infills and panels show, on the contrary, a slightly decreasing trend, starting from 60% for the damage level 1 for both structural components. This unforeseen trend can be related to the source of the damage information. For severe damages (D3 to D5), the damage description present in the reports prepared by professional to obtain regional funds, focus mainly on the description of the severe damages at the structures as columns and roof often avoiding to underline the possible presence of

minor damages on partitions or infills since, for those damage levels, the amount of the funds was not related to that.

The types of damages showed by each structural component, for each damage level, are illustrated from Figure 48 to Figure 51.

The types of damages considered for the columns are:

- Cracks;
- Spalling of concrete cover;
- Development of plastic hinge at the base of the columns;
- Drift < 2%;
- Drift >2%;
- Drift not evaluated;
- Short pillar;
- Rotation of the foundation.

The types of damages considered for the roof are:

- Slip of roof elements;
- Slip of main beams;
- Loose of support of roof elements from the main beam;
- Loose of support of the main beam from the column.

The types of damages considered for the masonry curtain walls are:

- Cracks on masonry curtain walls;
- Detachment without collapse of masonry curtain walls;
- Collapse of masonry curtain walls

The types of damages considered for the cladding panels are:

- Local damages on RC cladding panels;
- Movement of RC cladding panels without collapse;
- Damage of fastening device for panel-column connections;
- Collapse of RC cladding panels.

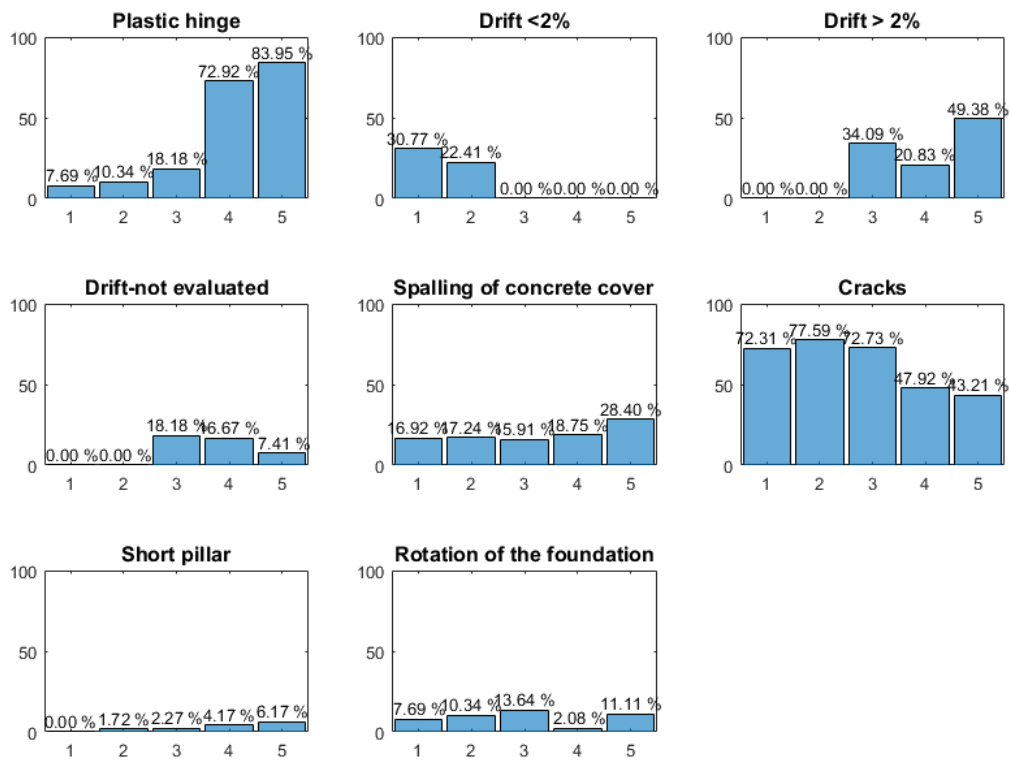


Figure 48. distribution of different types of column damage among the 5 damage levels.

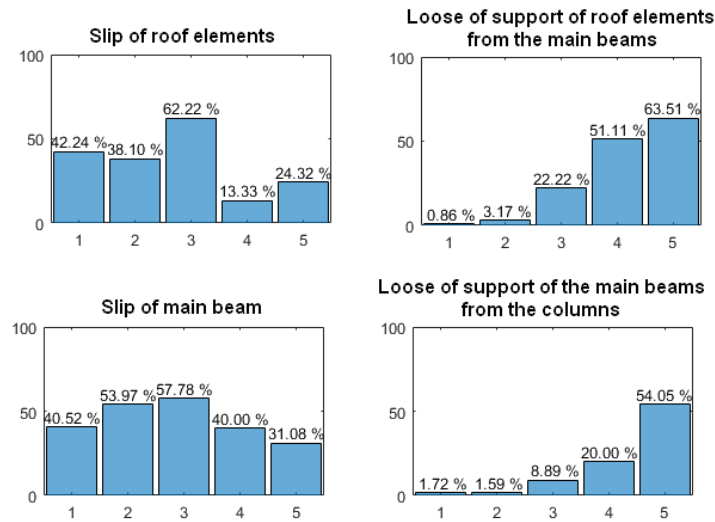


Figure 49. distribution of different types of roof damages among the 5 damage levels.

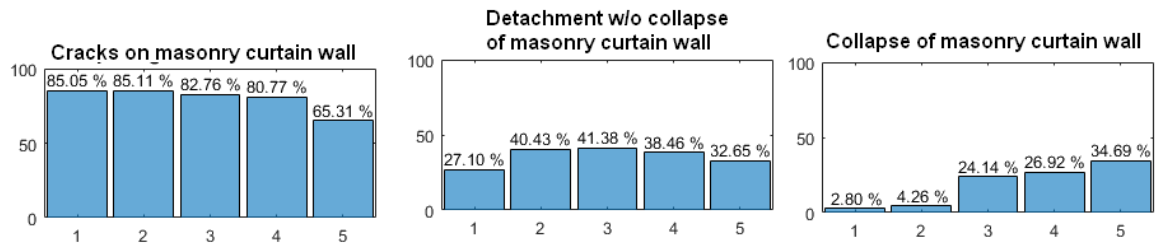


Figure 50. distribution of different types damages on masonry curtain wall among the 5 damage levels.

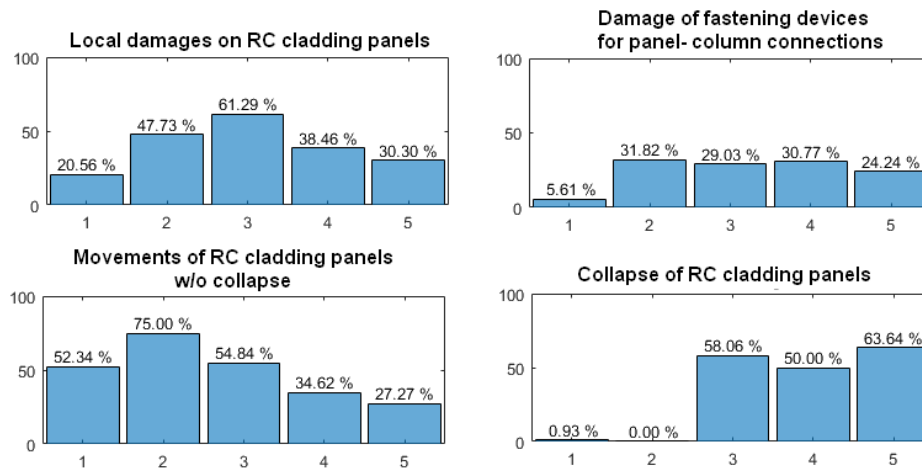


Figure 51. distribution of different types damages on RC cladding panels among the 5 damage levels.

#### 4.4 Summary of post-earthquake reconnaissance activity

The experience of a seismic event gives the possibility to develop a deeper knowledge on the seismic behavior of a structural typology.

The surveyed buildings considered in the previous sections emphasize typical weaknesses of different structural precast typologies in areas recently classified as seismically prone.

Other examples of damage can be found in a number of reconnaissance reports already available (EPICentre Field Observation Report No. EPI-FO-200512, 2012; EPICentre Field Observation Report No. EPI-FO-290512, 2012; Decanini et al., 2012). The damages described in this chapter allow the author to point out that: (1) The Emilia Romagna earthquakes mainly destroyed masonry and RC precast buildings. In both cases the observed structural damage was mostly caused by lack of proper connection detailing. (2) The majority of heavy damaged or collapsed industrial buildings were designed for gravity loads only. Lacking or ineffective connections between RC precast roof beams and columns induced partially constrained roof systems which slipped off under large relative displacements between top sections of columns.

Ineffective connections between vertical façade panels and the structure caused dangerous out-of-plane collapse mechanisms of the panels.

The real response of structural and non structural components can be compared to the results of numerical analyses in order to validate the modeling assumptions. Some validation of numerical models were performed in the past for some structural typologies, as historical constructions ([55]) and masonry structures ([56]). On the contrary, few similar studies were developed for precast industrial buildings ([57]; [50]). In [57] the authors demonstrated the vulnerability of the existing friction beam-to-column connections by means of nonlinear static and dynamic analyses.

Moreover, the Italian damage data collected by the author were used to make a comparison with the loss estimation obtained through the software SP3, developed by Haselton and Baker risk group, which implement FEMA P-58 [58] guidelines on risk assessment procedure and also REDi rating system [59] to generate repair time. This part of the research is still going on and will be part of further development.

## **5. OBSERVATIONAL FAILURE ANALYSIS OF PRECAST BUILDINGS AFTER THE 2012 EMILIA EARTHQUAKES AND RELATED RETROFIT INTERVENTIONS.**

### **5.1 Introduction**

In the present chapter, the preliminary results obtained from field survey data on damages in precast RC industrial buildings hit by the 2012 Emilia earthquakes are presented. The present chapter provides damage distributions in the area as a function of Pseudo-Spectral Acceleration for a period of 1 second (PSA at 1s).

In the largest part of the territory, the maximum seismic intensity was recorded during the May 20<sup>th</sup> or 29<sup>th</sup>, 2012, earthquakes [60]. Therefore, PSA were referred to these two events. A total of 1890 buildings were included in the study, corresponding to approximately 30% of the industrial buildings in the struck area. Depending on the damage entity, the buildings were classified into six damage levels, from no damage up to collapse, according to the European Macroseismic Scale EMS-98 (1998) as illustrated in chapter 2.2.

### **5.2 Parameters of seismic intensity adopted in the study**

Neglecting the stiffening effect of non-structural curtain walls, precast RC buildings located in the area typically show a fundamental period lying in the range 1–2 seconds [51]. In fact, the presence of curtain walls provided with strip windows, generally located in correspondence of the building perimeter, may lead to severe structural damages (see Chapter 4), but, especially in buildings with non-rigid roof slab and a very large dimension in plan, does not influence significantly the global behaviour in the direction orthogonal to that dimension.

In order to state a relationship between damages and ground motion intensity, the horizontal PSA at 1 s with a 5% damping ratio was used (subscript “h” is dropped for simplicity of notation). The vertical component of the ground motion was not considered in the present study, because it affects particularly structures with very low natural periods.

The PSA data were obtained from the shakemaps published online by INGV (2012), and computed using the ShakeMap software package [61]. That software was implemented by INGV to be used automatically in real time for Civil Protection purposes [62]. For all earthquakes with magnitude  $M_L \geq 3.0$ , maps of macroseismic intensities in terms PSA (but also PGV and PGA) are computed by INGV for the post-earthquake emergency management and, with regard to the industrial buildings hit by the 2012 Emilia earthquakes, they were also widely used to define the intervention strategies [60]. Values of PSA were provided by INGV only for the periods 0.3, 1, and 3 s. Then, the period of 1 s was selected in the present study as the closest to the main vibration period of the buildings. Anyway, at least for the spectra of the records collected during the second

mainshock, PSA at 1 s represents a good approximation of the mean value of the PSA in the interval 0.85–2 s (see Figure 52).

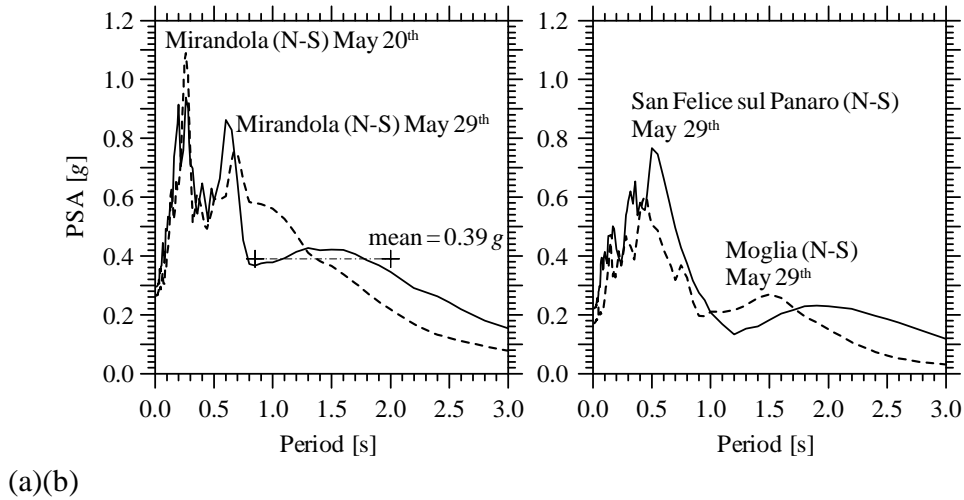


Figure 52. Horizontal PSA versus period for (a) the seismic station at Mirandola (first and second mainshocks), and (b) those at San Felice sul Panaro and Moglia (second mainshock)

Only the shakemaps of the two mainshocks (May 20<sup>th</sup> and 29<sup>th</sup>) were considered in the present study. In particular, for each building examined and included into the database, the value of PSA at 1 s corresponding to the nearest epicentre was retained. For comparison, also the maximum experienced PGA was considered. Because the strong motion data provided by INGV are referred to a dense grid with nodes spacing 1 km, according to the rule suggested by the Italian Building Code (2008), PGA and PSA at a given location in the map were obtained as the weighted mean values of the ground motion intensity measures at the four closest grid nodes, with the  $i$ -th weight being the reciprocal of the distance between the location and the  $i$ -th node. Less than 30% of the buildings included into the database are located closer to the epicentre of the first mainshock. For the remaining 70% buildings, the PSA at 1 s was that corresponding to the second mainshock.

The PSA of the two mainshocks presents some peculiar feature. For example, the PSA at 1 s obtained from the records of the seismic station of Mirandola for the first and second mainshocks was (INGV 2012)  $5.50 \text{ m/s}^2$  (0.56g) and  $3.70 \text{ m/s}^2$  (0.38g), respectively (see Figure 52 (a)). A value of PSA 50% larger for the May 20<sup>th</sup> mainshock appears quite unusual for two reasons: (1) the second mainshock was recorded at a much smaller epicentral distance, and (2) the magnitudes of the two mainshocks were comparable and no significant site effect can be expected in the area. With regard to the spectrum of the N-S component recorded during the first mainshock (Figure 52(a)), a PSA at 1 s approximately equal to three times the PSA at 2 s is observed. However, the heavy damages observed in the area around Mirandola were caused mainly by the second mainshock.

Cultrera et al. [63] showed that the increase in the number of stations between the two mainshocks led to a significant improvement of the ground motion estimates. Due to the small number of recording stations available during the first mainshock, the shakemaps of PGA and PSA at 3 s may be underestimated of about 0.20g and 0.14g, respectively, whereas, with the dense station coverage for the May 29<sup>th</sup> earthquake, the error reduces to about 0.10g and 0.05g, respectively. Underestimates of PGA were also underlined by Braga et al. [60].

### 5.3 First correlations between damage and seismic intensities

In the present study, the damage data for the 1890 buildings examined were processed to obtain correlations between damage level and epicentral distance or, alternatively, PSA at 1 s. In particular, with reference to the earthquakes occurred on May 20<sup>th</sup> and 29<sup>th</sup>, the distance from the nearest epicentre and corresponding PSA at 1 s were considered for each building. Table 4 shows, for each of the 5 damage levels, the number of buildings included into the database.

The locations of the industrial buildings belonging to damage levels D3, D4 and D5 are reported in Figure 53, where the highest concentration is observed around the epicentre of May 29<sup>th</sup> earthquake ( $M_L = 5.8$ ). Several buildings with heavy damages are also located at South-East of May 20<sup>th</sup> earthquake ( $M_L = 5.9$ ) epicentre. The cumulative frequencies of buildings with damage levels D3, D4 and D5 are reported in Figure 54(a) and Figure 54(b) versus epicentral distance and PSA at 1 s, respectively. For each damage level, the cumulative frequency is referred to the total number of buildings belonging to that level and included into the database. All collapsed buildings are located at less than 19 km from the nearest epicentre, and for 80% of them the epicentral distance does not exceed 9 km (D5 in Figure 54(a)). Moreover, 80% of the collapsed buildings experienced a PSA larger than 0.26g (D5 in Figure 54(b)). It is worth noting that, in Figure 54, the curves corresponding to damage levels D3 and D4 are very close to those corresponding to damage level D5, so confirming the difficulty, for the technicians charged of preparing the damage reports, of distinguishing between the three damage levels. This behaviour justifies the grouping of the three damage levels into one single damage class, as will be carried out in the following.

The locations of the buildings with slight to moderate damages (levels D1 and D2) are reported in Figure 55, where they appear scattered over the struck area, with the highest density in the Modena county. For the same buildings, the plots of the cumulative frequencies versus distance from the nearest epicentre and corresponding PSA at 1 s are reported in Figure 56(a) and Figure 56(b), respectively. All buildings with moderate damages lie at an epicentral distance not larger than 26 km, and 20% of them are located at less than 5 km from the nearest epicentre (D2 in Figure 56(a)). Moreover, 20% of the buildings with moderate damages experienced a PSA larger than 0.28g (D2 in Figure 56(b)). Finally, for 20% of the buildings with slight damages, the minimum

epicentral distance does not exceed 7 km (D1 in Figure 56(a)), and the experienced PSA at 1 s is larger than 0.27g (D1 in Figure 56 (b)).

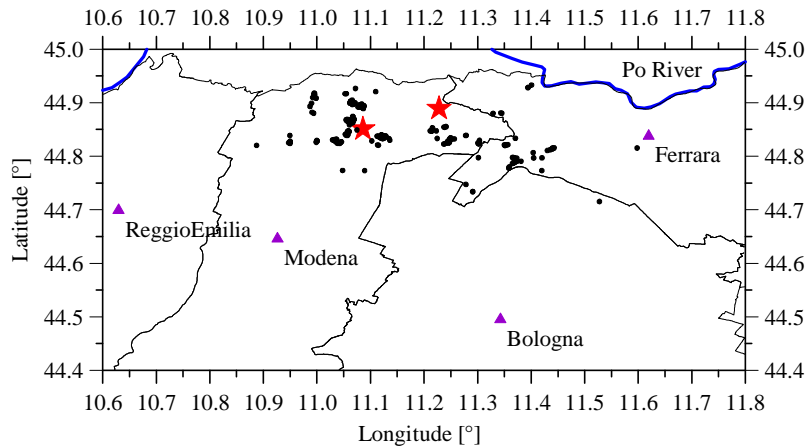


Figure 53. Map reporting the locations of severely damaged to collapsed buildings (damage levels D3, D4 and D5, black data points) and of epicentres of the two mainshocks (red stars)

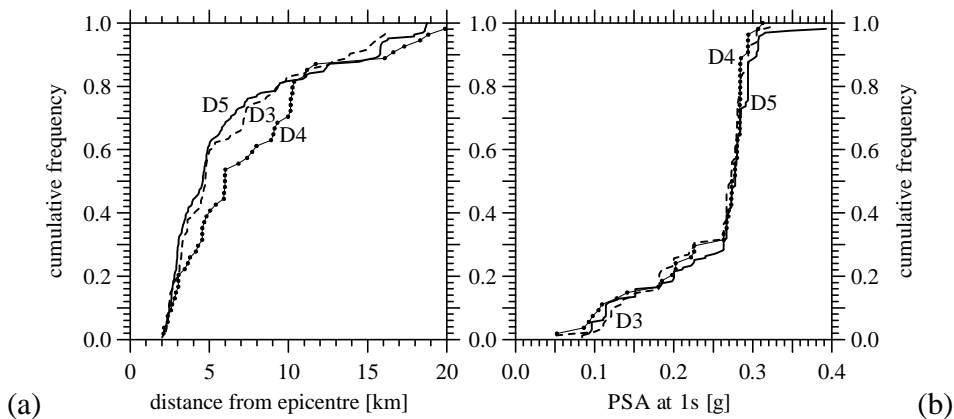


Figure 54. Cumulative frequencies of buildings belonging to damage levels D3 (dashed lines), D4 (line with symbols) and D5 (solid line) versus (a) distance from the nearest epicentre, and (b) corresponding PSA at 1 s

The 967 undamaged buildings included into the database are indicated in the map of Figure 57, where they appear almost uniformly distributed within the counties of Reggio Emilia, Modena, Bologna and Ferrara, and then also close to the earthquake epicentres. Note that only buildings lacking appropriate connections between precast elements and located in the struck area of Emilia-Romagna region were considered in the database.

The data reported show that even though six damage levels have been identified, the classification in one level or another may depend on the subjective judgement of the inspector.

For instance, the distinction between the distributions of buildings with damage levels D3, D4 and D5 is not clear (see Figure 54).

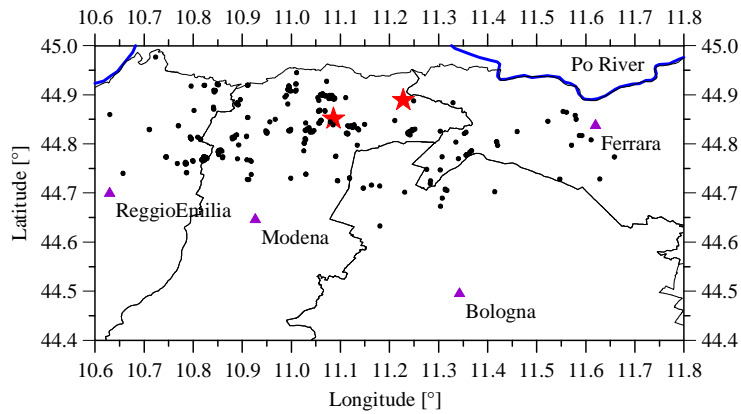


Figure 55. Map reporting the locations slightly to moderately damaged buildings (damage levels D1 and D2, black data points) and of epicentres of the two mainshocks (red stars)

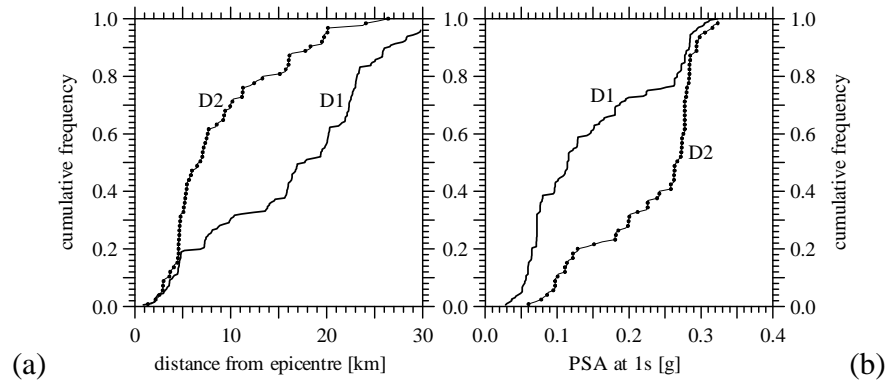


Figure 56. Cumulative frequencies of buildings belonging to damage levels D1 and D2 versus (a) distance from the nearest epicentre, and (b) corresponding PSA at 1 s

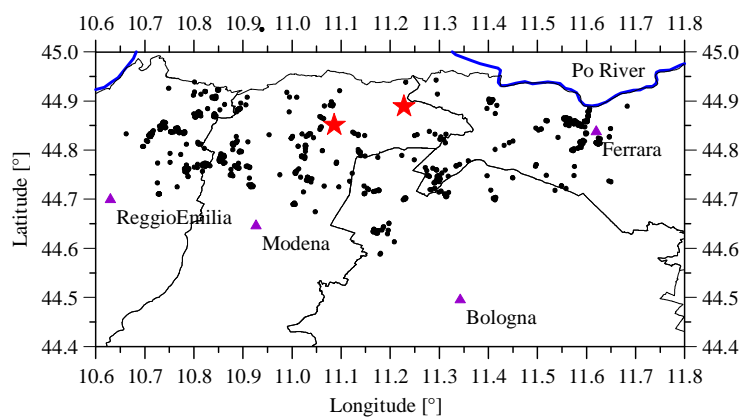


Figure 57. Map reporting the locations of undamaged buildings (damage level D0, black data points) and of epicentres of the two mainshocks (red stars)

Sometimes, also the distinction between damage levels D1 and D2 may be difficult. On the contrary, the distributions of groups of damage levels D3 to D5, D1 to D2, and D0 are clearly distinct (see Figure 53 Figure 55 and Figure 57 ). Therefore, in the further analyses, the damage data were grouped into three main classes, i.e., the class of the undamaged buildings (D0), that collecting the buildings with slight to moderate damages (D1+D2), and, finally, that of the severely damaged to collapsed buildings (D3+D4+D5). The corresponding cumulative frequencies are reported in Figure 58 versus the distance from the nearest epicentre. It can be noted from Figure 58 that 90% of the severely damaged to collapsed buildings (D3+D4+D5) lie within 16 km from the nearest epicentre. Moreover, for 90% of the buildings with slight to moderate damages (D1+D2), the minimum epicentral distance is less than 25 km.

Nevertheless, the circumstance that also quite close to the epicentres there is a significant number of undamaged buildings indicates that some precast building typologies did not suffer damages also in the presence of large ground accelerations.

The data are presented in an alternative form in Figure 59, to underline the percentages of buildings with different levels of damage as a function of their epicentral distance. In particular, the cumulative sum of buildings investigated is reported in Figure 59(a), whereas the percentage distribution of the buildings belonging to the three damage classes is reported in Figure 59(b). The investigated buildings with  $R_{epi} \leq 30$  km are distributed among the three damage classes according to the following percentages: 21% (D3+D4+D5), 31% (D1+D2) and 48% (D0). The buildings with severe damages up to collapse (D3+D4+D5 in Figure 59(b)) are 57 % of all buildings in the range 0–5 km, and about one half of the total stock for epicentral distances up to 10 km. Nevertheless, it is worth noting that 19% of the buildings within 10 km from the epicentre did not suffer any damage (D0 in Figure 59(b)).

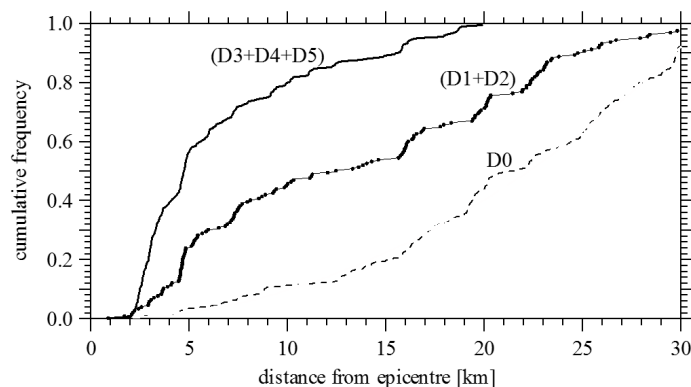


Figure 58. Cumulative frequencies of the three classes of damage levels plotted versus the distance from the nearest epicentre

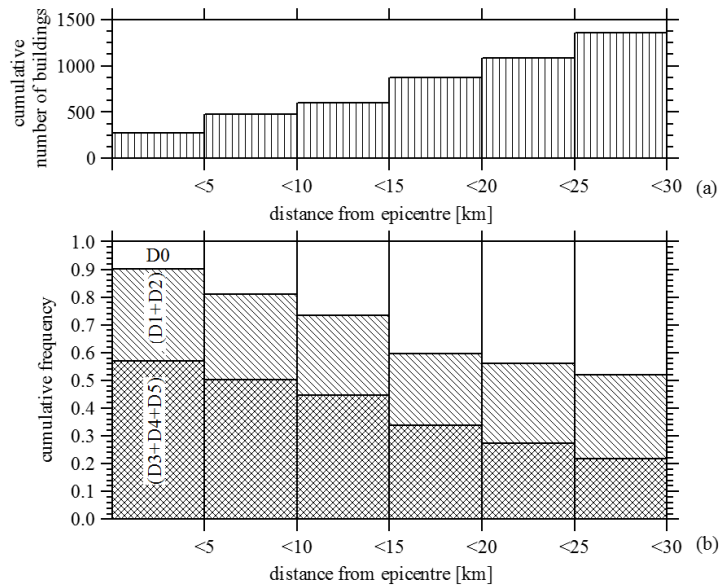


Figure 59. Bar charts with (a) cumulative number of buildings investigated, and (b) cumulative frequencies of buildings versus epicentral distance for the three classes of damage levels

The cumulative frequencies of the buildings belonging to the different classes of damage levels are reported in Figure 60 (a) versus the PSA at 1 s corresponding to the nearest epicentre. It can be observed that 90% of buildings with severe damages up to collapse (D3+D4+D5) experienced a PSA larger than 0.12g and 10% of them was subject to a PSA larger than 0.29g. Moreover, 90% of buildings with slight to moderate damages (D1+D2) experienced a PSA larger than 0.06g.

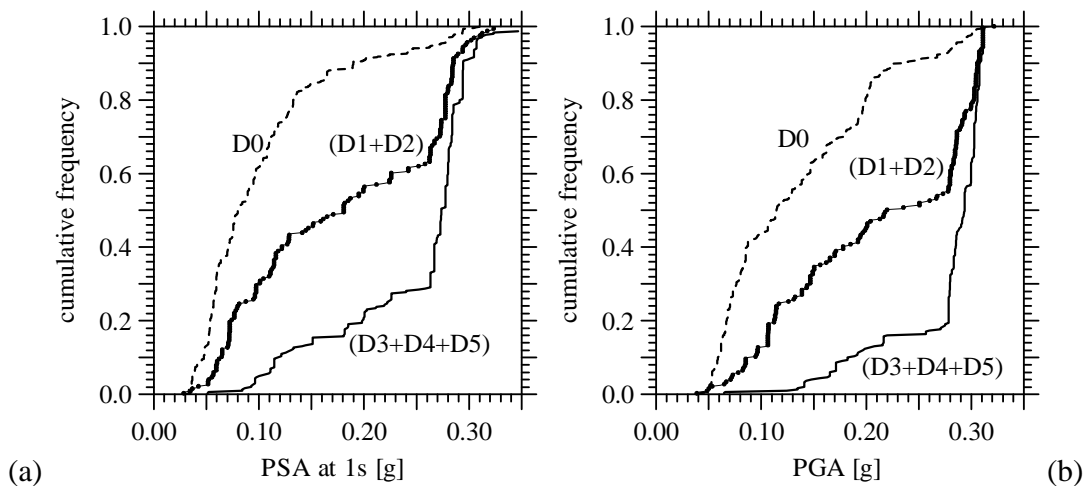


Figure 60. Cumulative frequencies of the three classes of damage levels versus (a) PSA at 1 s corresponding to the nearest epicentre, and (b) maximum experienced PGA

Distributions of the damage classes D1+D2 and D3+D4+D5 similar to those reported in Figure 60(a) are finally presented in terms of the maximum experienced PGA in Figure 60(b). It is worth noting that these curves show a sudden slope change at  $PGA \approx 0.28g$ , with a significant increase of the number of damaged buildings for PGA values greater than that value. In particular, the 598 buildings subjected to a  $PGA \geq 0.28g$  and located at epicentral distances lower than 12 km are distributed among the three damage classes according to the percentages reported in Table 8. Distribution among the three damage classes of the buildings affected by a  $PGA \geq 0.28g$  showing a clear predominance of class D3+D4+D5 (severe damage to total collapse).

Damage class	D0	D1+D2	D3+D4+D5	Total
No. of buildings	80	230	288	598
Percentage [%]	13	38	48	100

Table 8. Distribution among the three damage classes of the buildings affected by a  $PGA \geq 0.28g$

This circumstance would suggest the possibility that, for  $PGA \geq 0.28g$ , some damage mechanisms can be activated, depending on parameters not strictly related with the building characteristics: one of these causes can be the falling of the roof elements, or even main girders from their support (see Figure 10(a)), which is related to the overcoming of the friction resistance at the support level. Actually, the slope changes shown in Figure 60 are a consequence of the non-uniform distribution of buildings and of the spatial distribution of the parameters of seismic intensity. Only for the uniform distribution of the undamaged buildings (D0) the slope change is absent.

That said, the falling down collapse mechanism was very frequent in the epicentral areas, especially when the interaction between precast columns and non-structural walls took place.

As an example, consider a typical precast building with one single beam span and columns of height  $h$ . A general frame of the building is outlined in Figure 61 (a). According to Figure 61 (a), for a site which experienced a PGA of about  $0.28g-0.30g$ , and a natural period between 1 s and 2 s,  $PSA = \alpha g$ , where  $\alpha$  is about 0.4. If  $M$  indicates the upper mass (due to the presence of the roof slab elements and precast beam), the dead load acting on the two beam-column supports is  $F_{v1} = F_{v2} = Mg/2$ . The horizontal force due to the seismic excitation is then  $F_h = M PSA = \alpha Mg$ , and is equally divided between the two columns, i.e.,  $F_{h1} = F_{h2} = \alpha Mg/2$ . It can then be verified that the supports are perhaps able to support the horizontal forces by friction, being  $F_{h1}/F_{v1} = F_{h2}/F_{v2} = \alpha = 0.4$ , which is a typical value for the concrete-to-concrete friction coefficient (Tassios and Vintzēleou 1987). With an illustrative example considering a friction-based beam-column connection typical for the struck area, Liberatore et al. [8], showed that, if no vertical component of the ground motion is considered, a friction coefficient  $\alpha = 0.4$  is sufficient to avoid relative displacements between beam and column. Conversely, sliding may occur in some case due to the combined effect of horizontal and vertical components of the ground motion.

As a second case, consider a front frame with a masonry infill wall and a strip window on the top of it, whose height is  $h_1 = h/3$  (see Single-storey single-bay precast frame (a) without masonry infill and (b) with an infill wall provided with a strip window between precast beam and wall(b)). When the roof is oscillating due to the seismic excitation, the two columns exhibit different lateral stiffnesses because of the interaction with the infill: under the assumption that the left column has a deformable length equal to  $h_1$ , and thus behaves as a cantilever with the fixed cross-section located at  $h-h_1 = (2/3)h$  from the base, the lateral stiffness of the right column is  $K = 3EI/h^3$ , whereas that of the left column is 27 times greater. Hence, almost the whole horizontal force will be carried out by the left column (Figure 61(b)), i.e.,  $F_{h1} \cong \alpha M g$  and  $F_{h1}/F_{v1} = 2\alpha = 0.8$ . Though ignoring the possibility of a short column failure for the left column, such a ratio between horizontal and vertical forces, certainly greater than the concrete-to-concrete friction coefficient, indicates that the falling down of the beam from the column is to be expected. In the pushover curve of Fig. 2.4 reported by Casotto et al. [50] the collapse due to connection failure is reached before the attainment of the flexural strength in the columns.

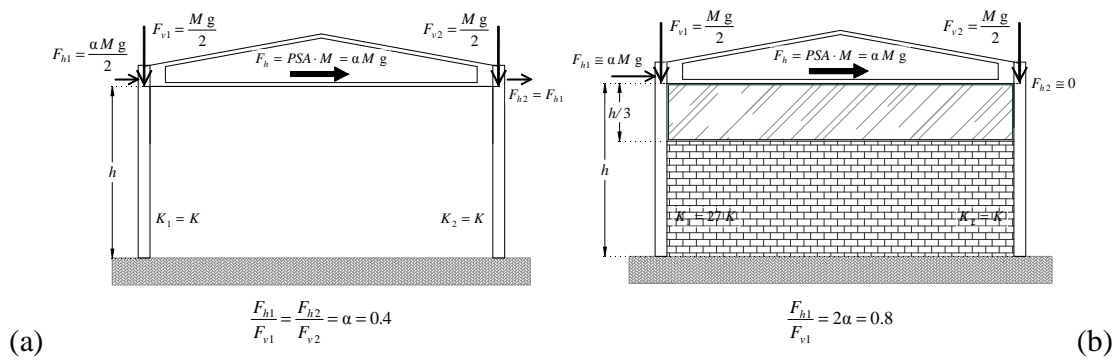


Figure 61. Single-storey single-bay precast frame (a) without masonry infill and (b) with an infill wall provided with a strip window between precast beam and wall

## 5.4 Conclusions

The results obtained from the analysis of damage data concerning more than 1800 precast RC industrial buildings hit by the 2012 Emilia seismic sequence are presented in the paper. About 96% of the buildings examined are located in the struck region at epicentral distances not larger than 30 km and represent about 30% of the total stock of industrial buildings in the area. The strong motion data used in the study were obtained from the shakemaps of the two mainshocks that occurred on May 20<sup>th</sup> and 29<sup>th</sup>, with  $M_L = 5.9$  and 5.8, respectively. In particular, for each building, three

parameters were considered to establish the earthquake intensity, i.e., distance from the nearest epicentre, PSA at 1 s associated with the nearest epicentre, and maximum experienced PGA.

A six level damage scale, substantially corresponding to those given by EMS-98, was defined. The first level (D0) corresponds to undamaged buildings, whereas damage levels D1 to D5 refer to increasing levels of damage, from slight damages on non-structural elements up to partial or full building collapse. Then, on the basis of some correlations observed, the damage data were grouped into the three classes D0, D1+D2, and D3+D4+D5.

It was found that approximately 90% of the buildings of damage class D3+D4+D5 included in the study are located within 16 km from the epicentre and experienced a PSA larger than 0.12g. For 10% of the severely damaged to collapsed buildings, the PSA was larger than 0.29g. It is worth observing that approximately 20% of the buildings that experienced a  $PSA \geq 0.20g$  were nevertheless undamaged. The circumstance that also close to the epicentres a significant number of buildings resulted undamaged indicates that some precast building typologies present a relatively low seismic vulnerability.

The damage distributions in terms of the maximum experienced PGA are characterized by a sudden increase in the number of damaged buildings for  $PGA \geq 0.28g$ . This slope change is a consequence of the non-uniform distribution of the buildings included into the database and of the spatial distribution of the PGA.

Since very heavy damages and collapses were observed in a significant number of buildings up to about 15 km from the epicentres, and moderate damages affected buildings located up to 25-30 km from the epicentres (Figure 60), further developments of the present investigation will be dedicated to a deeper analysis of the most common typologies of precast buildings, in order to put in evidence all possible sources of seismic vulnerability, as shown in the following chapter.

## **6. EMPIRICAL SEISMIC FRAGILITY FOR THE PRECAST RC INDUSTRIAL BUILDINGS DAMAGED BY THE 2012 EMILIA (ITALY) EARTHQUAKES**

### **6.1 Introduction**

In present economy, seismic loss estimation is extremely important for planning civil protection strategies and for predicting costs for restoring or retrofitting damaged buildings after earthquakes. Fragility curves are a fundamental tool for seismic risk assessment. These curves relate the probability of exceeding a particular damage level to ground-motion intensity [64] They can be obtained using different approaches, mainly statistical analysis of observational damage data or numerical modelling.

Observational damage data from past earthquakes are commonly used worldwide for the development of new empirical fragility curves or for validating existing ones based on mechanical models. D'Ayala et al. [65] used damage data from the 1755 Lisbon (Portugal) earthquake for estimating fragility functions suitable for Europe's historic city centres. Yamaguchi and Yamazaki [66] developed fragility functions for five different building typologies in Japan using damage data from the 1995 Kobe earthquake. Rossetto and Elnashai [67] derived empirical vulnerability curves for reinforced concrete (RC) buildings from 99 datasets collecting field observations from 19 earthquakes and including about 340000 buildings. Karababa and Pomonis [68] obtained a set of vulnerability curves for five building typologies in Lefkada Island, Greece. In their proposal, the authors used damage data collected after the earthquake that occurred in the island on August 14, 2003, and related the vulnerability of the buildings to the Parameterless Scale of Seismic Intensity (PSI) [69]. Molina et al. [70] recently used a damage database concerning about 67500 buildings struck by the 2010 Haiti earthquake for calibrating vulnerability curves for the city of Port-au-Prince. For the same destructive event, new fragility functions based on two separate methods of damage assessment, including field surveys and remote sensing, were obtained in [71]. With reference to Italian buildings, mainly comprised of low- to mid-rise masonry and RC structures, Rota et al. [72] proposed typological fragility curves based on earthquake damage data collected in the past 30 years. In Ref. [73], the possible sources of uncertainty that can affect empirical vulnerability curves were identified, such as the errors in ground shaking prediction and building exposure, the use of census data to establish the number of buildings in each municipality for each building typology, the incompleteness and deficiencies in survey forms, and the errors in data post-processing. For a recent, comprehensive review of the existing empirical fragility functions, see Ref. [74].

When numerical procedures are used to evaluate the seismic fragility of structures, damage is generally estimated using results obtained from numerical models. In nonlinear analysis methods, the attainment of a particular damage level, corresponding to a given limit state, can be defined in terms of material strains [75][76], interstorey drifts or chord rotations [77], and other Engineering

Demand Parameters [78]. Although the analysis method influences the vulnerability assessment of structures, Silva et al. [79] showed that, for a given structural typology, fragility curves are not particularly sensitive to the type of numerical analysis adopted. Of course, in order to be able to make reliable predictions, numerical models must be able to represent all the possible damage mechanisms that can affect the category of buildings under consideration, as well as possible inhomogeneities and irregularities. This aspect is crucial, for instance, for masonry structures, where both local and global collapse mechanisms must be captured by models, but also for precast RC industrial buildings. In fact, the dynamics of these structures can be strongly affected by infill walls or intermediate floors covering only a limited portion of the plan. These elements, because of limited structural redundancy, can facilitate the onset of failure mechanisms. For these reasons, observational models based on field results are very important to assess and calibrate numerical prediction models. The present chapter focuses on the definition of observational fragility curves for RC precast buildings using damage data collected after the Emilia seismic sequence that struck the north of Italy in 2012.

The present chapter presents the damage data collected, using both field surveys and technical reports prepared for obtaining public funds for reconstruction. The distribution of the buildings for which damage data were collected is analysed using cadastral data as a reference. Damage data are then used to define damage matrices from which empirical fragilities are estimated. Finally, parametric fragility curves for the different damage states under consideration are fitted using a Bayesian approach. Two main categories of models are adopted: fragility models based on the exceedance of individual damage states, and ordinal models that maintain ordinality among the fragility of damage states. The uncertainty on the ground-motion estimate is discussed and included in the ordinal model. When compared with fragility curves for RC buildings reported in the literature, the results presented here show that Italian precast structures for industrial-buildings are characterized by much higher seismic vulnerability than cast-in-place RC frame structures and therefore require specific fragility models.

## **6.2 Damage distribution vs. ground-motion intensity**

Over the largest part of the territory, the maximum ground-motion intensity was recorded during the two mainshocks, occurred on 20 May ( $M_w = 6.1$ ) and 29 May ( $M_w = 6.0$ ), 2012 [60]. Therefore, the measures of ground-motion intensity adopted in the present study refer to these two seismic events only.

### **6.2.1 Definition of ground-motion intensity**

The ground-motion intensity at the different building locations was obtained from the official shakemap data published online by Istituto Nazionale di Geofisica e Vulcanologia (INGV) [80].

These data provide information on the intensity of ground-shaking in terms of either PGA, PGV, and Pseudo-Spectral Accelerations (PSA) at 0.3 s, 1.0 s and 3.0 s, combining actual ground-motion recordings and predictions from attenuation relationships. These shakemaps are computed assuming that the ground-motion intensity at each location is lognormally distributed. For the fragility assessment presented in the following, after analysing the ground-motion accelerograms from the recording stations and the site-to-site variability of different possible ground-motion intensity measures, the maximum horizontal PGA was chosen as measure of ground-motion intensity. In fact, spectral accelerations at different natural periods were characterized by a very large variability.

Figure 62 Figure 1a-b show the shakemaps for the median value of the horizontal PGA referred to the 20 May and 29 May earthquakes, respectively. Figure 62-c-d show maps of the standard deviation of the natural logarithm of PGA for the two events. The uncertainty on the shakemaps for the two earthquakes is very different. In fact, many temporary ground-motion recording stations were installed after the first mainshock, and therefore the shakemaps for the subsequent shocks (and in particular for the earthquake occurred on 29 May, 2012) are more accurate. The logarithmic standard deviation of PGA will be used in the derivation of the fragility curves presented in Section 5.4. For a discussion on the level of approximation of the official shakemaps for the Emilia earthquakes see [63], [81].

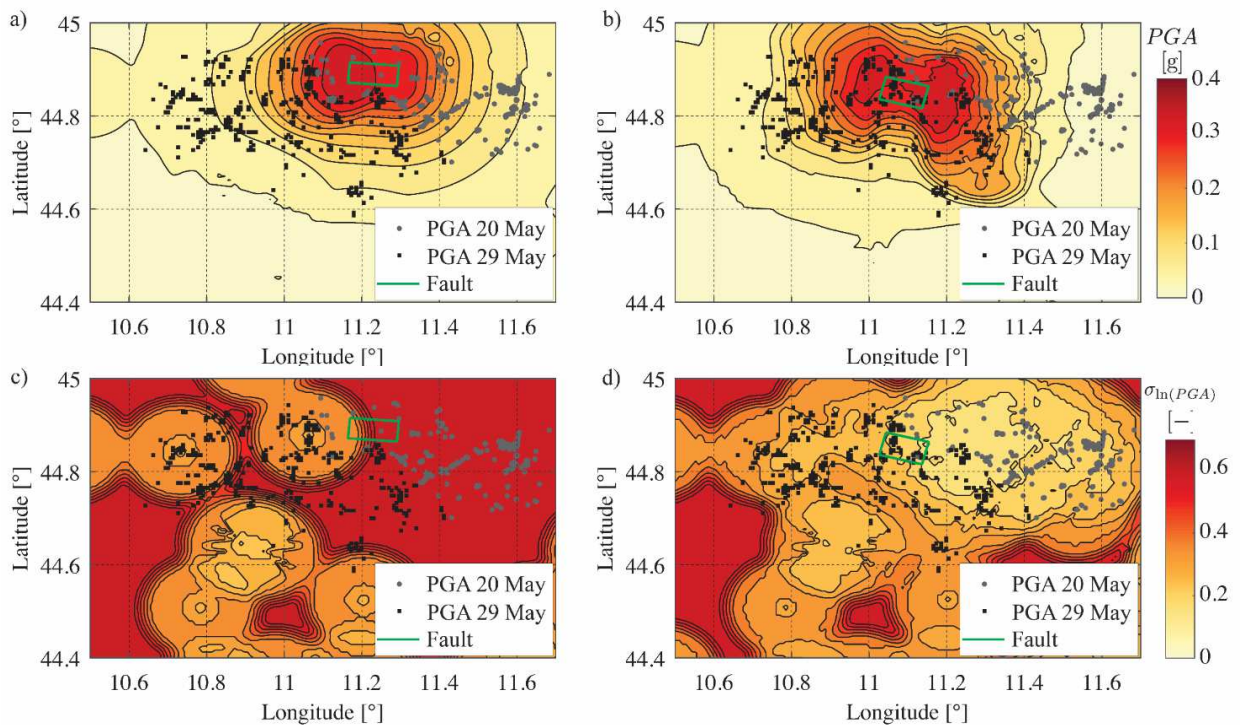


Figure 62. Shakemaps for (a-b) the median value of the horizontal PGA, and (c-d) for its logarithmic standard deviation (SD), for (a, c) the 20 May and (b, d) 29 May earthquakes. Grey dots and black squares indicate the locations of the buildings in database associated to the PGA of 20 May and 29 May, respectively.

Since the strong-motion parameters provided by INGV are referred to a dense spatial grid with nodes every 1 km, according to the rule suggested by the Italian Building Code [**Errore. L'origine riferimento non è stata trovata.**] the PGA at each building location was computed as the weighted mean value of the PGAs at the four closest grid nodes, with the  $i$ -th weight being the reciprocal of the distance between the location and the  $i$ -th node.

For each building, the value of the ground-motion intensity considered was the maximum between those related to the two mainshocks of 20 and 29 May. Grey dots and black squares in Figure 62 indicate the locations of the buildings in the database associated to the 20 May and 29 May PGA, respectively. Note that for most of the buildings associated to the 20 May ground-motion the logarithmic standard deviation (Figure 62 c-d), is as large as 0.6, which corresponds to the total standard deviation of the attenuation relationships used to compute the shakemaps.

Considering, as ground-motion intensity, the maximum PGA generated by the two mainshocks, corresponds to assuming that the damage produced by the two seismic events was not correlated. This assumption is supported by the outcomes of field surveys [7]. In fact, the prefabricated RC structures in the area were typically characterized by extremely fragile failure modes since they did not have any structural redundancy and featured friction-based connections between elements. Even when mechanical connectors were present, their strength was insufficient because they were not designed for seismic actions, but only to facilitate the assembly of prefabricated structural members during construction [7]. Therefore, these structures had no redistribution capacity. This behaviour was highlighted by some field surveys carried out after both the mainshocks, especially in the Mirandola area. This industrial area is particularly interesting because, during the two events, it experienced similar PGA values (recorded by a permanent accelerometric station), i.e.  $258 \text{ cm/s}^2$  and  $288 \text{ cm/s}^2$ , respectively. In spite of the similar PGA values, there were many cases of buildings totally undamaged after 20 May which collapsed on 29 May because of failures in friction-based connections, the most common of which were the unseating of either beams from columns or roofing elements from beams [7]. Of course, near-source effects might have contributed to the collapses occurred on May 29 [7].

### 6.2.2 Damage distribution versus PGA

The cumulative number of buildings with damage level  $D$  greater than or equal to either  $D_0$ ,  $D_1$ , or  $D_3$  is reported in Figure 63, together with the cumulative number of buildings estimated from cadastral data (see Sections 2.2 and 2.3), versus the maximum horizontal PGA.

For  $\text{PGA} \leq 0.28g$ , there are 1267, 385, and 72 buildings with damage  $D \geq D_0$ ,  $D \geq D_1$ , and  $D \geq D_3$ , respectively. For high accelerations the curves feature a sudden step. Since this peculiar shape can be observed also for  $D \geq D_0$  (i.e. the whole database) and for the building stock estimated from cadastral units, the step must be a consequence of the non-uniform distribution of buildings (see Section 2.3) and of the spatial distribution of PGA. In fact, the curve derived from cadastral data is completely independent from damage and unaffected by the procedure used to collect data. On the

other hand, it is worth noticing that the relative increment in the number of damaged buildings before and after the step is much higher for  $D \geq D_3$  (+323%) than for  $D \geq D_1$  (+122%) and  $D \geq D_0$  (+45%). Therefore, these different percentages might suggest that a portion of the sudden increment in the number of buildings with at least severe damage could be related to the activation of specific damage modes. Finally, the similitude of the shapes of the curves for  $D \geq D_0$  and for the building stock estimated from cadastral data is an indicator of the soundness of the data collection procedure.

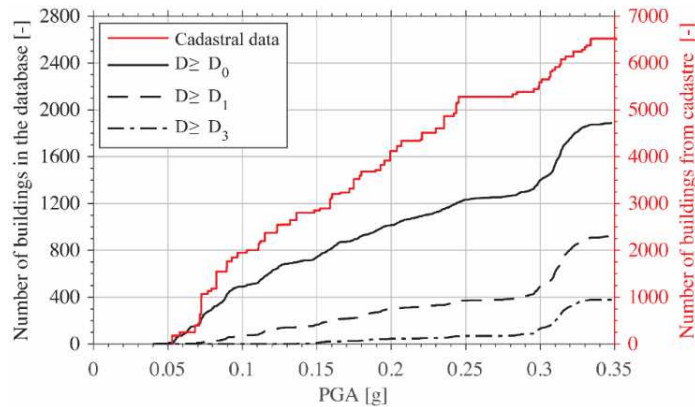


Figure 63. Cumulative number of industrial buildings, in the survey area, which experienced a peak ground acceleration less or equal to the PGA values reported in abscissa: building stock from cadastral data (right axis), all buildings in the database ( $D \geq D_0$ ), buildings with damage level  $D \geq D_1$ , and  $D \geq D_3$ .

## 6.3 Damage analysis and fragility

### 6.3.1 Damage data

In order to analyse the fragility of the buildings in the database, the 1890 damage data were categorized into the damage matrix reported in Table 9 [82], considering seven intervals for the PGA (column  $I_{PGA,i}$ ). The criteria used to define these intervals will be discussed at the end of Section 4.2 being related to fragility estimation. Table 9 provides, for each PGA interval, the number of buildings associated to each damage level. For example, among the 257 buildings that experienced a PGA between 0.297g and 0.313g, 35 were undamaged ( $D=D_0$ ), and 44, 52, 35, 25, and 35 buildings were classified in damage levels  $D_1$ ,  $D_2$ ,  $D_3$ ,  $D_4$ , and  $D_5$ , respectively.

Moreover, from Table 9 the cumulative damage matrix reported in Table 10 was obtained. This table shows the number of buildings which were exposed to a PGA belonging to the interval indicated in the first column, and that were associated to a damage level greater than or equal to  $D_j$ . For instance, 126 of the 257 buildings that experienced a maximum horizontal PGA between

0.297g and 0.313g had damage levels greater than  $D_3$ . Of course, the column  $D \geq D_0$  indicates the total number of buildings for each PGA interval.

$I_{PGA,i}$ [g]	$D = D_0$	$D = D_1$	$D = D_2$	$D = D_3$	$D = D_4$	$D = D_5$
[0.000 - 0.076[	249	21	1	0	1	0
[0.076 - 0.112[	205	57	6	0	0	0
[0.112 - 0.159[	158	80	10	4	8	10
[0.159 - 0.216[	153	74	18	7	3	15
[0.216 - 0.297[	133	51	27	19	14	26
[0.297 - 0.313[	35	44	52	35	25	66
[0.313 - 0.349[	34	44	60	40	25	80
<i>Total</i>	967	371	174	105	76	197

Table 9. Damage matrix for all buildings collected in the database: number of buildings for each damage level vs. intervals of PGA.

$I_{PGA,i}$ [g]	$D \geq D_0$	$D \geq D_1$	$D \geq D_2$	$D \geq D_3$	$D \geq D_4$	$D = D_5$
[0.000 - 0.076[	272	23	2	1	1	0
[0.076 - 0.112[	268	63	6	0	0	0
[0.112 - 0.159[	270	112	32	22	18	10
[0.159 - 0.216[	270	117	43	25	18	15
[0.216 - 0.297[	270	137	86	59	40	26
[0.297 - 0.313[	257	222	178	126	91	66
[0.313 - 0.349[	283	249	205	145	105	80
<i>Total</i>	1890	923	552	378	273	197

Table 10. Cumulative damage matrix for all buildings in the database.

### 6.3.2 Point estimates of fragility

Using the cumulative damage matrix, it is possible to obtain a first estimate of the fragility of the buildings. In fact, the probability of observing  $n_{i,j}$  buildings with damage  $D \geq D_j$  in the  $i$ -th ground-motion intensity interval  $I_{PGA,i}$  can be represented by the following binomial distribution [Errore. L'origine riferimento non è stata trovata.]:

$$P(n_{i,j} \text{ in } N_i \text{ with } D \geq D_j | PGA \in I_{PGA,i}) = \binom{N_i}{n_{i,j}} p_{i,j}^{n_{i,j}} (1 - p_{i,j})^{N_i - n_{i,j}} \quad (1)$$

where  $\binom{N_i}{n_{i,j}}$  indicates the binomial coefficient,  $N_i$  is the total number of buildings in the  $i$ -th PGA interval,  $I_{PGA,i}$  and  $p_{i,j}$  represents the probability of observing damage  $D \geq D_j$  in that interval. This probability can be estimated as:

$$p_{i,j} = n_{i,j} / N_i \quad (2)$$

and its variance as:

$$\text{var}(p_{i,j}) = p_{i,j} (1 - p_{i,j}) / N_i \quad (3)$$

where  $\hat{\cdot}$  indicates estimates.

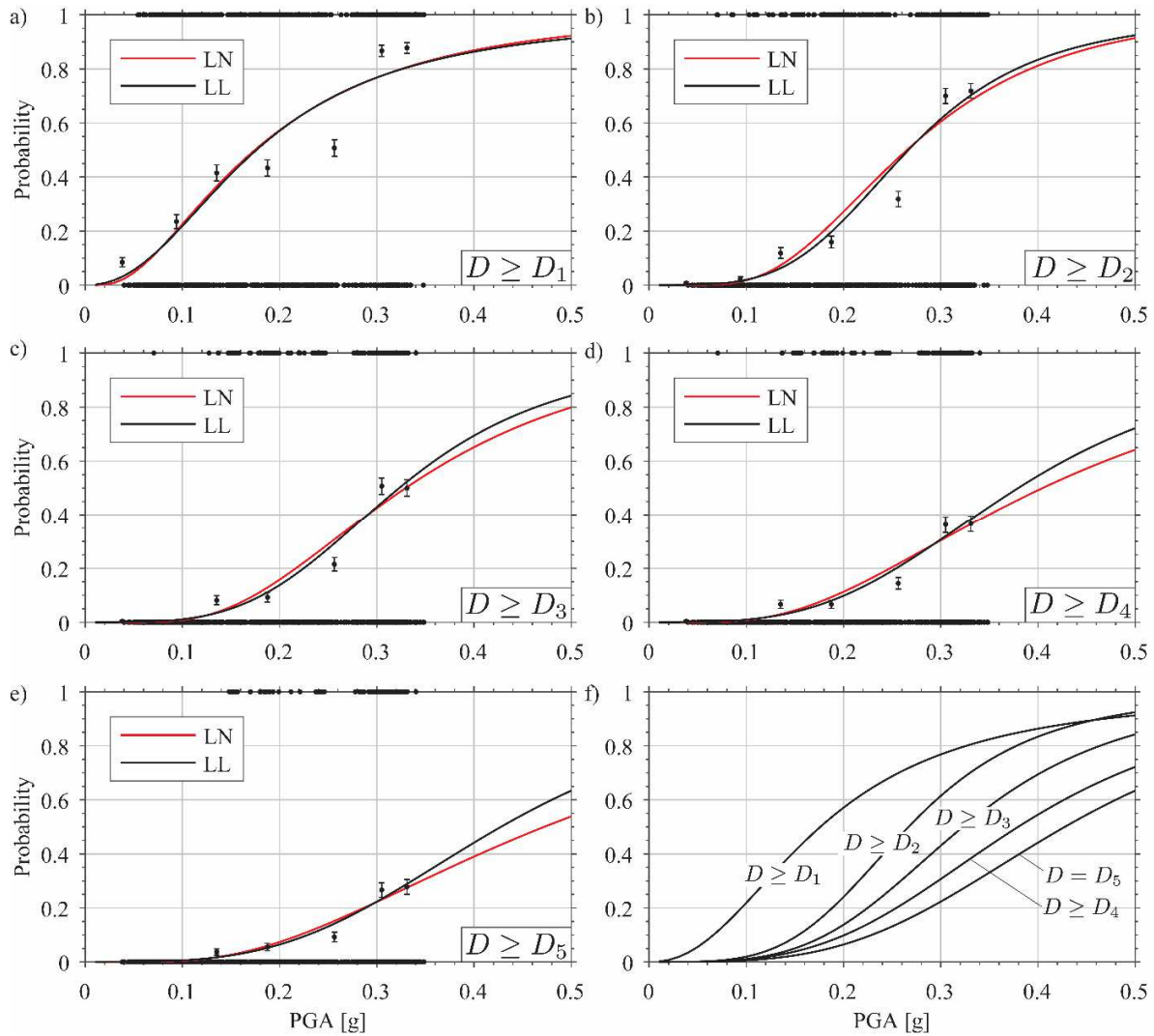


Figure 64. (a-e) comparison among failure probabilities for damage levels  $D_1$  to  $D_5$ , point-estimates from damage matrices (black circles), lognormal (LN) and log-logit (LL) parametric fragility curves obtained by maximum likelihood estimation; (f) LL parametric fragility curves for the various damage levels.

Using the data of the damage matrix reported in Table 10 together with Eq. (2), the failure probabilities for  $D \geq D_j$  ( $j = 1$  to 4) and  $D = D_5$  were estimated. These probabilities are given in Table 11. Estimated failure probability for each damage level. The central value  $\mu_{PGA,i}$  of each

interval, defined as the arithmetic mean of the PGA values, is also reported. The damage probabilities in Table 11 are also plotted in Figure 64. (a-e) comparison among failure probabilities for damage levels  $D_1$  to  $D_5$ , point-estimates from damage matrices (black circles), lognormal (LN) and log-logit (LL) parametric fragility curves obtained by maximum likelihood estimation; (f) LL parametric fragility curves for the various damage levels. (black circles), together with  $\pm 1$  standard deviation intervals obtained from Eq. (3).

The boundaries of the 7 PGA intervals were selected in order to: *i*) have a similar number of buildings in each interval (approximately 270) [82], see the column  $D \geq D_0$  of Table 10 and; *ii*) obtain, for each damage level, non-decreasing exceedance-probability values for increasing PGAs. It should be noted that the intervals adopted were used only to provide a graphical representation of fragility and do not affect the parametric fragility models discussed in the following.

$I_{PGA,i} [g]$	$\mu_{PGA,i} [g]$	$D \geq D_1$	$D \geq D_2$	$D \geq D_3$	$D \geq D_4$	$D = D_5$
[0.000 - 0.076]	0.04	0.08	0.01	0.00	0.00	0.00
[0.076 - 0.112]	0.09	0.24	0.02	0.00	0.00	0.00
[0.112 - 0.159]	0.14	0.41	0.12	0.08	0.07	0.04
[0.159 - 0.216]	0.19	0.43	0.16	0.09	0.07	0.06
[0.216 - 0.297]	0.26	0.51	0.32	0.22	0.15	0.10
[0.297 - 0.313]	0.31	0.86	0.69	0.49	0.35	0.26
[0.313 - 0.349]	0.33	0.88	0.72	0.51	0.37	0.28

Table 11. Estimated failure probability for each damage level.

## 6.4 Parametric fragility curves

### 6.4.1 General approach

Parametric fragility curves were fitted starting from the damage data described above. Various models and regression procedures have been proposed in the literature to obtain fragility curves from observational data, as described in the comprehensive review recently published by Lallemand et al. [83]. In the present work, different models were considered, adopting a Bayesian approach in order to estimate their parameters [83].

In the Bayesian framework adopted, a general parametric fragility model can be defined as a function dependant on ground-motion intensity  $IM$  and on a set of unknown regression parameters  $\Theta$ :

$$P_f(IM) = f(IM; \Theta). \quad (4)$$

In Bayesian statistics the current knowledge of  $\Theta$  is defined by a joint density  $f(\Theta)$  function, referred to as priori distribution. Once a vector  $y$  of observed data is available, the Bayes

theorem can be used to update the knowledge of the parameters, so obtaining a posterior distribution:

$$f(\Theta|\mathbf{y}) = \frac{P(\mathbf{y}|\Theta)f(\Theta)}{P(\mathbf{y})} = \frac{P(\mathbf{y}|\Theta)f(\Theta)}{\int P(\mathbf{y}|\Theta)f(\Theta)d\Theta} \quad (5)$$

where the function  $P(\mathbf{y}|\Theta)$  is referred to as likelihood function,  $L$ . The integrals involved in Eq. 5 can be complicated for some combinations of priori distributions and likelihood functions but they can be easily solved using computational algorithms based on Markov Chain MonteCarlo methods (MCMC) and Gibbs sampling [81].

#### 6.4.2 Fragility curves based on individual damage levels

The present Section describes the procedure adopted for fitting parametric fragility models for the general damage exceedance condition  $D \geq D_j$ . To this aim, the observed damage data is first transformed, for each damage level  $D_j$ , into a binary variable  $y_{i,j}$  which is equal to 1 if, in the  $i$ -th building, damage is not less than  $D_j$  and 0 otherwise. Assuming that the damage data  $y_{i,j}$  are independent and identically distributed (i.i.d.) the likelihood function  $L_j$  for the general damage level  $D_j$  can be defined as [Errore. L'origine riferimento non è stata trovata., 2, 83]:

$$L_j = P(\mathbf{y}_j|\Theta_j) = \prod_{i=1}^N (1 - p_{i,j}(IM_i; \Theta_j))^{(1-y_{i,j})} p_{i,j}(IM_i; \Theta_j)^{y_{i,j}} \quad (6)$$

where  $N$  indicates the total number of buildings observed,  $p_{i,j}$  represents the probability to exceed the damage level under consideration for the ground-motion intensity  $IM_i$ ,  $\Theta_j$  indicates the model parameters, and  $\mathbf{y}_j$  is a vector collecting the binary observations  $y_{i,j}$  for the damage level  $D_j$ , i.e.  $\mathbf{y}_j = [y_{1,j}, \dots, y_{N,j}]$ . Eq. 6 corresponds to assuming that each binary damage observation,  $y_{i,j}$ , follows a Bernoulli distribution,  $B$ , with probability  $p_{i,j}$ :

$$y_{i,j} \sim B(1, p_{i,j}(IM, \Theta_j)) \quad (7)$$

It is worth noticing that the whole dataset is used for evaluating the likelihood function (6) for each damage level  $D_j$ .

In the present work, two different models were considered for expressing  $p_{i,j}$  as a function of ground-motion intensity: a lognormal (LN) and a log-logit (LL) model. In the first case the failure probability  $p_{i,j}$  is written as

$$p_{i,j} = \Phi\left(\frac{\ln(IM_i) - \mu_j}{\sigma_j}\right) \quad (8)$$

where  $\Phi(\cdot)$  indicates the standard normal cumulative distribution function. For each damage level  $D_j$ , the model parameters are  $\Theta_j = [\mu_j, \sigma_j]$ . In the second case, the failure probability is written as

$$\text{logit}(p_{i,j}) = \beta_{0,j} + \beta_{1,j} \ln(IM_i), \quad (9)$$

and the model parameters are  $\Theta_j = [\beta_{0,j}, \beta_{1,j}]$ . In both models the logarithm of the ground-motion intensity was considered as covariate, in order to avoid non zero damage probability for  $IM = 0$ .

Bayesian regression was carried out using the software R and JAGS [4, 5] in order to estimate the parameters of the models. Convergence of the MCMC chains was checked by computing the potential scale reduction factor [81]. Three MCMC chains were used. Uninformative distributions were adopted as priori distributions of the model parameters. The two different models, i.e. LN and LL, were compared using the Deviance Information Criterion (DIC), which is preferable than other criteria as AIC and BIC when using MCMC Bayesian regression [81]. The DIC is computed based on the deviance of a model and its number of parameters and, given the same goodness of fit to a dataset, will favour models with less parameters [81].

Figure 64 shows the fragility curves obtained using the LN and the LL models. Black dots at the top and bottom of each panel represent the binary damage data,  $y_j$ , used for fitting the models for each damage state  $D_j$ . Table 12. Mean value (E) and standard deviation (SD) of the posterior distribution of the parameters of the log-logistic models (LL) for the different damage states. lists the mean values (used as estimates of the parameters) and the standard deviation of the posterior distribution for the two parameters of the LL model. For all the damage states considered the DIC indicated the LL model as preferable, even if by a low margin.

Note that the curve for  $D \geq D_1$  slightly overlaps the curve for  $D \geq D_2$  starting from PGA values larger than 0.45 g, which is clearly unjustifiable from a theoretical point of view. It is worth noticing that the dataset used has a maximum PGA value of 0.35g and, obviously, extrapolations of the fragility curves are more uncertain. A possible solution to overcome this issue is using statistical models that force ordinality of the damage states [**Errore. L'origine riferimento non è stata trovata.**]. This approach will be discussed in the following.

	$D \geq D_1$	$D \geq D_2$	$D \geq D_3$	$D \geq D_4$	$D = D_5$
$E[\beta_0][-]$	3.902	5.268	4.329	3.360	3.001
$SD[\beta_0][-]$	0.192	0.301	0.344	0.371	0.445
$E[\beta_1][1/\ln(g)]$	2.247	3.987	3.839	3.467	3.527
$SD[\beta_1][1/\ln(g)]$	0.108	0.214	0.258	0.281	0.344

Table 12. Mean value (E) and standard deviation (SD) of the posterior distribution of the parameters of the log-logistic models (LL) for the different damage states.

### 6.4.3 Fragility curves using ordinal models

In the present section, an ordinal log-logistic (OLL) model is presented with the aim of avoiding overlapping fragility curves. In particular, a link GLM (Generalised Linear Model) was used [6]. Alternative approaches are presented in Agresti [7]. In the model adopted in this section all the damage states are considered together and a single likelihood function is defined. In this section, the damage for the  $i$ -th building is defined in terms of an ordinal damage variable  $y_i$ , which can assume integer values from 0 to 5, corresponding to damage levels ranging from  $D_0$  to  $D_5$ , respectively.

The OLL model first requires to define a continuum latent variable  $y_i^*$ , which is here assumed to have a logistic distribution, on which linear regression is carried out, considering the logarithm of the ground-motion intensity as covariate:

$$y_i^* = \ln(IM_i)\beta + \epsilon_i, \quad \epsilon \sim \text{Logistic}(0, s), \quad i = 1, \dots, N, \quad (10)$$

where  $\beta$  is an unknown regression parameter,  $\epsilon$  is a logistically distributed random variable with 0 mean and scale parameter  $s$ . Using a normal distribution for  $\epsilon$  would generate a cumulative probit model. In the present work, a proportional odds model was assumed, i.e. the  $\beta$  parameter value does not depend on the damage level [7]. This assumption is required in order to avoid overlapping fragility curves. The continuum latent variable  $y_i^*$  is mapped to the ordinal damage variable  $y_i$  corresponding to damage levels  $D_0$  to  $D_5$  (see Table 2), using the following scheme:

$$\begin{aligned} y_i^* \leq \tau_0 &\Rightarrow y_i = 0 \\ \tau_{j-1} < y_i^* \leq \tau_j &\Rightarrow y_i = j, \quad 1 \leq j \leq 4 \\ y_i = 5 &\Leftrightarrow y_i^* > \tau_4 \end{aligned} \quad (11)$$

where  $j$  indicates the general damage level, and  $\tau_0$  to  $\tau_4$  are unknown threshold, to be defined by regression, fulfilling the ordering constraint  $\tau_0 < \tau_1 < \tau_2 < \tau_3 < \tau_4$ . The probability of observing the different damage levels can be computed as:

$$\begin{aligned} P[y_i = 0] &= P[y_i^* \leq \tau_0] \\ P[y_i = j] &= P[\tau_{j-1} < y_i^* \leq \tau_j], \quad 1 \leq j \leq 4 \\ P[y_i = 5] &= P[y_i^* > \tau_4] \end{aligned} \quad (12)$$

which can be easily evaluated using the cumulative logistic distribution function as illustrated by Figure 65. (a) PDF and (b) CDF for  $y_i^* | IM_i, \beta$  and  $y_j^* | IM_j, \beta$ , with  $IM_j > IM_i$  and  $\beta > 0$ . The boundaries of the intervals used to map the continuum latent variables  $y_i^*$  and  $y_j^*$  to the ordinal damage variables  $y_i$  and  $y_j$  are indicated by dashed lines. The areas corresponding to the probability of observing damage  $D_i = D_1$  (i.e.  $y_i = 1$ ) and  $D_j = D_1$  (i.e.  $y_j = 1$ ) are hatched in (a). **Errore. L'origine riferimento non è stata trovata.** Finally, assuming that data are i.i.d. and defining an indicator variable  $\delta_{i,j}$  which is 1 if  $y_i = j$  (i.e. if damage in the  $i$ -th building is equal to  $D_j$ ) and 0 otherwise, the likelihood function  $L$  for the model can be written as:

$$L = \prod_{i=1}^N \prod_{j=0}^5 P[y_i = j]^{\delta_{i,j}} \quad (13)$$

The parameters of the so defined model are unidentifiable. In fact, any change in the scale parameter  $s$  in Eq 10 can be balanced by changes in  $\tau$  and  $\beta$ . Therefore, this model requires a set of normalization constraints. In the present work, the scale parameter  $s$  was set to 1 [6]. For the same reason, no intercept parameter was defined in Eq. 10. In fact, this latter would be balanced by shifting all the threshold values  $\tau_0, \dots, \tau_4$ . Under these assumptions, the parameters of the model are  $\Theta = [\beta, \tau_0, \tau_1, \tau_2, \tau_3, \tau_4]$ .

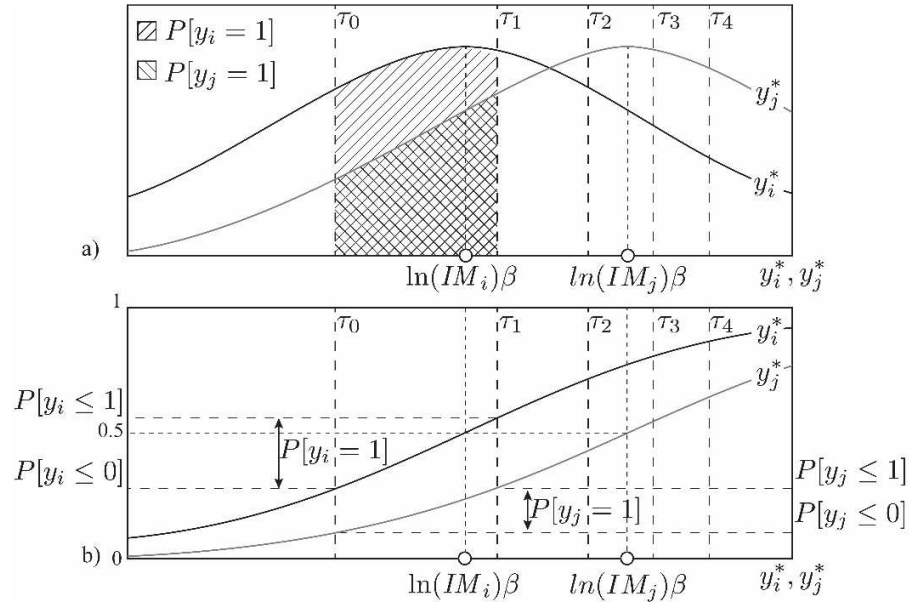


Figure 65. (a) PDF and (b) CDF for  $y_i^* | IM_i, \beta$  and  $y_j^* | IM_j, \beta$ , with  $IM_j > IM_i$  and  $\beta > 0$ . The boundaries of the intervals used to map the continuum latent variables  $y_i^*$  and  $y_j^*$  to the ordinal damage variables  $y_i$  and  $y_j$  are indicated by dashed lines. The areas corresponding to the probability of observing damage  $D_i = D_1$  (i.e.  $y_i = 1$ ) and  $D_j = D_1$  (i.e.  $y_j = 1$ ) are hatched in (a).

As suggested in [89], uninformative normal priori distributions were used for the model parameters. Furthermore  $\beta$  and  $\tau_0, \dots, \tau_4$  were assumed as independent a priori [89]. Convergence of the MCMC chains was checked, as discussed in Section 5.2. The mean value and the standard deviation of the posterior distribution of the parameters are reported in **Errore. L'origine riferimento non è stata trovata.**

Considering the linear structure of the regression model in Eq. (10), associated to a non-negative value of the estimate for the  $\beta$  parameter, and that cumulative distribution functions are non-decreasing, it is evident that this model will lead to non-overlapping fragility curves.

<i>Model</i>	$E[\beta][1/\ln(g)]$	$E[\tau_0][−]$	$E[\tau_1][−]$	$E[\tau_2][−]$	$E[\tau_3][−]$	$E[\tau_4][−]$
<i>OLL</i>	2.554	-4.508	-3.299	-2.616	-2.136	-1.708
<i>OLL-R</i>	3.306	-5.727	-4.243	-3.404	-2.823	-2.315
	$SD[\beta][1/\ln(g)]$	$SD[\tau_0][−]$	$SD[\tau_1][−]$	$SD[\tau_2][−]$	$SD[\tau_3][−]$	$SD[\tau_4][−]$
<i>OLL</i>	0.103	0.183	0.167	0.161	0.161	0.163
<i>OLL-R</i>	0.187	0.318	0.276	0.255	0.245	0.239

Table 13. Mean value (E) and standard deviation (SD) of the posterior distribution of the parameters of the ordinal log-logistic models with (OLL-R) and without (OLL) ground-motion uncertainty.

#### 6.4.4 Ground-motion uncertainty

An important factor to consider in fragility estimation is the uncertainty in ground-motion data. The adopted shakemaps (see Section 6.2.1) assume that the ground-motion intensity, i.e. PGA in this paper, at each site has a lognormal distribution with median value and logarithmic standard deviation as provided in Figure 62. In other words, the true value of the ground-motion intensity, at the  $i$ -th building location, is not known and can be written as [8]:

$$\ln(IM_i^{true}) \sim \mathcal{N}(\ln(IM_i), \sigma_{\ln(IM),i}); \quad (14)$$

where  $\mathcal{N}$  indicates the normal distribution,  $IM_i$  is the median ground-motion intensity at the  $i$ -th building location (provided by the shakemaps in Figure 62 a-b) and  $\sigma_{\ln(IM),i}$  its corresponding logarithmic standard deviation (see Figure 62 c-d). Figure 66 shows the uncertainty on the PGA associated to each building in the database (see also Figure 62). Vertical bars represent  $\pm 1$  standard deviation intervals on the logarithm of PGA, centred on the median PGA value. In general, the PGAs associated to larger standard deviations are mostly those obtained from the shakemaps for the 20 May earthquake (see red points in Figure 66 and Figure 62 c). It is worth noticing that for the buildings with damage states  $D_3$  to  $D_5$  (Figure 66 d-f) small PGA values systematically feature larger standard deviations than large PGA values.

The error model defined in Eq. (14) is normally referred to as Berkson error model [9]. It differs from traditional covariate error models (e.g. error in variables models) in which one assumes that the measured value of the covariate can be defined as the summation of a true value and a random error term with zero mean [92]). Eq (14) assumes that, on average, the ground-motion prediction is unbiased as suggested by Straub and Der Kiureghian [8]. This assumption is also justified based on the procedure adopted for computing shakemaps [10]. The Berkson error model can be included in MCMC-based Bayesian regression by considering that the IM value at each building location is random. In particular the median ground-motion intensity  $IM_i$  in Eq. (10) is replaced by the random variable  $IM_i^{true}$ . Then, during the MCMC simulations random samples of this latter variable are generated using the PDF defined in Eq. (14).

MCMC Bayesian regression was carried out according to the procedure and criteria described in the previous sections. The mean values and standard deviations of the posterior distributions of the model parameters are reported in Table 13, and the corresponding fragility curves are plotted in Figure 67, together with curves obtained from the models discussed in the previous sections. It is worth noticing that the curves obtained considering the uncertainty on PGA (OLL-R) are, in general, steeper than those provided by the OLL model. This result can be explained considering the non-uniform uncertainty of the PGA associated to the damage data (Figure 66). In fact, as discussed above, low PGA values have larger uncertainties. Therefore, these data are penalized in the regression which will favour points with smaller uncertainties. On the other hand, the standard deviation of the posterior distribution of the OLL-R parameters (see Table 13) is larger than for the OLL model and therefore the confidence on the fragility curve (not plotted here) is reduced.

Clearly, the proportional odds ordinal models provide a worst fit to the data if compared with those discussed in Section 6.4.1, being these latter fitted independently for each damage level. A better fit to the data could be possible introducing higher-order terms (e.g.  $\beta_1 \ln(IM_i)^2$ ) to the linear regression in Eq. (10), but in that case it might be possible to obtain decreasing curves which are not justified theoretically [**Errore. L'origine riferimento non è stata trovata.**]. Furthermore, a direct comparison of the goodness of fit of the ordinal model with those in Section 6.4.2 is not possible because each of these latter uses the full dataset, which is converted into a binary observation variable that will assume different values for each damage level. The models related to the different damage states are therefore fitted independently and have different likelihoods. The ordinal model, on the other hand, uses the full dataset for defining a single likelihood function to obtain fragilities for all damage states. Given these considerations and the different number of regression parameters – in the LL and LN models 2 parameters per damage level are adopted, while in the OLL models 6 parameters in total – the OLL and OLL-R models obviously provide a worst fit to the data if compared to those Section 6.4.2, but have the important advantage of providing non-overlapping fragility functions.

Finally, comparing the fragilities presented in the present work with those available in the literature for cast in place RC frame structures, e.g. [67], it is easy to notice the much higher vulnerability of prefabricated structures, especially as far as the most severe damage levels are considered ( $D_3$ ,  $D_4$  and  $D_5$ ). For example, in Figure 5(c) of [67], providing fragility curves for European-type RC buildings derived from a large observational dataset, the PGA values corresponding to 50% failure probability for the "Extensive", "Partial Collapse", and "Collapse" damage states are 1.65g, 2.11g, and 2.27g, respectively. On the contrary, the PGA values corresponding to 50% failure probability for the fragility curves proposed in the present paper for damage states  $D \geq D_3$ ,  $D \geq D_4$  and  $D = D_5$  are as low as 0.36g, 0.43g, and 0.50g, respectively.

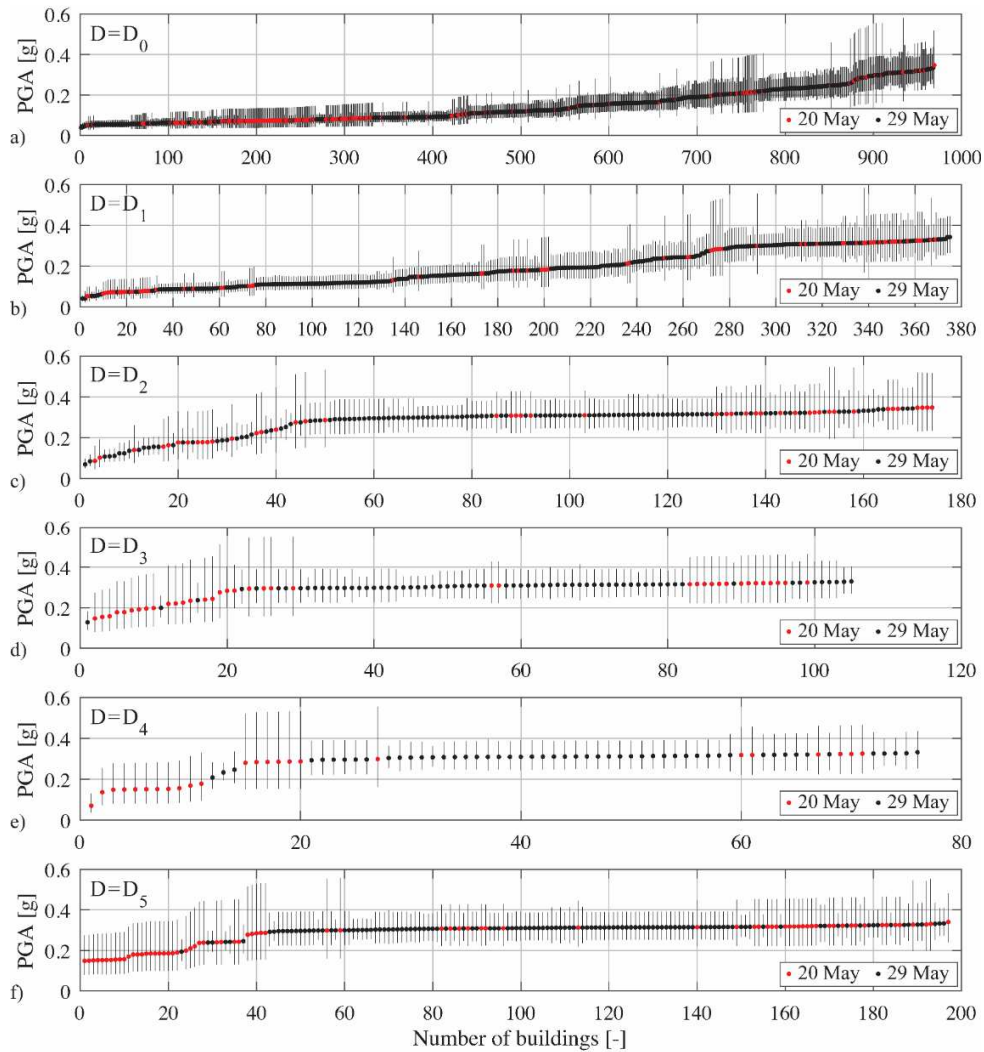


Figure 66. Dataset used for the ordinal regression. Figures a) to f) correspond to damage levels  $D_0$  to  $D_5$ , respectively. Each point represents the median PGA value assigned to a building, colours indicate the earthquake that produced the ground-motion (20 May and 29 May). Vertical bars represent  $\pm$  standard deviation intervals on the logarithm of PGA, centred on the median PGA value.

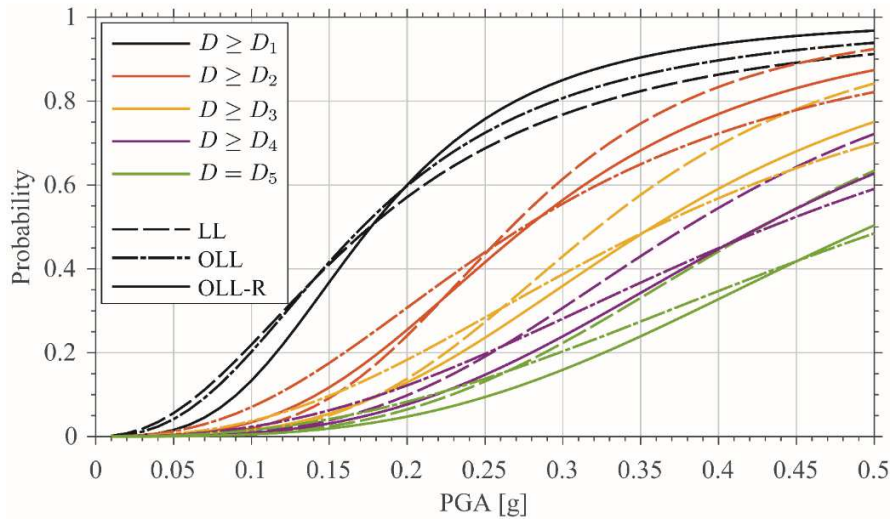


Figure 67. Comparison of fragility curves obtained from the log-logit models (LL), the ordinal log-logistic model (OLL) and the ordinal log-logistic model taking ground-motion uncertainty into account (OLL-R).

### 6.5 Fragility curve distinguished for the different types of precast buildings

The building stock was subdivided into 6 classes with homogenous attributes according to paragraph 4.2. The general approach is the same described at the paragraph 6.1.

In the present work a log-logit (LL) multivariate regression model is used and the failure probability  $p_{i,j}$  is written as

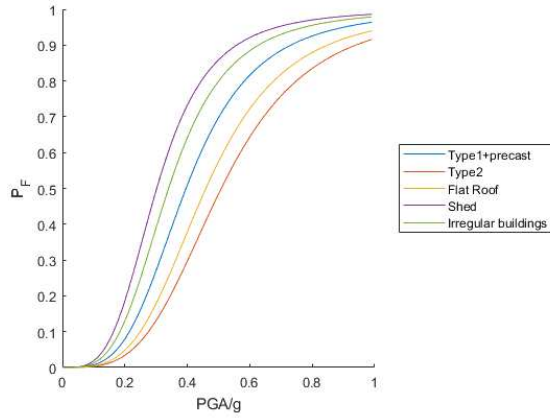
$$\text{logit}(p_{i,j}) = \beta_0 + \beta_1 X_1 + \beta_2 X_2 + \dots + \beta_p (\ln(\text{IM})) \quad (15)$$

Where  $\beta_0; \beta_1; \beta_2; \dots; \beta_p$ , are the model parameters. The first parameter is the constant and then there is a parameter for each building type.

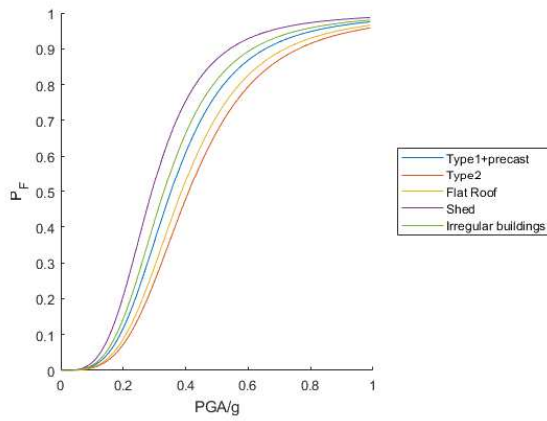
Therefore, Figure 68 shows the fragility curves for each building class considering no ordinal models. Each damage level as to be considered separately.

Type 1 and type 0 are grouped in the same class since the fragility curves were perfectly overlapped. According with the following curves Type 4 (shed) is the most vulnerable typology, followed by Type 5 (Irregular buildings) Type 1 (dsr masonry infills), Type 3 (flat roof) and Type 2 (dsr precast external panels).

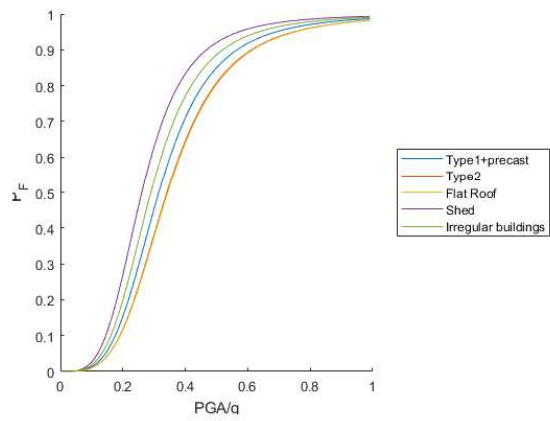
### Damage level 5



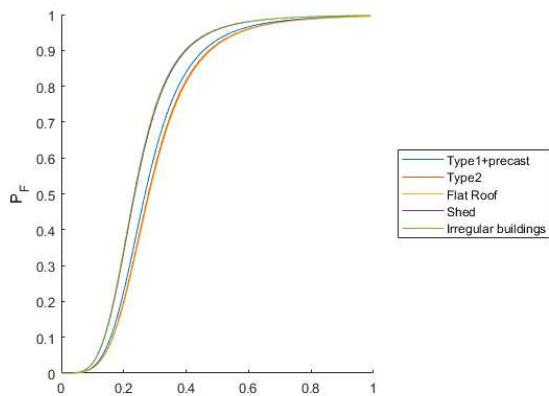
### Damage level 4



### Damage level 3



### Damage level 2



### Damage level 1

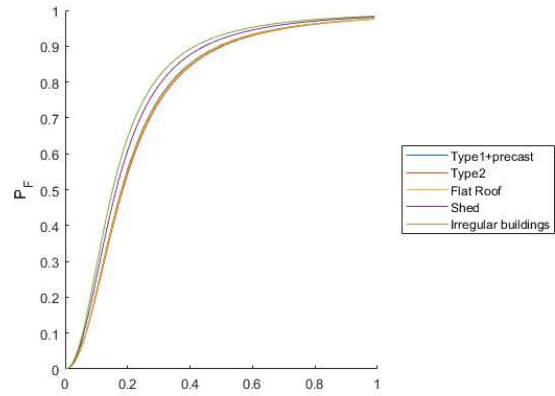


Figure 68. Comparison of the fragility curves for each building class, for each damage level, considering no ordinal models.



## 7. Conclusions

### 7.1 General conclusions

A database of seismic damage on 1890 precast RC buildings was assembled using data collected after the 2012 Emilia earthquake. Both field surveys and information provided by structural engineers appointed, by owners, to design retrofit/strengthening interventions for damaged buildings were used. The information acquired was essential to build a new precast concrete building database. The consistency of the building database was analysed using cadastral data as reference.

About 96% of the buildings examined are located in the struck region at epicentral distances not larger than 30 km and represent about 30% of the total stock of industrial buildings in the area. The strong motion data used in the study were obtained from the shakemaps of the two mainshocks that occurred on May 20<sup>th</sup> and 29<sup>th</sup>, with  $M_L = 5.9$  and 5.8, respectively. In particular, for each building, three parameters were considered to establish the earthquake intensity, i.e., distance from the nearest epicentre, PSA at 1 s associated with the nearest epicentre, and maximum experienced PGA.

A six level damage scale, substantially corresponding to those given by EMS-98, was defined. The first level (D0) corresponds to undamaged buildings, whereas damage levels D1 to D5 refer to increasing levels of damage, from slight damages on non-structural elements up to partial or full building collapse. Then, on the basis of some correlations observed, the damage data were grouped into the three classes D0, D1+D2, and D3+D4+D5.

It was found that approximately 90% of the buildings of damage class D3+D4+D5 included in the study are located within 16 km from the epicentre and experienced a PSA larger than 0.12g. For 10% of the severely damaged to collapsed buildings, the PSA was larger than 0.29g. It is worth observing that approximately 20% of the buildings that experienced a  $PSA \geq 0.20g$  were nevertheless undamaged. The circumstance that also close to the epicentres a significant number of buildings resulted undamaged indicates that some precast building typologies present a relatively low seismic vulnerability.

The damage distributions in terms of the maximum experienced PGA are characterized by a sudden increase in the number of damaged buildings for  $PGA \geq 0.28g$ . This slope change is a consequence of the non-uniform distribution of the buildings included into the database and of the spatial distribution of the PGA.

Since very heavy damages and collapses were observed in a significant number of buildings up to about 15 km from the epicentres, and moderate damages affected buildings located up to 25-30 km from the epicentres (Figure 60), further developments of the present investigation will be

dedicated to a deeper analysis of the most common typologies of precast buildings, in order to put in evidence all possible sources of seismic vulnerability, as shown in the following chapter.

Damage matrices were evaluated from the database and observational parametric fragilities were computed using a simulation based Bayesian approach. Two different classes of models were fitted: *i*) models considering the different damage levels independently and *ii*) an ordinal logistic model which leads to non-overlapping fragility curves. In fact, being the dataset limited to 0.35 g, fragility curves obtained from the individual damage states were slightly overlapped for larger PGA values. Furthermore, uncertainty on PGA was discussed and included in the ordinal model adopting a Berkson error model.

The fragility curves obtained in the present work, when compared to literature fragilities for cast in place RC frame buildings, indicate that precast industrial buildings are significantly more vulnerable. Therefore, specific fragility models should be used for assessing the seismic risk related to prefabricated buildings.

Finally, it should be noted that Emilia earthquakes caused PGA values not larger than 0.35 g and no information was available on the behaviour of the buildings under consideration for stronger ground-motions. Therefore, the fragility curves obtained, in particular those related to the most severe damage states considered could be biased, and should be used with care for stronger ground-motions. Nevertheless, the fragility models presented may provide important information for validating fragility curves obtained from numerical models.

## **7.2 Further developments**

Communicating seismic risk and structural performance is a complex but essential task assigned to the technical community, in order to enable owners of earthquake prone buildings and other stakeholders to consider the implementation of seismic vulnerability reduction interventions and to make informed retrofit decisions.

In the last few years, in the spirit of Performance- Based Design, a great amount of research efforts were carried out focusing on the evaluation of the consequences for the building owners and occupants of the occurrence of a seismic event (PEER PBEE methodology – Porter, 2003; Mitrani-Reiser, 2007; Ramirez and Miranda, 2009; ATC-58, 2012; Welch, Sullivan et al., 2014).

There are many loss estimation models available in the literature today, the most simplified ones aim at evaluating the direct economic losses due to building repair or replace while the more comprehensive ones also consider indirect consequences, namely the downtime, injuries and casualties, due to either a specified earthquake scenario or expected on a structure within a certain time frame.

In the light of the above, the last phase of the research activity was related to the application of Performance-Based-Earthquake-Engineering (PBEE) methodology according to FEMA P-58 guidelines. In particular, to exercise and evaluate P-58 guidelines, while making a comparison

with the Italian damage data collected, was used the software SP3, developed by Haselton and Baker risk group. This software implement P-58 risk assessment procedure and also REDi rating system to generate repair time. From the tests carried on a sample of buildings of the same structural typology, the software SP3 seems to provide a good prediction in term of damage level, but the component cost estimation for different levels of damages is overestimated compared to the actual Italian repair cost. After analyzing different price lists for different retrofit interventions some consequence functions in terms of repair costs were recalibrated.

Significant cases study were then chosen to perform a loss assessment analysis and evaluate the cost-effectiveness of alternative retrofit options to support decision making to better suit the client priorities and needs. The use of SP3 software, compared with PACT software belonging to FEMA -58 guidelines results computationally less expensive and would easily be used in common practice. For all of those reasons this part of the research, that is still going on, will be object of further development.

## REFERENCES

- [1] R. K. Khare, M. M. Maniyar, S. R. Uma, and V. B. Bidwai, "Seismic performance and design of precast concrete building structures: An overview," *J. Struct. Eng.*, vol. 38, no. 3, pp. 272–284, 2011.
- [2] H. Muguruma, M. Nishiyama, and F. Watanabe, "Lessons learned from the Kobe earthquake - a Japanese perspective," *PCI J.*, vol. 40, no. 4, pp. 28–42, 1995.
- [3] M. Posada and S. L. Wood, "Seismic Performance of Precast Industrial Buildings in Turkey," *7th U.S. National Conference on Earthquake Engineering*. Boston, U.S., p. Paper 543, 2002.
- [4] M. H. Arslan, H. H. Korkmaz, and F. G. Gulay, "Damage and failure pattern of prefabricated structures after major earthquakes in Turkey and shortfalls of the Turkish Earthquake code," *Eng. Fail. Anal.*, vol. 13, no. 4, pp. 537–557, Jun. 2006.
- [5] E. Akpınar, H. M. Atalay, S. Özden, and H. Erdoğan, "Performance of precast concrete structures in October 2011 Van earthquake, Turkey," *Mag. Concr. Res.*, vol. 66, no. 11, pp. 543–552, Jun. 2014.
- [6] G. Toniolo and A. Colombo, "Precast concrete structures: The lessons learned from the L'Aquila earthquake," *Struct. Concr.*, vol. 13, no. 2, pp. 73–83, 2012.
- [7] M. Savoia, C. Mazzotti, N. Buratti, B. Ferracuti, M. Bovo, V. Ligabue, and L. Vincenzi, "Damages and collapses in industrial precast buildings after the Emilia earthquake," *International J. Earthq. Eng. (Ingegneria Sismica)*, vol. 29, no. 2–3, pp. 120–131, 2012.
- [8] L. Liberatore, L. Sorrentino, D. Liberatore, and L. D. Decanini, "Failure of industrial structures induced by the Emilia (Italy) 2012 earthquakes," *Eng. Fail. Anal.*, vol. 34, pp. 629–647, Dec. 2013.
- [9] P. Yanev, "Performance of industrial facilities," *Earthq. Spectra*, vol. 5, no. (3), pp. 101–113, 1989.
- [10] A. H. Hadjian, "The Spitak, Armenia earthquake of 7 December 1988 — why so much destruction," *Soil Dyn. Earthq. Eng.*, vol. 12, no. 1, pp. 1–24, Jan. 1993.
- [11] M. Saatcioglu, D. Mitchell, R. Tinawi, N. J. Gardner, A. G. Gillies, A. Ghobarah, D. L. Anderson, and D. Lau, "The August 17, 1999, Kocaeli (Turkey) earthquake — damage to structures," *Can. J. Civ. Eng.*, vol. 28, no. 4, pp. 715–737, Aug. 2001.
- [12] E. Yüksel and M. Sürmeli, "Failure analysis of one-story precast structures for near-fault and far-fault strong ground motions," *Bull. Earthq. Eng.*, vol. 8, no. 4, pp. 937–953, Aug. 2010.

- [13] H. Sezen and A. S. Whittaker, “Seismic Performance of Industrial Facilities Affected by the 1999 Turkey Earthquake,” *J. Perform. Constr. Facil.*, vol. 20, no. 1, pp. 28–36, Feb. 2006.
- [14] K. A. Korkmaz and A. E. Karahan, “Investigation of Seismic Behavior and Infill Wall Effects for Prefabricated Industrial Buildings in Turkey,” *J. Perform. Constr. Facil.*, vol. 25, no. 3, pp. 158–171, Jun. 2011.
- [15] G. A. S. Miyamoto and A. Wada, “RECONNAISSANCE REPORT OF THE 2008 SICHUAN EARTHQUAKE, DAMAGE SURVEY OF BUILDINGS AND RETROFIT OPTIONS,” *Proc. 14th World Conf. Earthq. Eng. Beijing, China, Oct.*, 2008.
- [16] J. D. Marshall and N. C. Gould, “The Performance of Low-Rise Industrial Facilities in the 2010 Haiti and 2011 Christchurch, New Zealand Earthquakes,” *Proc. 15th World Conf. Earthq. Eng. Lisbon, Port. Sept.*, 2012.
- [17] F. Biondini, B. Dal Lago, and G. Toniolo, “Role of wall panel connections on the seismic performance of precast structures,” *Bull. Earthq. Eng.*, vol. 11, no. 4, pp. 1061–1081, Aug. 2013.
- [18] I. Faggiano, B. Iervolino, I. Magliulo, G. Manfredi, G. Vanzi, “Il comportamento delle strutture industriali nell’evento de L’Aquila,” *Progett. Sismica*, vol. 1, no. 3, pp. 203–208, 2009.
- [19] M. Dolce and D. Di Bucci, “National Civil Protection Organization and technical activities in the 2012 Emilia earthquakes (Italy),” *Bull. Earthq. Eng.*, vol. 12, no. 5, pp. 2231–2253, Oct. 2014.
- [20] R. Paolucci, F. Pacor, R. Puglia, G. Ameri, C. Cauzzi, and M. Massa, “Record Processing in ITACA, the New Italian Strong-Motion Database,” in *Earthquake Data in Engineering Seismology - Predictive Models, Data Management and Networks*, S. Akkar, P. Gülkan, and T. van Eck, Eds. Springer Netherlands, 2011.
- [21] F. Bozzoni, C. G. Lai, and L. Scandella, “Preliminary results of ground-motion characteristics,” *Ann. Geophys.*, vol. 55, no. 4, pp. 609–614, 2012.
- [22] E. Priolo, M. Romanelli, C. Barnaba, M. Mucciarelli, G. Laurenzano, L. Dall’Olio, N. Abu Zeid, R. Caputo, G. Santarato, L. Vignola, C. Lizza, and P. Di Bartolomeo, “The Ferrara thrust earthquakes of May-June 2012: preliminary site response analysis at the sites of the OGS temporary network,” *Ann. Geophys.*, vol. 55, no. 4, pp. 591–597, 2012.
- [23] P. Di Manna, P. Di Manna, L. Guerrieri, L. Piccardi, E. Vittori, D. Castaldini, A. Berlusconi, L. Bonadeo, V. Comerci, F. Ferrario, R. Gambillara, F. Livio, M. Lucarini, and A. M. Michetti, “Ground effects induced by the 2012 seismic sequence in Emilia: implications for seismic hazard assessment in the Po Plain,” *Ann. Geophys.*, vol. 55, no. 4, Oct. 2012.
- [24] M. Savoia, N. Buratti, and L. Vincenzi, “Damage and collapses in industrial precast

- buildings after the 2012 Emilia earthquake,” *Eng. Struct.*, vol. 137, pp. 162–180, Apr. 2017.
- [25] A. Masi, G. Santarsiero, A. Digrisolo, L. Chiauuzzi, and V. Manfredi, “Procedures and experiences in the post-earthquake usability evaluation of ordinary buildings,” *Boll. di Geofis. Teor. ed Appl.*, vol. 57, no. 2, pp. 199–200, 2016.
- [26] V. Castelli, F. Bernardini, R. Camassi, C. H. Caracciolo, E. Ercolani, and E. Postpischl, “Looking for missing earthquake traces in the Ferrara-Modena plain: an update on historical seismicity,” *Ann. Geophys.*, vol. 5, no. 4, pp. 519–524, 2012.
- [27] M. Pieri and G. Groppi, “Subsurface geological structure of the Po Plain, Italy,” C.N.R. (Italian National Council for Research), 1981.
- [28] G. G. Ori and P. F. Friend, “Sedimentary basins formed and carried piggyback on active thrust sheets,” *Geology*, vol. 12, no. 8, pp. 475–478, 1984.
- [29] S. Zerbini, F. Matonti, and C. Doglioni, “Crustal movements in northeastern Italy from permanent GPS stations,” in *Geophysical Research Abstracts, Proceedings of European Geosciences Union 2006*, 2006, vol. 8, p. 6257.
- [30] R. Devoti, G. Pierantonio, A. Pisani, F. Riguzzi, and E. Serpelloni, “Present day kinematics of Italy,” *J. Virtual Explor.*, vol. 36, 2010.
- [31] A. Gorini, M. Nicoletti, P. Marsan, R. Bianconi, R. Nardis, L. Filippi, S. Marcucci, F. Palma, and E. Zambonelli, “The Italian strong motion network,” *Bull. Earthq. Eng.*, vol. 8, no. 5, pp. 1075–1090, 2010.
- [32] G. Di Capua, G. Lanzo, V. Pessina, S. Peppoloni, and G. Scasserra, “The recording stations of the Italian strong motion network: geological information and site classification,” *Bull. Earthq. Eng.*, vol. 9, no. 6, pp. 1779–1796, 2011.
- [33] M. Bresolin, “Effetto di diverse tecniche di rinforzo di lai lignei sul comportamento sismico di so,” 2013.
- [34] Italian Ministry of Public Works, “D.M. 3/12/1987 – Norme tecniche per la progettazione, esecuzione e collaudo delle costruzioni prefabbricate.” 1987.
- [35] Presidente del Consiglio dei Ministri, “OPCM 3274/2003 – Primi elementi in materia di criteri generali per la classificazione sismica del territorio nazionale e di normative tecniche per le costruzioni in zona sismica (in Italian).” 2003.
- [36] Italian Ministry of Public Works, “Norme Tecniche per le Costruzioni (in Italian).” 2008.
- [37] G. M. Verderame, F. De Luca, M. T. De Risi, C. Del Gaudio, and P. Ricci, “A three level vulnerability approach for damage assessment of infilled RC buildings: The Emilia 2012 case (V 1.0),” pp. 1–49, 2012.
- [38] “Italian Building Code (2008), D.M. 14/01/2008, Rome.,” 2008.

- [39] A. Benavent-Climent, H. Akiyama, F. López-Almansa, and L. . Pujades, “Prediction of ultimate earthquake resistance of gravity-load designed RC buildings,” *Eng. Struct.*, vol. 26, no. 8, pp. 1103–1113, Jul. 2004.
- [40] Italian National Research Council - CNR, “Istruzioni per il progetto, l’esecuzione e il controllo delle strutture prefabbricate in conglomerate cementizio e per le strutture costruite con sistemi industrializzati – CNR 10025 (in Italian).” 1984.
- [41] European Committee for Standardization - CEN, “Eurocode 2: Design of concrete structures - Part 1-1: General rules and rules for buildings.” 2004.
- [42] I. N. Psycharis and H. P. Mouzakis, “Shear resistance of pinned connections of precast members to monotonic and cyclic loading,” *Eng. Struct.*, vol. 41, pp. 413–427, 2012.
- [43] P. Negro and G. Toniolo, “Design Guidelines for Connections of Precast Structures under Seismic Actions,” Joint Research Centre of the European Commission, 2012.
- [44] Ministro dei Lavori Pubblici, “D.M. 14/2/1992 - Norme tecniche per l’esecuzione delle opere in cemento armato normale e precompresso e per le strutture metalliche.” 1992.
- [45] Italian Ministry of Public Works, “D.M. 9.1.1996 – Norme Tecniche per il calcolo, l’esecuzione ed il collaudo delle strutture in cemento armato, normale e precompresso e per le strutture metalliche (in Italian).” 1996.
- [46] Italian Ministry of Public Works, “D.M. 16/1/1996 - Norme Tecniche relative alle costruzioni in zona sismica,” 1996.
- [47] F. Minghini, E. Ongaretto, V. Ligabue, M. Savoia, and N. Tullini, “Observational failure analysis of precast buildings after the 2012 Emilia earthquakes,” *Earthq. Struct.*, vol. 11, no. 2, 2016.
- [48] C. Baggio, A. Bernardini, R. Colozza, L. Corazza, M. Della Bella, G. Di Pasquale, M. Dolce, A. Goretti, A. Martinelli, and G. Orsini, “Field Manual for post-earthquake damage and safety assessment and short term countermeasures (AeDES).”
- [49] 18 pp Goretti, Anvitational workshop report, Pasadena, CA, USA and G. Di Pasquale, “An overview of post-earthquake damage assessment in Italy. Earthquake Eng. Res. Inst.,” *Earthq. Eng. Res. Inst. Invit. Work. report, Pasadena, CA, USA, 18 pp*, 2002.
- [50] C. Casotto, V. Silva, H. Crowley, R. Nascimbene, and R. Pinho, “Seismic fragility of Italian RC precast industrial structures,” *Eng. Struct.*, vol. 94, pp. 122–136, 2015.
- [51] D. A. Bournas, P. Negro, and F. F. Taucer, “Performance of industrial buildings during the Emilia earthquakes in Northern Italy and recommendations for their strengthening,” *Bull. Earthq. Eng.*, vol. 12, no. 5, pp. 2383–2404, 2014.
- [52] A. Belleri, M. Torquati, P. Riva, and R. Nascimbene, “Vulnerability assessment and retrofit

- solutions of precast industrial structures,” *Earthquakes Struct.*, vol. 8, no. 3, pp. 801–820, 2015.
- [53] Liberatore Sorrentino Liberatore Decanini, “Failure of industrial structures induced by the Emilia (Italy) 2012 earthquakes,” 2013.
- [54] B. Kafle, N. T. K. Lam, E. Lumantarna, E. F. Gad, and J. L. Wilson, “Overturning of precast RC columns in conditions of moderate ground shaking,” *Earthquakes Struct.*, vol. 8, no. 1, pp. 1–18, Jan. 2015.
- [55] G. Milani and M. Valente, “Comparative pushover and limit analyses on seven masonry churches damaged by the 2012 Emilia-Romagna (Italy) seismic events: Possibilities of non-linear finite elements compared with pre-assigned failure mechanisms,” *Eng. Fail. Anal.*, vol. 47, pp. 129–161, Jan. 2015.
- [56] E. Artioli, R. Battaglia, and A. Tralli, “Effects of May 2012 Emilia earthquake on industrial buildings of early ’900 on the Po river line,” *Eng. Struct.*, vol. 56, no. November, pp. 1220–1233, 2013.
- [57] M. Ercolino, G. Magliulo, and G. Manfredi, “The lesson learnt after Emilia-Romagna earthquakes on precast RC structures: a case-study,” no. 2008, 2016.
- [58] J. W. Baker, G. Cremen, and S. Giovinazzi, “Benchmarking FEMA P-58 performance predictions against observed earthquake data - A preliminary evaluation for the Canterbury earthquake sequence,” *New Zeal. Soc. Earthq. Eng. Conf.*, no. Figure 1, pp. 1–7, 2016.
- [59] I. Almufti, M. Willford, M. Delucchi, C. Davis, B. Hanson, D. Langdon, D. Friedman, L. Johnson, G. Nielsen, N. O. Riordan, C. Roberts, M. Steiner, A. Wilson, A. Wolski, and T. Mote, “REDi™ Rating System,” no. October, 2013.
- [60] F. Braga, R. Gigliotti, G. Monti, F. Morelli, C. Nuti, W. Salvatore, and I. Vanzi, “Speedup of post earthquake community recovery: the case of precast industrial buildings after the Emilia 2012 earthquake,” *Bull. Earthq. Eng.*, vol. 12, no. 5, pp. 2405–2418, Oct. 2014.
- [61] D. J. Wald, B. C. Worden, V. Quitoriano, and K. L. Pankow, “ShakeMap® Manual TECHNICAL MANUAL, USERS GUIDE, AND SOFTWARE GUIDE Prepared by,” 2006.
- [62] A. Michelini, L. Faenza, V. Lauciani, and L. Malagnini, “Shakemap Implementation in Italy,” *Seismol. Res. Lett.*, vol. 79, no. 5, pp. 688–697, Sep. 2008.
- [63] G. Cultrera, L. Faenza, C. Meletti, V. D’Amico, A. Michelini, and A. Amato, “Shakemaps uncertainties and their effects in the post-seismic actions for the 2012 Emilia (Italy) earthquakes,” *Bull. Earthq. Eng.*, vol. 12, no. 5, pp. 2147–2164, Oct. 2014.
- [64] T. Rossetto, P. Gehl, S. Minas, C. Galasso, P. Duffour, J. Douglas, and O. Cook, “FRACAS:

- A capacity spectrum approach for seismic fragility assessment including record-to-record variability,” *Eng. Struct.*, vol. 125, no. August, pp. 337–348, 2016.
- [65] D. D’Ayala, R. Spence, C. Oliveira, and A. Pomonis, “Earthquake loss estimation for Europe’s historic town centres,” *Earthquake Spectra*, vol. 13, no. 4, pp. 773–793, 1997.
- [66] N. Yamaguchi and F. Yamazaki, “Fragility Curves for Buildings in Japan Based on Damage Surveys After the 1995 Kobe Earthquake,” *12th World Conf. Earthq. Eng.*, pp. 1–8, 2000.
- [67] T. Rossetto and A. Elnashai, “Derivation of vulnerability functions for European-type RC structures based on observational data,” *Eng. Struct.*, vol. 25, no. 10, pp. 1241–1263, 2003.
- [68] F. S. Karababa and A. Pomonis, “Damage data analysis and vulnerability estimation following the August 14, 2003 Lefkada Island, Greece, Earthquake,” *Bull. Earthq. Eng.*, vol. 9, no. 4, pp. 1015–1046, 2011.
- [69] G. Orsini, “A model for buildings’ vulnerability assessment using the parameterless scale of seismic intensity (PSI),” *Earthquake Spectra*, vol. 15, no. 3, pp. 463–483, 1999.
- [70] S. Molina, Y. Torres, B. Benito, M. Navarro, and D. Belizaire, “Using the damage from 2010 Haiti earthquake for calibrating vulnerability models of typical structures in Port-au-Prince (Haiti),” *Bull. Earthq. Eng.*, vol. 12, no. 4, pp. 1459–1478, 2014.
- [71] U. Hancilar, C. Tuzun, C. Yenidogan, M. Erdik, and K. Observatory, “Introduction Earthquake Loss Estimation Routine ( ELER ) Spectral Capacity Based Vulnerability Assessment Casualty Assessment Conclusions,” no. September, 2010.
- [72] M. Rota, A. Penna, and C. L. Strobbia, “Processing Italian damage data to derive typological fragility curves,” *Soil Dyn. Earthq. Eng.*, vol. 28, no. 10–11, pp. 933–947, 2008.
- [73] M. Colombi, B. Borzi, H. Crowley, M. Onida, F. Meroni, and R. Pinho, “Deriving vulnerability curves using Italian earthquake damage data,” *Bull. Earthq. Eng.*, vol. 6, no. 3, pp. 485–504, 2008.
- [74] T. Rossetto, I. Ioannou, and D. N. Grant, “Existing Empirical Fragility and Vulnerability Relationships: Compendium and Guide for Selection,” *GEM Tech. Rep.*, vol. 1, p. 77, 2015.
- [75] H. Crowley, R. Pinho, and J. J. Bommer, “A Probabilistic Displacement-based Vulnerability Assessment Procedure for Earthquake Loss Estimation,” *Bull. Earthq. Eng.*, vol. 2, no. 2, pp. 173–219, 2004.
- [76] N. Buratti, B. Ferracuti, and M. Savoia, “Response Surface with random factors for seismic fragility of reinforced concrete frames,” *Struct. Saf.*, vol. 32, no. 1, pp. 42–51, Jan. 2010.
- [77] M. A. Erberik, “Fragility-based assessment of typical mid-rise and low-rise RC buildings in Turkey,” *Eng. Struct.*, vol. 30, no. 5, pp. 1360–1374, May 2008.
- [78] A. Babič and M. Dolšek, “Seismic fragility functions of industrial precast building classes,”

- Eng. Struct.*, vol. 118, pp. 357–370, 2016.
- [79] V. Silva, H. Crowley, H. Varum, R. Pinho, and R. Sousa, “Evaluation of analytical methodologies used to derive vulnerability functions,” *Earthq. Eng. Struct. Dyn.*, vol. 43, no. 2, pp. 181–204, Feb. 2014.
- [80] “INGV (2012), Italian National Institute of Geophysics and Volcanology. ShakeMap Home Page,” 2012. [Online]. Available: <http://shakemap.rm.ingv.it/shake/index.html>. [Accessed: 17-Dec-2017].
- [81] F. Braga, R. Gigliotti, G. Monti, F. Morelli, C. Nuti, W. Salvatore, and I. Vanzi, “Post-seismic assessment of existing constructions: evaluation of the shakemaps for identifying exclusion zones in Emilia,” *Earthquakes Struct.*, vol. 8, no. 1, pp. 37–56, Jan. 2015.
- [82] M. J. O’Rourke and P. So, “Seismic fragility curves for on-grade steel tanks,” *Earthq. Spectra*, 2000.
- [83] D. Lallemand, A. Kiremidjian, and H. Burton, “Statistical procedures for developing earthquake damage fragility curves.”
- [81] Gelman A, Carlin JB, Stern HS, Dunson DB, Vehtari A, Rubin DB. Bayesian Data Analysis. 3rd ed. Chapman & Hall/CRC Press; 2013.
- [2] Koutsourelakis PS, Pradlwarter HJ, Schuëller GI. Reliability of structures in high dimensions. *Proceedings in Applied Mathematics and Mechanics* 2003; 3(1): 495–496.
- [3] Shinozuka M, Feng MQ, Lee J, Naganuma T. Statistical Analysis of Fragility Curves. *Journal of Engineering Mechanics* 2000; 126(12): 1224–1231.
- [4] R Development Core Team. R: A Language and Environment for Statistical Computing. Vienna, Austria: R Foundation for Statistical Computing; 2008.
- [5] Plummer M. JAGS: A Program for Analysis of Bayesian Graphical Models Using Gibbs Sampling. *Proceedings of the 3rd International Workshop on Distributed Statistical Computing*, Wien, Austria, 20-22 March: 2003.
- [6] Jackman S. Bayesian Analysis for the Social Sciences. John Wiley & Sons; 2009.
- [7] Agresti A. Analysis of ordinal categorical data. Wiley; 2010.
- [8] Straub D, Der Kiureghian A. Improved seismic fragility modeling from empirical data. *Structural Safety* 2008; 30(4): 320–336.
- [9] Carroll RJ, Carroll RJ. Measurement error in nonlinear models: a modern perspective. Chapman & Hall/CRC; 2006.
- [10] Worden C., Wald DJ. ShakeMap Manual Online: technical manual, user’s guide, and software guide. 2016. DOI: 10.1234/012345678.